Magnetic multilayers

Magnetic Multilayers

H.J.G. Draaisma

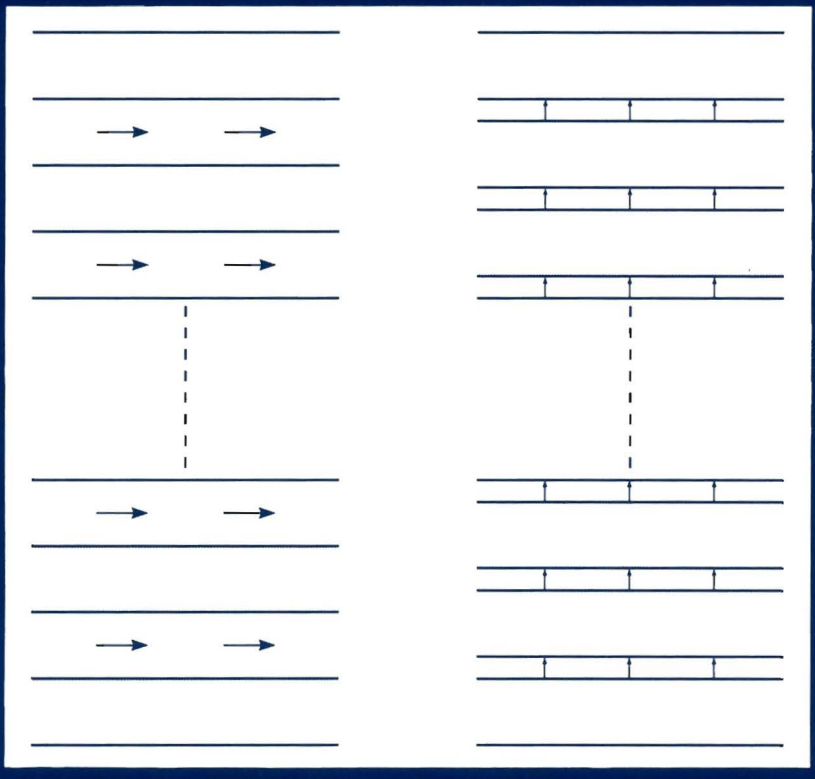

The cover shows schematically the preferential magnetization
in Pd/Co multilayers for a Co layer thickness above and below a critical thickness

MAGNETIC MULTILAYERS

PROEFSCHRIFT

TER VERKRIJGING VAN DE GRAAD VAN DOCTOR AAN DE TECHNISCHE UNIVERSITEIT EINDHOVEN, OP GEZAG VAN DE RECTOR MAGNIFICUS, PROF. IR. M. TELS, VOOR EEN COMMISSIE AANGEWEZEN DOOR HET COLLEGE VAN DEKANEN IN HET OPENBAAR TE VERDEDIGEN OP DINSDAG 4 OKTOBER 1988 TE 16.00 UUR

DOOR

HENRICUS JOHANNES GEORGE DRAAISMA

GEBOREN TE LEIDSCHENDAM

Dit proefschrift is goedgekeurd door de promotoren:

Prof. dr. ir. W.J.M. de Jonge en

Prof. dr. A.R. Miedema.

Copromotor: Dr. ir. F.J.A. den Broeder

The work described in this thesis is part of a joined research project of the Philips Research Laboratories, group "Magnetism" and the Eindhoven University of Technology, group "Cooperative Phenomena", Solid State Division, Department of Physics, both in Eindhoven, The Netherlands.

It is important for him who wants to discover,

not to confine himself to one chapter of science,

but to keep in touch with various others.

Jacques Hadamard

aan mijn ouders

TABLE OF CONTENTS

Chapter 1 INTRODUCTION

One of the challenges in solid state physics is to manipulate the properties of a material by arranging the atoms on predetermined sites in a lattice. This is sometimes called "atomic engineering". In semiconductors the growth of layers of different composition onto each other has led to the development of the solid state laser and the discovery of the quantum Hall effect. The control of crystalline and compositional perfection for metal systems is not as well developed as for semiconductors, but interesting results have already been obtained in the fields of magnetism, superconductivity, elastic behaviour, diffusion and the development of novel materials. In this thesis we report the results of an experimental study of the magnetic properties and phenomena which may occur when a thin film is built up of successive atomic layers of different metals.

In this introduction we will motivate the present study and describe the multilayers that are the subject of this thesis. Further some results reported in the literature on this subject will be mentioned and an overview over the material contained in this thesis will be given. A review of developments in both semiconductor and metallic modulated structures has appeared recently [1].

1.1 Metallic multilayers

Metallic multilayers are thin films in which the composition is modulated by alternating deposition of different metals. The term metallic is used to make a distinction with semiconductor multilayers and because most of the materials are metallic. The films are usually prepared by common vacuum deposition methods such as evaporation and sputtering. Other names used for this new class of thin film materials are compositionally modulated alloys, metallic superlattices, layered ultra-coherent structures etc., depending on the point of view one likes to emphasize. The alternation between two materials can be done gradually to obtain a smooth transition of one material into the other or abruptly to obtain a sharp interface. Whether this can be realized depends of course on the characteristics of the materials involved and on the growth conditions.

Fig. 1.1 shows a schematic representation of the multilayer systems studied in this thesis. This multilayer can be characterized by the individual layer thicknesses t_A and t_B and the total number of bi-layers (N). A typical property of the multilayer is that in the direction perpendicular to the film plane the structure repeats itself with a certain period, called the modulation length D, which, in this case, is equal to the sum of the layer thicknesses $t_A + t_B$. The individual thicknesses range approximately from 2 to 100 Å which means from one to several atomic layers. The total thickness of the film is mostly about 0.3 μm. The individual layers can be amorphous or crystalline, they can have the same or a different crystal structure and they can

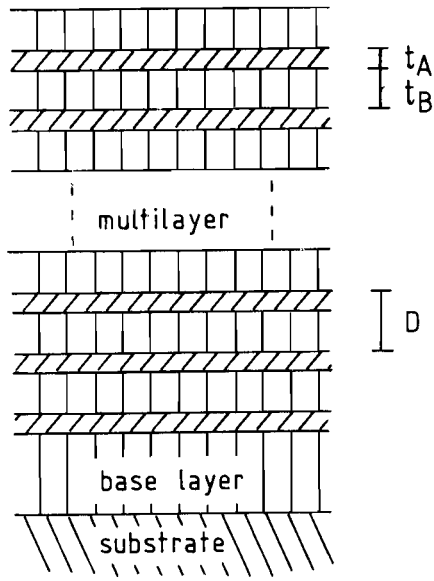

Fig. 1.1 *Schematic drawing of a multilayer with sharp interfaces. Indicated are the individual layer thicknesses* t_A *and* t_B *and the modulation length D.*

have the same or different lattice constants. By epitaxial or pseudomorphic growth (i.e. a growth mode in which the deposited layer adapts itself in one way or the other to the surface on which it is deposited), metastable phases can be obtained, which yield potential possibilities to create novel materials.

When all the atoms are neatly arranged on a lattice and the modulation can be described completely by the repetition of a large unit cell in the direction perpendicular to the film, one can speak of a true superlattice. In this case, lattice planes perpendicular to the film plane can be discerned. The interface between two materials can be called coherent if each atom in one material has the same relative

position to the atoms in the other material. When the lattice mismatch results in a regular array of dislocations at the interface, the interface becomes more incoherent (Fig. 1.2). Though it is often claimed that a multilayer is a coherent structure, it is hard to find experimental evidence for it.

The interest in the physical properties of these artificial structures has various origins. The limited thickness of the individual layers, the large number of interfaces and the adjustable coupling over or through the layers are just a few of the challenging aspects for very different fields of physics. We will first consider some of the magnetic properties and then pay attention to some other fields of interest.

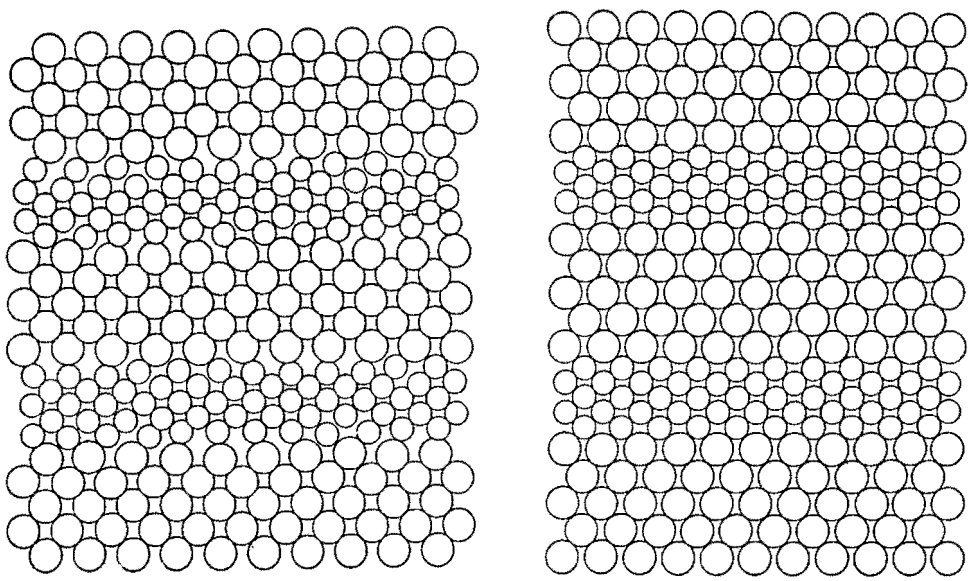

Fig. 1.2 *Model of incoherent* (a) *and coherent* (b) *interfaces between the layers of the two materials.*

1.2 Magnetic properties

The interest in the magnetic properties of multilayers in which one of the materials is ferromagnetic in its bulk form, concerns several effects. First of all, the reduction of the thickness of the individual magnetic layers imposes a two-dimensional (2D) character on the magnetic system, which is of interest to the theory of phase transitions. For instance, the temperature dependence of the magnetization is predicted to be linear when the thickness is reduced [2]. Examples of this behaviour have been found in Fe/V [3] and Cu/Ni [4] multilayers.

Secondly, there are interface effects depending on the kind of material that is neighbouring the magnetic layers. The interface can lead to a reduced magnetic moment on the outer atomic layers, but also enhancements are predicted from band structure calculations. The observation of "dead layers" in Fe and Ni films [5] has stimulated the search for these effects, but the results are not unambiguous. A review comparing theory and experiment has been given in [6]. A more important effect of the interface is that the anisotropic environment can lead to a preferential direction for the magnetization. This was already pointed out by Néel for the surface of a magnetic material [7] and experimentally the values predicted by this phenomenological theory were found to be in the same order of magnitude [8]. In principle, these effects can be and have been measured in single, very thin layers, whether or not sandwiched between layers of another material. Multilayers have the advantage to increase the accuracy with which the

measurements can be made and to allow structure determinations by X-ray or electron diffraction. Also when applications of these effects on ultra-thin scale are pursued in a thin film, it is necessary to repeat the layer sequence.

A third source of interest is the long range coupling across a non-magnetic metal, e.g. by RKKY-coupling. This is claimed to be found in Gd/Y [9] and Dy/Y [10] multilayers where the nesting of the Fermi surfaces in the Y layers seems to be responsible for this coupling [11]. The interaction of alternating sign between the magnetic moments can lead to interesting new spin structures, dependent on the thickness of the layers [12].

At the fourth place, superlattice effects are expected by the superposition of the properties of the individual layers. For example, the superposition of the Damon-Eschbach (DE) modes, which are surface spin-wave excitations, leads to modification of the spin-wave mode spectra [13].

Finally, structural modifications, induced by neighbouring layers, might bring about metastable phases, such as other lattice parameters or other crystal structures, which can lead to new magnetic properties, as appears from theoretical calculations [14].

1.3 Applications in magnetic recording

Magnetic recording takes place in many situations in which a signal is to be saved for later use. In Fig. 1.3 a sketch of a common way of magnetic recording is given. During the write process the storage

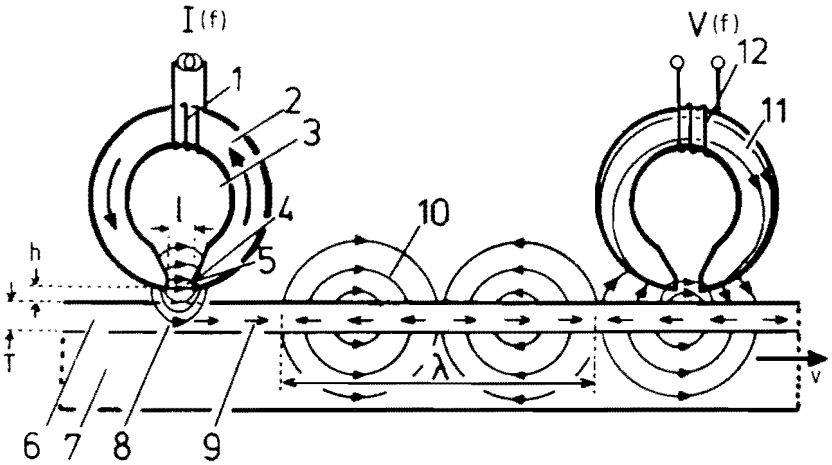

Fig. 1.3 *Principle of the magnetic recording process: the write mode (left-hand side) and the read-mode (right-hand side). Indicated are 1) the coil generating the flux to write, 2) the core of highly permeable material, 3) the coil window, 4) the head tip, 5) the head gap of length l, 6) the magnetic medium, thickness T, 7) the non-magnetic carrier, 8) the recording field, 9) the magnetization pattern, wavelength λ, 10) the magnetic stray field, 11) the flux picked up by the head and 12) the coil in which a voltage is induced.*

medium and head move with a velocity v relative to each other, so that a current with frequency f will result in a magnetization pattern in the medium of wavelength λ, obeying the relation

$$\lambda = \frac{v}{f} . \qquad (1)$$

The magnetization is consolidated by the use of a magnetic medium with relatively high coercivity, which means that the magnetization

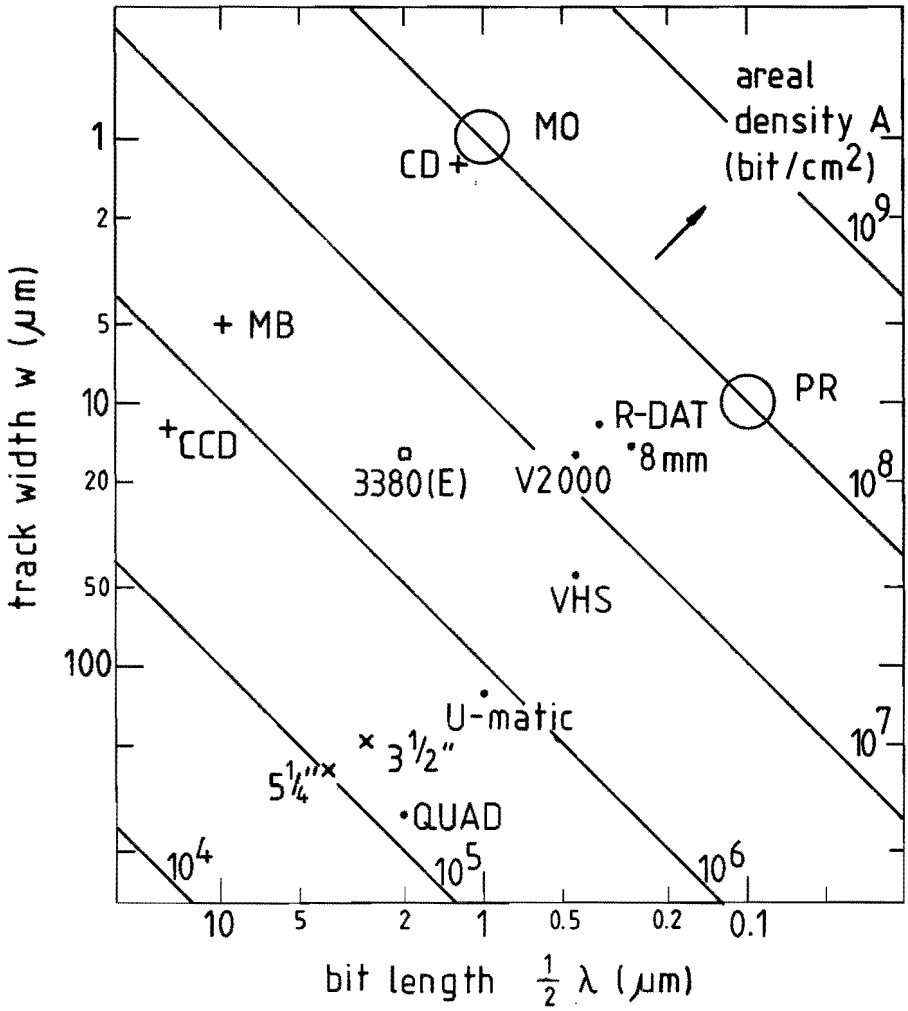

Fig. 1.4 *The recording density of some past, present and future systems, as a function of their typical dimensions. The magnetic recording systems are divided in helical scan (•), floppy disk (×) and rigid disk systems (□). Further indicated are charge coupled devices (CCD), magnetic bubbles (MB) and compact disc (CD). The goals to be realized for magneto-optical (MO) and perpendicular recording (PR) are approximately indicated.*

can only change if, roughly spoken, the applied field exceeds the coercive field of the medium.

Since its discovery, magnetic recording has grown out to an important industrial activity [15]. A historical overview is given in [16] and several textbooks on this subject are available [17]. Here we want to pay some attention to the role that magnetic thin films and possibly multilayers can play in magnetic recording. Before we do this, we note that one of the important trends is to increase the information density A. For the magnetization pattern described above one could define this density as

$$A = \frac{2}{\lambda w} , \qquad (2)$$

with w as the track width. To increase A, the wavelength λ of the magnetization pattern and/or the trackwidth w are to be reduced. In Fig. 1.4 the areal density for some past, present and future systems is shown. For comparison some non-magnetic memory technologies are included in the figure. The helical scan and floppy disk systems are in-contact recording methods, with the disadvantage that wear takes hold of the specially designed dimensions of the recording head. As far as the magnetic recording concerns, there is little difference between in-contact and hard disk recording except that the distance between head and medium is larger in the latter one. Magneto-optical (MO) and perpendicular recording (PR) are future systems for which the goals in density are given.

For a review concerning the application of homogeneous thin films

in magnetic recording we refer to [18]. We will shortly discuss four possible applications of multilayer thin films in magnetic recording: a) as perpendicular recording medium, b) as magneto-optical medium, c) as recording head material and d) as magneto-resistive element.

a) To increase the information density in magnetic recording, the interest in perpendicular recording has revived since 1977 [19]. In this recording mode the domains in the magnetic medium are not oriented in the plane of the film, as usually, but perpendicular to it, as shown in Fig. 1.5. When the domain length decreases, the demagnetization energy more and more opposes the domain pattern longitudinal to the plane, whereas it supports the perpendicular domain pattern. Especially the domain transitions, whence the outcoming flux originates, are expected to be smaller and sharper between the perpendicular domains.

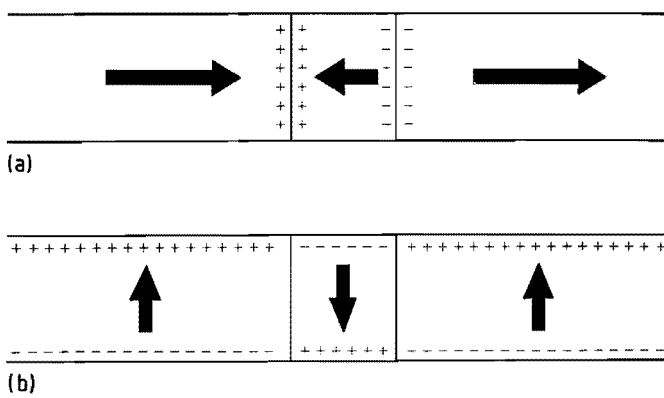

Fig. 1.5 *Magnetic domains oriented parallel* (a) *and perpendicular* (b) *to the film. When the average domain length decreases, the magnetostatic energy supports configuration* (b), *whereas it opposes the antiparallel alignment of the domains in* (a).

To orient the domains perpendicular to the film plane, intrinsic anisotropy is needed to overcome the demagnetization of a thin film. In Co-Cr alloys this is the case when the Co concentration is below 80 at.% and the c-axis of the hexagonal structure is oriented perpendicular to the film [20]. Depending on the preparation conditions, the anisotropy in these films can vary and experimentally it is found that better recording behaviour is obtained when the anisotropy is larger [21]. In multilayers the anisotropy needed can be provided by the interface between a magnetic and non-magnetic material [22]. If the transition between two domains can be considered as a Bloch wall, a larger anisotropy causes a sharper transition between two domains. The thickness of a Bloch wall is $\delta \approx 4\ (A/K)^{1/2}$, in which A is the exchange stiffness (mostly about $2 \cdot 10^{-11}$ J/m) and K the intrinsic anisotropy constant. For $Co_{80}Cr_{20}$ $K \approx 10^{-5}$ J/m^3, so $\delta \approx 500$ Å, which is fairly large when we consider $\lambda \approx 1000$ Å. Another important parameter is the relative perpendicular remanence of the thin film material, which should be close to 1. For Co-Cr it is only about 0.2 and this may be the cause of the high noise level [23]. This property can hardly be predicted in advance, but is more or less coincidental. Manipulations of the individual layer thicknesses and/or growth conditions may systematically influence this property for multilayers.

b) A new mode of high density, erasable recording is, as already indicated in Fig. 1.4, magneto-optical recording [24]. Sometimes it is called thermomagnetic recording [25]. Though there are variations, its main principle is that a ferrimagnetic material is operated as medium whence the domains are read by means of the Kerr rotation of the pola-

rized light that is reflected from the medium. The material used nowadays is mostly an amorphous alloy of Gd or Tb with Fe or Co. Its thickness is only about 600 Å, which is passed two times by the light beam. The material has a compensation point around room temperature, so that the net magnetization is nearly zero. The effective Kerr effect is caused by the (Fe,Co) sublattice magnetization and can only be used if the domains are oriented perpendicularly to the plane. A relatively small anisotropy, probably resulting from pair ordening in the alloy, is sufficient to take care of this since there is no magnetostatic energy involved. The coercivity is strongly temperature dependent because it is very large when the net magnetization is zero and decreases as the magnetization increases with the temperature. This property is used in the write process in which the medium is locally heated and the magnetization is switched by a small magnetic field.

Also in this case multilayers may be useful to increase the anisotropy and sharpen the transitions. A preliminary investigation on Tb/Fe multilayers has been reported [26]. Further, multilayers seem to have a better corrosion behaviour, which is an important problem for the current materials. Last but not least, multilayers composed of other materials may show a large Kerr rotation by the change of the dielectric constants at the interfaces between the materials [27].

c) A magnetic head is usually made of (Mn,Zn) ferrite, which has a saturation magnetization, $\mu_o M_s$, of about 0.5 T. In the write process enough flux should leave the gap of the head to magnetize the medium, i.e. the magnetic field in the medium should exceed the coercivity. As the tendency is to increase the coercivity, the magnetic head suffers

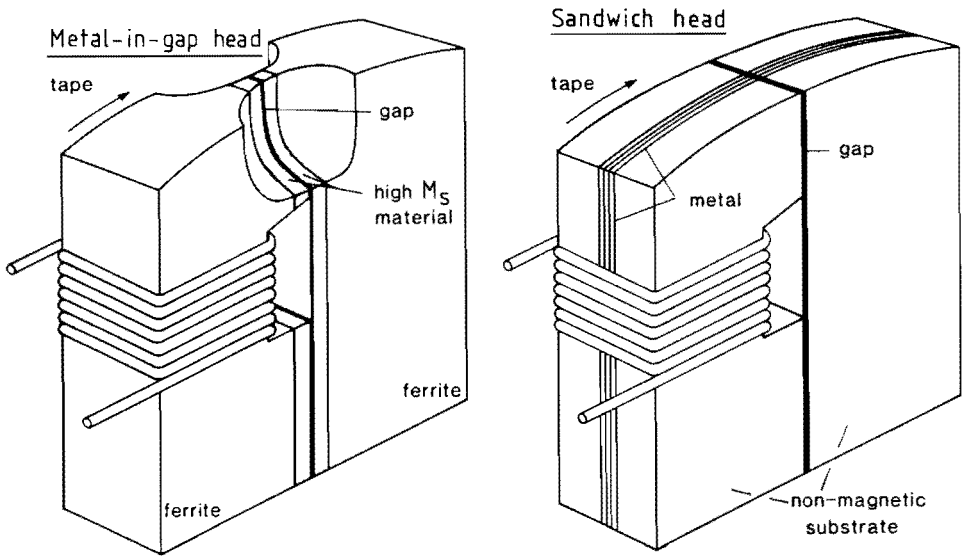

Fig. 1.6(a) *Configuration of the Metal-in-Gap (MIG) head. The ferrite is covered with a metallic thin film with high saturation magnetization,* M_s. (b) *Configuration of the sandwich head in which a metallic thin film is completely carrying the flux through the head.*

from saturation in the pole tips, where the flux is concentrated. One way to overcome this problem is to cover these tips with a thin metallic film with a high saturation magnetization ($\mu_o M_s \approx 1$ T). In Fig. 1.6(a) a schematic drawing of this metal-in-gap (MIG) configuration is shown. These films should be magnetically very soft ($\mu_o H_c \leq 0.1$ mT) and therefore have a low anisotropy and a low magnetostriction. At present, permalloy ($Ni_{79}Fe_{21}$) and sendust ($Fe_{74}Si_{16}Al_{10}$) are used [28]. Another way is to make the head of another material with higher

M_s. Since these are metals, the head must be extremely thin to avoid losses due to eddy currents in the head. Therefore the head material is to be supported by non-magnetic bearers. The configuration used is a so-called sandwich head, in which an amorphous ribbon or a thin film is placed between two glass bearers (see Fig. 1.6(b)). The material is often lamellated to further reduce the eddy current losses. In both of these heads a multilayer thin film can be used to tune the optimal characteristics of the film. Fe/C multilayers are investigated for this purpose [29]. The C layers are introduced to keep the Fe crystallites small, which improves the soft magnetic properties.

d) Finally, multilayers may show a large magnetoresistance anisotropy $\frac{\Delta \rho}{\rho}$ which would make them ideal elements for the detection of magnetic fields [30]. Apart from this anisotropy, the film should be magnetically soft. At present, in the form of thin films, Ni-Fe-Co alloys show the largest anisotropy with $\frac{\Delta \rho}{\rho} \approx 3$ %, but permalloy films ($Ni_{79}Fe_{20}$) are used as thin film read heads in magnetic recording with an anisotropy of 1 %. The scattering of electrons at the interface between two materials can be spin-dependent, as it is for electrons scattered from the surface of materials [31]. Since the mean free path of electrons in metals at room temperature is of the order of 100 Å, there is a realistic possibility to have interface dominated electron scattering. Thus interface scattering can lead to a large magnetoresistance anisotropy. No decisive results have been reported so far, probably because of the dominating scattering from grain boundaries.

1.4 Non-magnetic multilayers

Multilayers are suitable samples for the investigation of physical properties which depend on characteristic lengths. The basic parameters in superconductivity, such as the coherence length, the penetration depth, the proximity effect and localization can be determined by the variation of the thickness of the layers [32]. In addition, changes in the electron-electron interaction, changes in the Cooper pair state and new materials or phases can influence the transition temperature [33].

Multilayers are also produced as X-ray [34] and neutron mirrors [35]. When deposited on curved surfaces, reflective X-ray optical elements can be made, which open the possibility of X-ray imaging.

The supermodulus effect was one of the first spectacular and intriguing properties of multilayer thin films. Young's modulus in Au/Ni, Cu/Pd, Ag/Pd and Cu/Au [36] multilayers appeared to be more than two times higher than in the corresponding alloy. Explanations have been searched for in the contact of the Fermi surface with extra band gaps in the electron band structure [37] and in the lattice deformation due to the lattice mismatch [38], but no definite explanation is yet available. On the other hand in Mo/Ni multilayers lattice softening is found [39].

Interdiffusion, amorphization and interfacial reactions are studied in multilayers because of the small length scale one can use. Especially in the case of the diffusion in metallic glasses multilayers open the possibility to use temperatures below the crystallization

temperature [40]. Diffusion coefficients as low as 10^{-26} m^2/s can be determined.

Effects on the electric conductivity are expected by the large number of interfaces in the film. Especially the behaviour at the interface of a ferromagnetic and a non-ferromagnetic material is not known [41]. Up to now, no interesting experimental results have been reported, probably because the scattering at grain boundaries, which are introduced during the growth, still dominates. The continuing progress in preparation techniques is necessary to exploit this fruitful area.

1.5 Scope of this thesis

In this thesis the results of an experimental study of some magnetic properties of multilayers are presented. In chapter 2 the growth of multilayers and the role of epitaxy will be discussed. Further, a description of the two preparation methods as used for this study is given. Chapter 3 discusses methods which have been used to characterize the multilayer thin films. This concerns both the crystalline structure and the composition profile which have been realized. In chapter 4 the magnetic measurements which have been performed, are described. Also the different methods are compared concerning their suitability and relevance for the study of magnetic multilayers. In chapter 5 the results for Pd/Co multilayers are presented along with some related subjects, such as the influence of the perpendicular

domain pattern on the magnetization curve and the contribution of the dipole-dipole interaction to the surface anisotropy.

Parts of chapter 3 and 5 have already been published or submitted for publication. We have chosen to embody the corresponding texts in this thesis in essentially the same form as they have been or will be published. As a consequence, some parts of these chapters may seem somewhat redundant for the reader of this thesis. On the other hand, this choice has the advantage that these parts can be read rather independently.

references

[1] "Synthetic Modulated Structures", Ed. L.L. Chang and B.C. Giessen, Academic Press, Orlando (1985)

[2] M.J. Klein and R.S. Smith, Phys. Rev. **81** (1951) 378

[3] H.K. Wong, H.Q. Yang, B.Y. Yin, Y.H. Shen, W.Z. Cao, J.B. Ketterson, and J.E. Hilliard, J. Appl. Phys. **55** (1984) 2494

[4] B.J. Thaler, J.B. Ketterson, and J.E. Hilliard, Phys. Rev. Lett. **41** (1978) 336

[5] L. Liebermann, J. Clinton, D.M. Edwards, and J. Mathon, Phys. Rev. Lett. **25** (1970) 232

[6] G. Bayreuther, J. Magn. Magn. Mater. **38** (1983) 273

[7] M.L. Néel, J. de Phys. et le Rad. **15** (1954) 225

[8] U. Gradmann, J. Magn. Magn. Mater. **54-57** (1986) 723

[9] J. Kwo, E.M. Gyorgy, D.B. McWhan, M. Hong, F.J. DiSalvo, C. Vettier, and J.E. Bower, Phys. Rev. Lett. **55** (1985) 1402
C.F. Majkrzak, J.W. Cable, J. Kwo, M. Hong, D.B. McWhan, Y. Yafet, J.V. Waszczak, and C. Vettier, Phys. Rev. Lett. **56** (1986) 2700

[10] S. Sinha, J. Cunningham, R. Du, M.B. Salamon, and C.P. Flynn, J. Magn. Magn. Mater. **54-57** (1986) 773
R.W. Erwin, J.J. Rhyne, M.B. Salamon, J. Borchers, S. Sinha, R. Du, J.E. Cunningham, and C.P. Flynn, Phys. Rev. B **35** (1987) 6808

[11] Y. Yafet, J. Kwo, M. Hong, C.F. Majkrzak, and T. O'Brien, J. Appl. Phys. **63** (1988) 3453

[12] L.L. Hinchey and D.L. Mills, J. Appl. Phys. **57** (1985) 3687

[13] P.Grünberg, J. Appl. Phys. **57** (1985) 3673

[14] P. Marcus and V.L. Moruzzi, J. Appl. Phys. **63** (1988) 4045

[15] R.W. Wood, Proc. IEEE **74** (1986) 1557

[16] M. Camras, "Magnetic Tape Recording", van Nostrand Reinhold, New York (1985)

[17] R.M. White, "Introduction to Magnetic Recording", IEEE-press, New York (1985)
"Magnetic Recording vol.I: Technology", Ed. C.D. Mee and E.D. Daniel, McGraw-Hill, New York (1987)

[18] J.K. Howard, J. Vac. Sci. Technol. A **4** (1986) 1

[19] S. Iwasaki and Y. Nakamura, IEEE Trans. Magn. MAG-**13** (1977) 1272
S. Iwasaki and K.Ouchi, IEEE Trans. Magn. MAG-**14** (1978) 849

[20] T. Wielinga, "Investigations on Perpendicular Magnetic Recording", PhD Thesis, Enschede (1983)

[21] I. Hatakeyama in "Recent Magnetics for Electronics", Ed. Y. Sakurai, Ohmsha and North-Holland, Amsterdam (1986)

[22] H.J.G. Draaisma, W.J.M. de Jonge, and F.J.A. den Broeder, J. Magn. Magn. Mater. **66** (1987) 351

[23] R.W. de Bie, S.B. Luitjens, V. Zieren, C.P.G. Schrauwen, and J.P.C. Bernards, IEEE Trans. Magn. MAG-**23** (1987) 2091

[24] M. Hartmann, B.A.J. Jacobs, and J.J.M. Braat, Philips Techn. Rev. **42** (1985) 37
M.H. Kryder, J. Appl. Phys. **57** (1985) 3913

[25] A.E. Berkowitz and W.H. Meiklejohn, IEEE Trans. Magn. MAG-**11** (1975) 996

[26] N. Sato, J. Appl. Phys. **59** (1986) 2514

[27] H. Feil and C. Haas, Phys. Rev. Lett. **58** (1987) 65

[28] C.W.M.P. Sillen, J.J.M. Ruigrok, A. Broese van Groenou, and U. Enz, IEEE Trans. Magn. MAG-**24** (1988) 1802

[29] T. Kobayashi, R. Nakatani, S. Ootomo, and N. Kumasaka, J. Appl. Phys. **63** (1988) 3203

[30] U. Dibbern, Sens. and Act. **10** (1986) 127

[31] J. Kirschner, "Polarized Electrons at Surfaces", Springer, Berlin (1985)

[32] K. Kanoda, H. Mazaki, N. Hosoito, and T. Shinjo, Phys. Rev. B **35** (1987) 8413

[33] S.T. Ruggiero, Superl. and Microstr. **1** (1985) 441

[34] T.W. Barbee, Jr., Optical Engineering **25** (1986) 898

[35] F. Mezei, NATO ASI on Physics, Fabrication and Applications of Multilayered Structures, Ile de Bendor 1987
A.M. Saxena and B.P. Schoenborn, Acta Cryst. A **33** (1977) 805

[36] W.M.C. Yang, T. Tsakalos, and J.E. Hilliard, J. Appl. Phys. **48** (1977) 876
G.E. Henein and J.E. Hilliard, J. Appl. Phys. **54** (1983) 728

[37] P.C. Clapp, in "Modulated Structure Materials", Ed. T. Tsakalakos, Martinus Nijhoff, Dordrecht (1983)

[38] A.F. Jankowski and T. Tsakalos, J. Appl. Phys. F **15** (1985) 1279

[39] M.R. Khan, C.S.L. Chun, G.P. Felcher, M. Grimsditch, A. Kueny, C.M. Falco, and I.K. Schuller, Phys. Rev. B **27** (1983) 7186

[40] F. Spaepen, NATO ASI on Physics, Fabrication and Applications of Multilayered Structures, Ile de Bendor 1987

[41] P.C. van Son, H. van Kempen, and P. Wyder, Phys. Rev. Lett. **58** (1987) 2271

Chapter 2 PREPARATION AND GROWTH

The deposition of multilayers proceeds analogous to the deposition of a homogeneous thin film exept for the composition modulation control. In this chapter we will consider some elements of the growth of thin films which are relevant to the preparation of multilayers and give an overview of epitaxial relations which may occur between metallic elements. Furthermore we will describe the additional features which are used to deposit multilayers. Finally we give a description of the preparation facilities employed in this study.

2.1 Growth of thin films

On a microscopic scale usually four steps in the growth of a thin film are discerned: 1) nucleation, 2) outgrowth of the nuclei into islands, 3) coalescence of the islands and 4) filling of the channels [1]. The way these stages are completed depends on the growth mechanism involved. Three major growth mechanisms are distinguished: 1) In the Frank-van der Merwe (FvdM) mechanism atomic layers grow layer-by-layer, so the four stages are completed before a new atomic layer nucleates. 2) In the Volmer-Weber mechanism (VW) islands grow without

a complete coverage of the substrate. 3) In the Stranski-Krastanov (SK) mechanism first one or more atomic layers are formed, but then islands grow without covering the full film. These mechanisms are sketched in Fig. 2.1. The occurrence of these mechanisms depends on the materials involved, the temperature and crystallographic orientation of the substrate, the deposition rate, the kinetic energy of the incoming particles, the bombardment of the substrate by other particles etc.

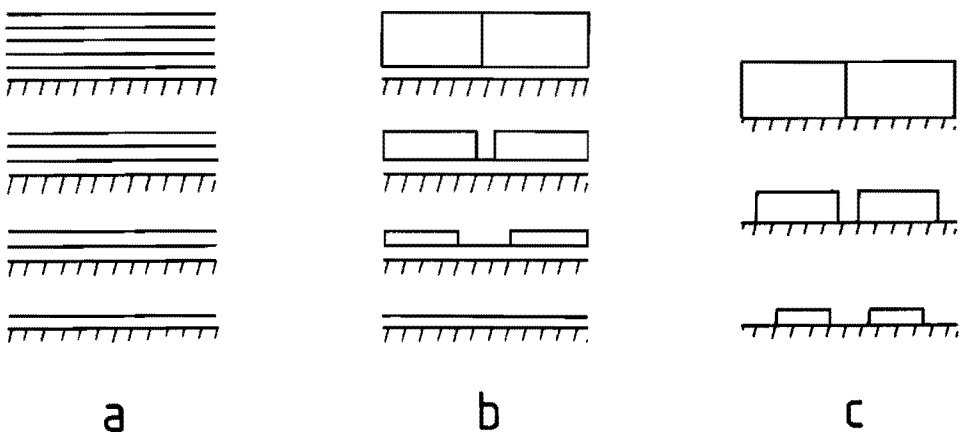

Fig. 2.1 *Schematic illustration of the three growth mechanisms indicated in the text:* a) *Frank-van der Merwe*, b) *Volmer-Weber and* c) *Stranski-Krastanov*.

In classical models of thin film growth a dominant role is played by the surface and interfacial energies [2], of which values have been given by Miedema [3] and Miedema and Den Broeder [4]. However, there is still discussion in the literature about the correlation of the growth mode with the thermodynamic properties of the materials [5].

The temperature of the substrate is important for the amount of

surface- and interdiffusion that may occur. At higher temperatures more diffusion leads leads to larger crystallites [6], but the inter-diffusion leads to smoother transitions from one layer into the other.

To make a multilayer of materials A and B the FvdM mechanism for the growth of A on B and for B on A is preferred. It must be realized however, that the thermodynamically stable growth mode will not set in at low temperature and high deposition rate. In that case, kinetically determined localized condensation of the incident atoms may result in a metastable layered structure.

2.2 Crystallographic orientation of the layers

Depending on the deposition rate, the temperature and other deposition parameters, the average size of the crystallites, or grain size, varies from only a few atoms to as large as the substrate. In the lower limit the layer is no longer crystalline, but amorphous, while in the upper limit we speak of a single crystal film. The orientation of the crystallites in the layer relative to the film plane can be a) epitaxial, b) textured and c) random. In Fig. 2.2 the difference between these types is indicated for a layer in which the crystallites are cubic.

The deposition of multilayers mostly starts with a base layer on the substrate. In this study we used glass (D263) and oxidized silicon substrates, which have an amorphous surface structure. A crystalline base layer on these substrates has a texture corresponding to its crystal structure. In the case of a face centered cubic (fcc) material

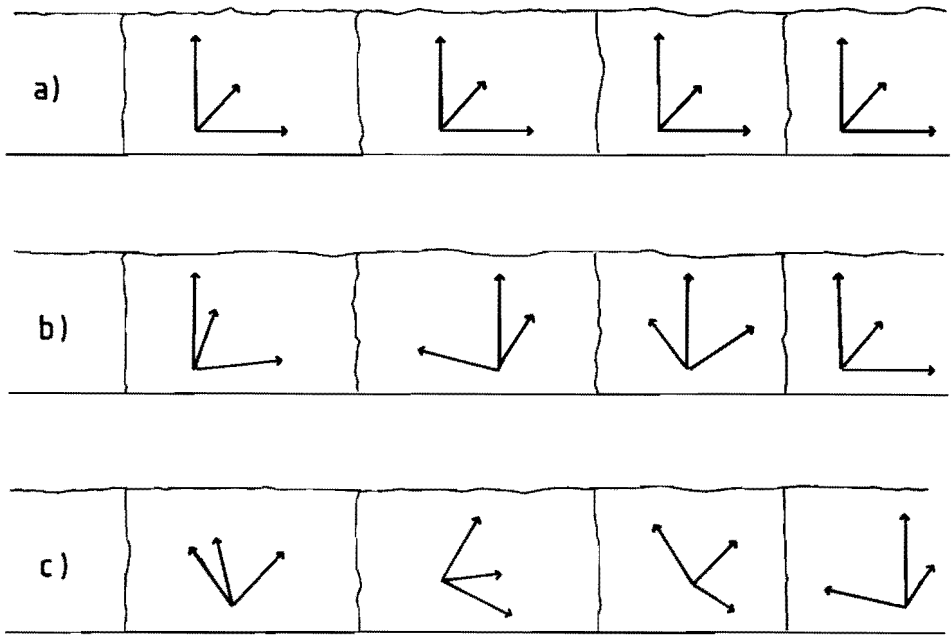

Fig. 2.2 *Orientation of some cubic crystallites in a deposited layer:* a) *epitaxial*, b) *textured and* c) *random*.

such as Pd the preferred axis perpendicular to the film plane is the [111] direction. In the case of a body centered cubic (bcc) material as Fe, this is the [110] direction. In both cases the closest packed planes of the crystal structure are parallel to the surface of the film.

When another material is deposited onto these crystallites, three types of epitaxial growth may occur: 1) strained layer growth, 2) pseudomorphic growth and 3) fixed relative orientation growth.

1) Strained layer growth occurs when there is a small lattice mismatch between the similar crystal structures of the different materials. An expansion in the plane of the layer is accompanied by a contraction

perpendicular to it and vice versa. This type is theoretically predicted by van der Merwe up to a certain layer thickness of a few atomic layers [7]. Above this critical thickness dislocations will relax the strain. Bean et al. have found this type of growth in the case of Ge-Si on Si [8].

2) Pseudomorhic growth means that the crystal structure of the material at the surface is transferred to the deposited layer. This is the case for Fe deposited on Cu (111) and on Cu(100). Fe does not adopt the bcc structure, but the fcc structure up to a certain thickness [9].

3) Fixed relative orientation growth takes place when the structures of successive layers have preferred orientations relative to each other. Various combinations of surface structures are treated theoretically by Bauer et al. [10].

2.3 Preparation of multilayers

In order to control the composition of the particle flux arriving at the surface of the film, three different methods are used: The first method is to rotate the substrate above the different sources. This is done both with electron beam evaporation sources [11] and sputter sources [12]. Also a continuously rotating shutter, which opens and closes the direct path from the source to the substrate, has been used [13]. A disadvantage of this method is that to change the relative thicknesses of the layers, the sputter or evaporation rates of the sources has to be changed. Alternatively one can keep the rate

of the sources at a constant level and use shutters to interrupt the particle flux at preset times and/or rotate the substrate away from the source. For evaporation sources the rate can be kept at a constant level by regulating the power of the electron beam coupled to the rate measurement of a quartz crystal sensor [14]. For sputtering sources a fairly constant rate can be ensured by keeping the power, that is put into the plasma, constant [15]. Finally, a third way to control the particle flux way is to use a feedback system, based on flux measurement by a mass spectrometer, which can be employed to obtain a continuous rate and/or thickness control [16].

The range of evaporation rates which can be controlled is different for the various methods. Combined with the different vacuum conditions, the properties of the multilayers prepared in the various ways do not have to be the same. A detailed comparison between the methods has not yet been made.

2.4 The electron beam evaporation apparatus

The electron beam evaporation apparatus consists of a vacuum vessel which can be heated to a temperature of 250 ^{o}C, so that a base pressure of 10^{-10} Torr can be obtained. This is caused primarily by H_2O desorption from the inner walls. Three electron guns with a maximum power of 6 kW are mounted in the side wall, aiming the electrons at an angle of 90 deg. into water-cooled copper crucibles. In Fig. 2.3 the position of one of the crucibles relative to the revolving substrate holder and

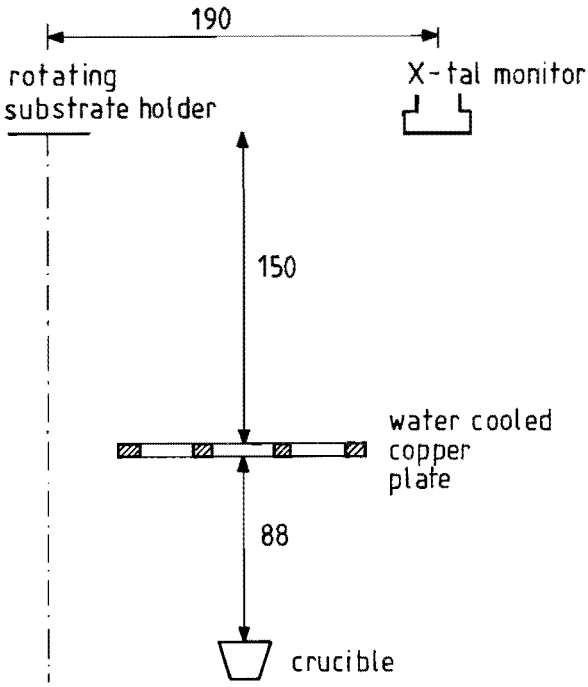

Fig. 2.3 *Relative position of a crucible in the electron beam evaporation apparatus to the rotating substrate holder and the crystal monitor.*

one of the crystal monitors is shown. These monitors are resonating quartz crystals whose resonance frequency is dependent on the mass of the deposited film. They are connected to the rate controllers IC6000 (Inficon) which control the power of the electron guns to obtain the wanted evaporation rate. Above the crucibles water-cooled copper plates are mounted in a configuration as shown in Fig. 2.4, to keep the vapour in a limited space. In each plate three holes give way to the vapour stream. A3, B3 and C3 are intended to let the vapour reach the crystal monitors. Above A2, B2 and C2 mirrors are mounted to ob-

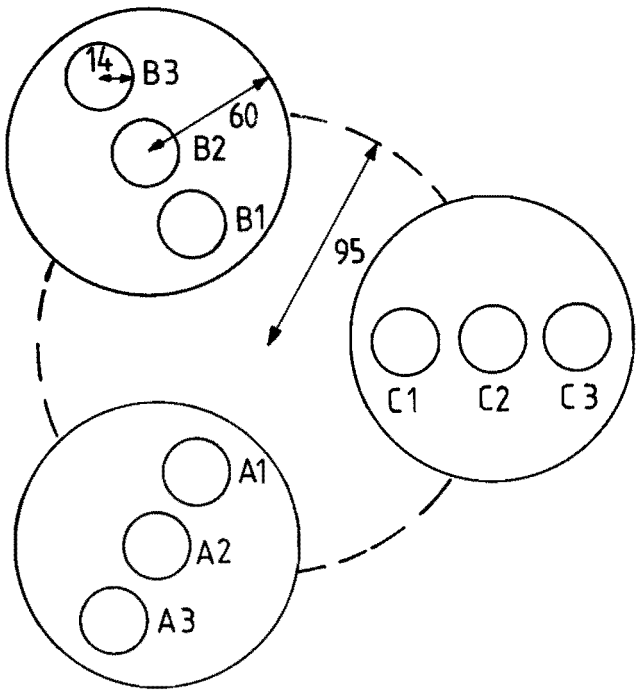

Fig. 2.4 *Orientation of the three water-cooled copper plates above the crucibles. The purpose of the holes is explained in the text.*

serve the electron spot in the crucible. The holes A1, B1 and C1 can be opened and closed seperately by shutters to alternate the composition of the vapour. The revolving substrate holder has a diameter of 36 mm and can be heated up to 800 ^{o}C during deposition.

We operated this apparatus by setting the evaporation rate to a certain value, mostly 1 Å/s, and controlling the layer thicknesses by opening and closing the shutters at given times. This was automated with an Apple IIe computer. We used no delay time between the deposition of the individual layers of the different materials.

The glass substrates were etched in a mixture of H_2O_2 and H_2SO_4 and

rinsed in H_2O with C_2H_5OH, according to a standard procedure. Inside the vacuum vessel no further cleaning was applied.

A multilayer is typified by the individual layer thicknesses and the number of times these layers are repeated. In fact, not the thickness but the mass of the deposited material is controlled and the thickness is calculated via the bulk density. It has to be kept in mind that the density of the material in the multilayer may be different, e.g. when the layer is strained.

A check of the average accuracy of the deposition rate can be made by chemically analyzing the composition of the multilayer. In Table 2.1 some typical results of Pd/Co multilayers are given. The measured amount of Co agrees very well with the intended amount, but the amount of Pd is in general somewhat higher.

Table 2.1 *Comparison between the nominal amount (m_o) and measured amount (m) of Pd and Co in Pd/Co multilayers prepared by evaporation. The masses are given in μg. In the last column the total mass ($m_{tot.}$) of the film as measured from the weight gain of the substrate plus film is given.*

sample	m_o(Pd)	m(Pd)	m_o(Co)	m(Co)	$m_{tot.}$
200ÅPd+34*(10.3ÅCo+45ÅPd)	99.8	111	15.0	15.3	125.8
200ÅPd+300*(2ÅCo+4.5ÅPd)	89.4	120	25.6	26	151.1
200ÅPd+150*(4ÅCo + 9ÅPd)	89.4	90	25.6	27	113.9
200ÅPd+150*(2ÅCo+13.5ÅPd)	128.4	166	12.8	12.9	184.1

2.5 The ion beam sputtering apparatus

In a sputtering apparatus the plasma generation and the film deposition usually take place in the same vacuum chamber. In an ion beam sputtering system these two processes are separated: The ions are extracted from a plasma chamber and are accelerated to a target from which material is sputtered. This material is deposited on substrates opposite to the target. In our ion beam sputtering apparatus the target, with a diameter of 10 cm, consisted of two halves of different materials. The Ar^+ ions were accelerated with 1.5 kV and deflected electrostatically (± 125 V) to the two targets periodically in order to deposit layers of the two materials. The thickness of the layers was controlled by the measurement of the amount of charge collected on the target. The Ar pressure in the deposition chamber during deposition was $2 \cdot 10^{-5}$ Torr and the distance between target and substrate 8 cm which meant that the sputtered atoms were not "thermalized" [17], because at this pressure the mean free path in the chamber is about 2 m. The substrate holder could be heated up to 300 ^{o}C. The maximum deposition rate was about 0.5 Å/s. For a more detailed description we refer to Smits [18].

It was found that in this apparatus the divergence of the Ar^+ beam was too large to obtain a complete separation of the deposited materials. Approximately 10 - 25 % of the beam current hit the wrong target with the result that the individual layers were composed of both materials, each with its own concentration. This problem can be avoided if the targets are mounted on a rotating assembly [19].

references

[1] L. Eckertová, "Physics of Thin Films", Plenum Press, New York (1977)
K.L. Chopra, "Thin Film Phenomena", McGraw-Hill, New York (1969)
L.I. Maissel and R. Glang, "Handbook of Thin Film Technology", McGraw-Hill, New York (1970)

[2] R.W. Vook, Int. Met. Rev. **27** (1982) 209

[3] A.R. Miedema, Z. Metallkunde **69** (1978) 287

[4] A.R. Miedema and F.J.A. den Broeder, Z. Metallkunde **70** (1979) 14

[5] F.C.M.J.M. van Delft, A.D. van Langeveld, and B.E. Nieuwenhuys, Thin Solid Films **123** (1985) 333

[6] C.R.M. Grovenor, H.T.G. Hentzell, and D.A. Smith, Acta Metall. **32** (1984) 773

[7] F.C. Frank and J.H. van der Merwe, Proc. Roy. Soc. A **198** (1949) 205

[8] J.C. Bean, L.C. Feldman, A.T. Fiory, S. Nakahara, and I.K. Robinson, J. Vac. Sci. Technol. A **2** (1984) 436

[9] U. Gradmann and P. Tillmanns, Phys. Stat. Sol. (a) **44** (1977) 539
S.A. Chambers, T.J. Wagener, and J.H. Weaver, Phys. Rev. B **36** (1987) 8992

[10] E. Bauer and J.H. van der Merwe, Phys. Rev. B **33** (1986) 3657

[11] H.K. Wong, H.Q. Yang, B.Y. Yin ,Y.H. Shen, W.Z. Cao, J.B. Ketterson, and J.E. Hilliard, J. Appl. Phys. **55** (1984) 2494

[12] P.F. Carcia and A. Suna, J. Appl. Phys. **54** (1983) 2000

[13] H.E. Cook and J.E. Hilliard, J. Appl. Phys. **40** (1969) 2191

[14] J.Q. Zheng, J.B. Ketterson, C.M. Falco, and I.K. Schuller, J. Appl. Phys. **53** (1982) 3150

[15] Y. Togami, T. Morishita, and K. Tsushima, Jap. J. Appl. Phys. **26** (1987) 635

[16] W. Sevenhans, J.-P. Locquet, and Y. Bruynseraede, Rev. Sci. Instrum. **57** (1986) 937

[17] K. Meyer, I.K. Schuller, and C.M. Falco, J. Appl. Phys. **52** (1981) 5803

[18] J.W. Smits, J. Vac. Sci. Technol. **19** (1981) 704

[19] F. Spaepen, A.L. Greer, K.F. Kelton, and J.L. Bell, Rev. Sci. Instrum. **56** (1985) 1340

Chapter 3 CHARACTERIZATION

After deposition of the multilayer several techniques can be applied to analyze the crystallographic structure and the composition profile along the normal to the film. In this chapter we will discuss some of these techniques and report on the results for the multilayers which are studied in this thesis.

3.1 X-ray diffraction from incommensurable artificial superlattices

Introduction

X-ray diffraction is often used as a primary routine probe to determine the structural properties of compositionally modulated thin films and multilayers in a non-destructive way. The usual technique employs the ϑ-2ϑ scan with the scattering vector perpendicular to the plane of the film. Mostly Cu Kα radiation (λ = 1.542 Å) is applied and the diffracted intensity is recorded conventionally as a function of the angle 2ϑ [1].

At low angles ($2\vartheta \approx$ 0-12 deg.) intensity peaks in the diffractogram appear which are caused by the periodic variation of the scattering factor [1,2]. The repeating distance of this variation is the modula-

tion length. At high angles intensity peaks are the result of diffraction from a crystalline lattice with periodically varying lattice constant and/or scattering factor. In the literature these are commonly referred to as "satellites" around the "main peak" originating from the "average lattice" (see e.g. McWhan [3]).

For the interpretation of the experimental diffractograms three different descriptions of the diffraction process are used. The optical theory neglects the atomic nature of matter and replaces the scattering factor of the atoms by the refractive index. This theory can only describe the low-angle peaks [4]. In the kinematical theory the amplitude and phase of the diffracted wave is calculated by summation of the amplitudes and phases of waves from the individual scattering centres. No account is given of extinction as is done in the dynamical theory for diffraction. A comparison between these theories for diffraction from superlattices is given by Bartels [5]. For polycrystalline metallic multilayers, with usually small crystallites, the kinematical theory is most suitable.

The structural properties one likes to determine from X-ray diffraction are the modulation length, the distances between the lattice planes, the composition of each plane, the texture of the crystallites, the coherence length, etc. Several models have been proposed to interpret the diffractograms, ranging from an idealized structure model, which gives a qualitative agreement with the experimental diffractogram [6,7] to computer simulations in which diffuseness at the interfaces, grain size and fluctuations in the layer thicknesses are investigated [8,9]. It is noted that several combinations of parame-

ters result in the same calculated diffractogram. McWhan [10] suggests to use different wavelengths e.g. from synchroton radiation, to discriminate between these combinations by the wavelength dependence of the scattering factor.

An important qualitative distinction can be made between multilayers consisting of two amorphous materials, one amorphous and one crystalline material, and two crystalline materials. In the case of two amorphous materials only low-angle diffraction peaks occur, whereas in the case of two crystalline materials also high-angle peaks can be expected. When the multilayer consists of one amorphous and one crystalline material, there is in principle nothing that prevents the occurrence of high-angle peaks. Sevenhans et al. [11] showed however, that the cumulative disorder that originates from fluctuations in the thickness of the amophous layers, results in the disappearance of the reflections other than from the pure crystalline layer.

The problem of commensurability is not often addressed in papers on artificially modulated structures. In general, in preparing crystalline multilayers by e.g. sputtering or vapour deposition, the individual layers do not consist of an integral number of atomic layers. Thus when an average thickness t_A of material A is reached, material B is deposited on a non-finished atomic layer of A etc. This means that, in general, the multilayer period D does not consist of an integer number of atomic layers A and B, or, in other words, that the periodicity is incommensurable with the average underlying lattice. In diffractograms the order numbers of the peaks are counted relatively to a central peak (indicated by ...,-2,-1,0,+1,+2,...) without giving significance to the commensurability of the layers.

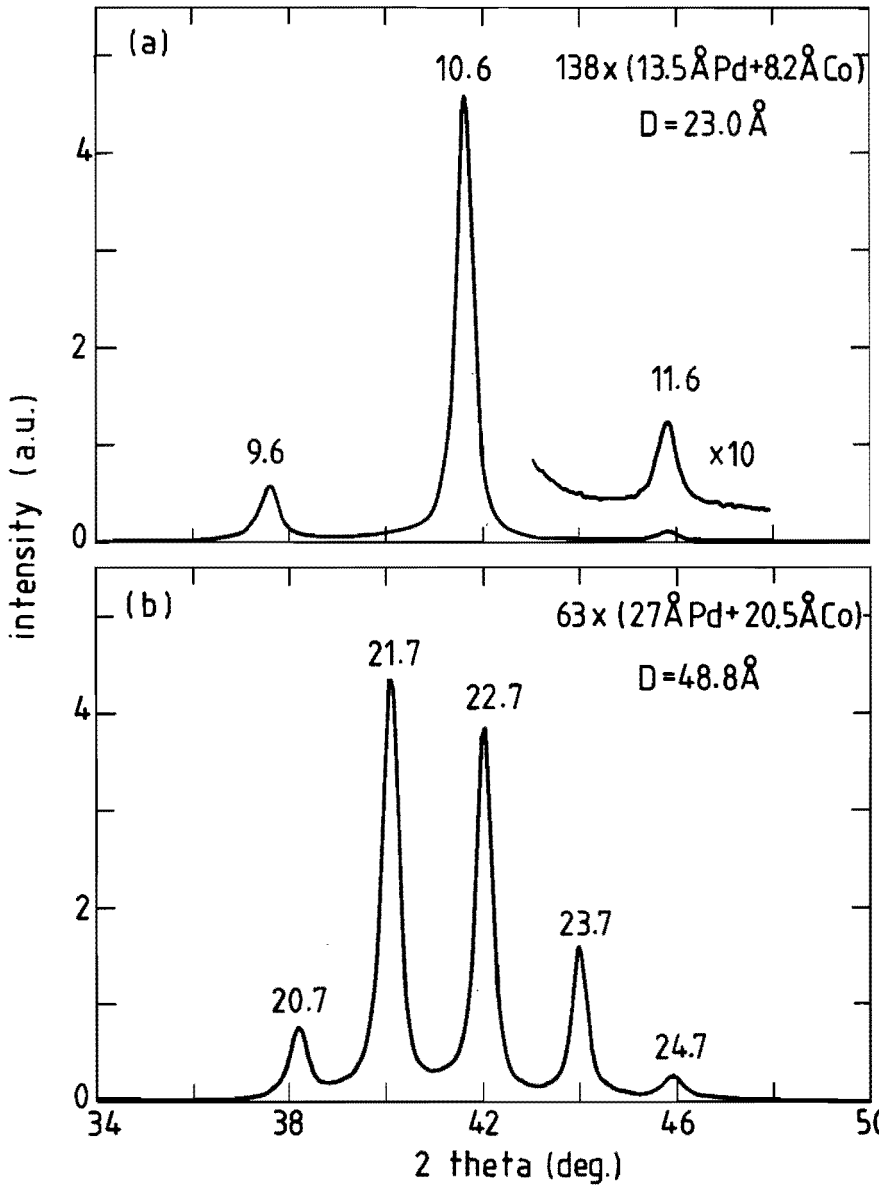

Fig. 3.1 *Experimental diffractograms of Pd/Co multilayers with layer thicknesses as indicated in the figures. The modulation length D is determined as the least square fit of the peak positions to relation* (1).

In this section we show how incommensurability affects the diffraction pattern. We will concentrate on the positions of the reflections, rather than on their intensities or linewidths, because these are strongly influenced by the texture of the crystallites in the sample. The results will be compared with experimental diffractograms of Pd/Co multilayers.

Experiments

The Pd/Co multilayers were produced by electron beam evaporation in ultra-high vacuum onto substrates of silicon and glass at 20 ^{o}C (see section 2.4). The deposition rate was 1 Å/s, as monitored by quartz oscillators, and shutters were used to alternate the constituents. The diffractograms are measured in a standard powder diffractometer (Philips PW1380) using the ϑ-2ϑ mode with Cu Kα radiation (λ = 1.542 Å). The film is oriented in such a way that the scattering vector is perpendicular to the film plane. Two characteristic diffractograms are given in Fig. 3.1. The individual layer thicknesses as set before the deposition and the number of times the bilayers are repeated are indicated in the figure. The diffraction peaks appear in the vicinity of the $(111)_{fcc}$ reflection of Pd and the $(00.2)_{hcp}$ reflection of Co. Therefore the multilayers have a fibre texture in which $(111)_{fcc}$ Pd layers alternate with $(00.2)_{hcp}$ or $(111)_{fcc}$ Co layers. It turns out that the observed diffraction peaks can be labelled according to the relation

$$2\,D\,\sin(\vartheta(x)) = x\,\lambda\ , \qquad (1)$$

in which the labels x of subsequent peaks differ by 1. In this way the modulation length D can be calculated from

$$D = \frac{\lambda}{2(\sin(\vartheta(x+1)) - \sin(\vartheta(x)))} \qquad (2)$$

Actually, the modulation lengths D indicated in Fig. 3.1(a) and (b) are calculated from a least square fit of the linear relation (1) using all the diffraction peaks in the figures. In this way both D and an absolute label x for each peak are obtained. In the following we will discuss the meaning of these labels. At low angles reflections are found which also obey relation (1), but for these the labels are integers. In this angle range corrections for non-ideal alignment of the sample and/or refraction [12] may be necessary.

Kinematical description

A description of the kinematical theory for multilayers has been given many times [3,5-10] and will not be repeated here. We present a structural model of a multilayer consisting of two crystalline materials. The diffractogram of this model is then calculated from the usual formulas of the kinematical description. The influence of different parameters in the model will be traced.

In our model a multilayer of the elements A and B consists of a total of N atomic layers on lattice planes parallel to the film plane. Each atomic layer contains an atomic concentration c of element A, yielding a concentration profile $c(i)$, $i=1,..,N$. Depending on c, a

thickness t_α is attributed to the atomic layer, e.g. following Végard's law:

$$t_\alpha(i) = c(i)\, d_A + (1-c(i))\, d_B \ , \tag{3}$$

and the distance d between two successive lattice planes is given by

$$d(i) = \frac{1}{2}\,(t_\alpha(i) + t_\alpha(i-1)) \ , \quad i=2,\ldots,N \ . \tag{4}$$

In the case that the materials A and B have the same lattice parameters in their pure state, t_a and d will be independent of i. Introducing a z-axis perpendicular to the film, the first lattice plane is located at $z=0$, and the following planes at

$$z(n) = \sum_{i=2}^{n} d(i) \ , \quad n=2,\ldots,N \ . \tag{5}$$

In a rectangular modulated film the concentration is described by

$$\begin{aligned} c(z) &= 1 \ , \quad 0 \le z < t_A \\ &= 0 \ , \quad t_A \le z < t_A + t_B \end{aligned} \tag{6}$$

and is further periodic in z with period $t_A + t_B$, t_A and t_B being the thicknesses of the individual layers A and B. In our model the concentration is not a continuous function of z, but only defined on discrete lattice planes, so that this description (6) is not complete. When t_A and/or t_B are not equal to the thickness of an integral number

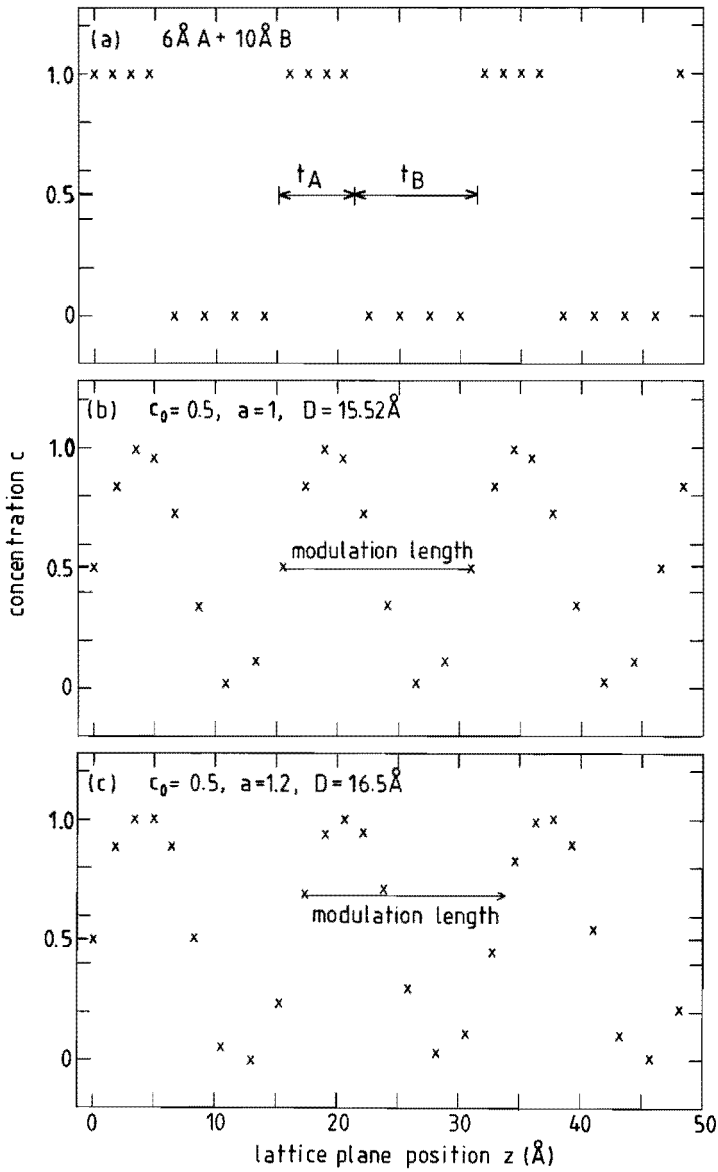

Fig. 3.2 *Examples of composition profiles in a multilayer. The crosses indicate the position and composition of an atomic layer.* (a) *rectangular, commensurable profile,* (b) *sinusoidal, commensurable profile and,* (c) *sinusoidal, incommensurable profile.*

of atomic layers, extra atomic layers are added with intermediate concentration. This concentration is not necessarily the same at each interface between the materials A and B.

Likewise the sinusoidal composition modulation is described by

$$c(i) = c_0 + \frac{1}{2}\, a\, \sin(2\pi\, \frac{z(i)}{D}) \qquad (7)$$

in which c_0 is the average composition, a is the (peak to peak) amplitude of the modulation and D the modulation length. When after one modulation length there is an atomic layer with exactly the same composition, the concentration profile is called commensurable (see Fig. 3.2).

To calculate the diffractogram of these structures we attribute to each atomic layer a scattering coefficient $f(i)$ using

$$f(i) = c(i)\, f_A + (1-c(i))\, f_B \qquad (8)$$

where f_A and f_B are the scattering coefficients of the individual elements including the Debye-Waller factor. These values are calculated for each scattering angle using a series expansion given in the International Tables [13]. The reflected intensity I as a function of the angle ϑ is calculated from

$$I(\vartheta) \sim L(\vartheta)\, \left| \sum_{n=1}^{N} f(n)\, \exp(4\pi i z(n) \frac{\sin(\vartheta)}{\lambda}) \right|^2 \qquad (9)$$

where $L(\vartheta)$ is the Lorentz factor.

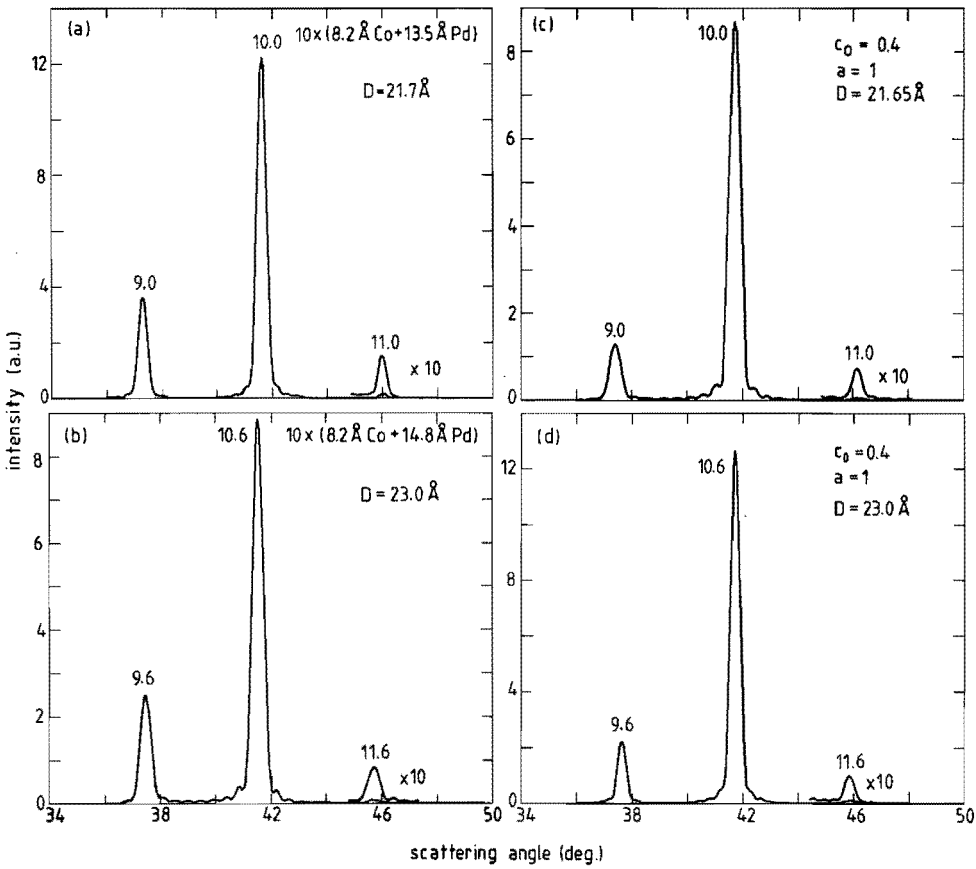

Fig. 3.3 *Calculated diffractograms for* (a) *a rectangular, commensurable* Pd/Co *superlattice;* (b) *a rectangular, incommensurable* Pd/Co *superlattice;* (c) *a sinusoidal, commensurable* Pd/Co *superlattice;* (d) *a sinusoidal, incommensurable* Pd/Co *superlatice.*

We have used this model to simulate diffractograms of Pd/Co multilayers. For the distances between the individual lattice planes we used for the Co layers the (00.2) lattice spacing of pure Co (d_{Co} = 2.05 Å) and for Pd the (111) lattice spacing of pure Pd (d_{Pd} = 2.25 Å). For atomic layers containing both elements we used a linearly interpolated value, in accordance with the lattice parameters for Pd-Co alloys [14]. In Fig. 3.3(a) the result of this calculation is shown for a multilayer consisting of 10 times 4 atomic layers Co (8.2 Å) and 6 atomic layers Pd (13.5 Å). The positions of the diffraction peaks are analyzed in the same way as for the experimental diffractograms. The fringes with low intensity result from the limited thickness of the crystal in the calculation. For this commensurable multilayer all labels of the peaks are integers. Though the calculated intensity profile resembles the experimental one in Fig. 3.1(a), the difference is clear from the labels of the peaks. From chemical analysis we know that the amount of Pd deposited in the multilayers is higher than it was meant to be. When the Pd thickness in our model is increased, we obtain extra atomic layers composed of both Pd and Co, and the multilayer becomes incommensurable. In Fig. 3.3(b) we show the diffractogram resulting for a Pd layer thickness of 14.8 Å, which is 6.6 atomic layers. The labels belonging to the peaks have now become non-integer and are identical to the experimental diffractogram in Fig. 3.1(a). It should be stressed here that this result in no way originates from the difference in lattice parameter between Co and Pd. Non-integer labels also occur for incommensurable multilayers with identical lattice parameters of the two constituents. To investigate the influence of

the composition of the individual atomic layers on the diffractogram, we have performed the same calculation for a sinusoidal profile. Fig. 3.3(c) shows that the intensities of the satellite reflections relative to the main reflection have somewhat decreased. Their positions and labels however, have not changed. The label of the main reflection x_o in a rectangular profile can be obtained from

$$x_o = \frac{t_A}{d_A} + \frac{t_B}{d_B} \quad . \tag{10}$$

which is similar to the observations of Window [15]. In (10) each term represents a (non-integer) number of atomic layers. In non-rectangular profiles x_o can be expressed as

$$x_o = \frac{D}{\bar{d}} \quad . \tag{11}$$

where $\bar{d}$ is introduced as the average distance between lattice planes in the multilayer [16].

If we perform the calculation of the intensity profile in the low-angle range for the same incommensurable concentration profile which leads to Fig. 3.3(b) at high angles, only integer diffraction peaks are obtained, as shown in Fig. 3.4. This can be expected since details of the crystalline structure play no role in this range. The transition between the integer labelled and non-integer labelled peaks takes place at intermediate angles. Experimentally the observed intensity in

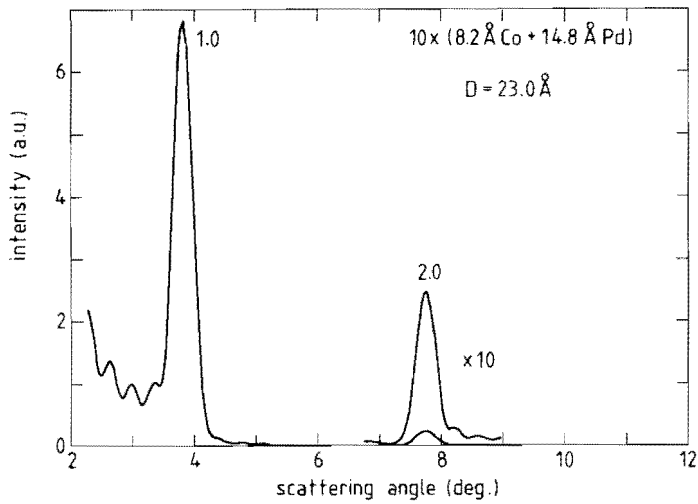

Fig. 3.4 *Low-angle diffractogram for the rectangular, incommensurable Pd/Co superlattice as used in* Fig. 3.3(b). *In contrast to that figure, reflections can be labelled with integers.*

this range is always low and no diffraction peaks are observed. In the calculated diffractogram we do observe peaks, although at a lower level of intensity relative to the low and high angle ranges. Fig. 3.5 shows this result for the Pd/Co concentration profile which was also used for Figs. 3.3(b) and 3.4. Two sets of peaks can be distinguished. The integer labelled peaks decrease in intensity with increasing angle, whereas the non-integer peaks increase in intensity.

Finally, also the diffractogram at higher scattering angles was investigated. Fig. 3.6 shows the results in the range where the (00.4) reflection of pure Co and the (222) reflection of pure Pd occur. Again relation (1) applies and some labels (x = 19.2, 21.2) are twice the labels in Fig. 3.3(b). Additional reflections occur (x = 20.2, 22.2)

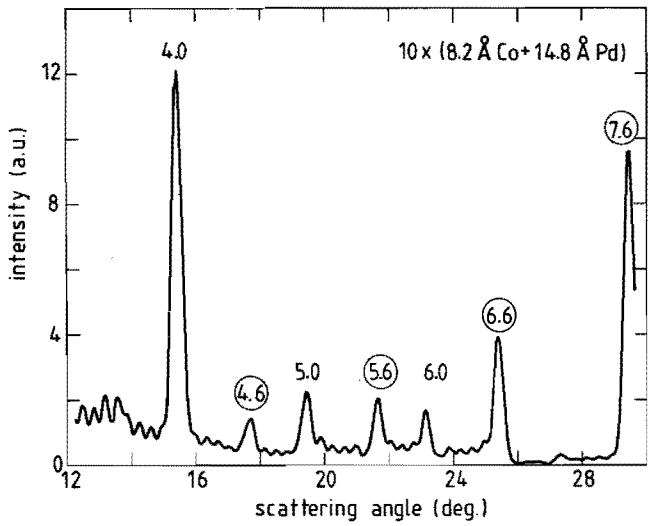

Fig. 3.5 *The transition between integer and non-integer labelled peaks takes place at angles intermediate between those of* Fig. 3.3(b) *and* Fig. 3.4.

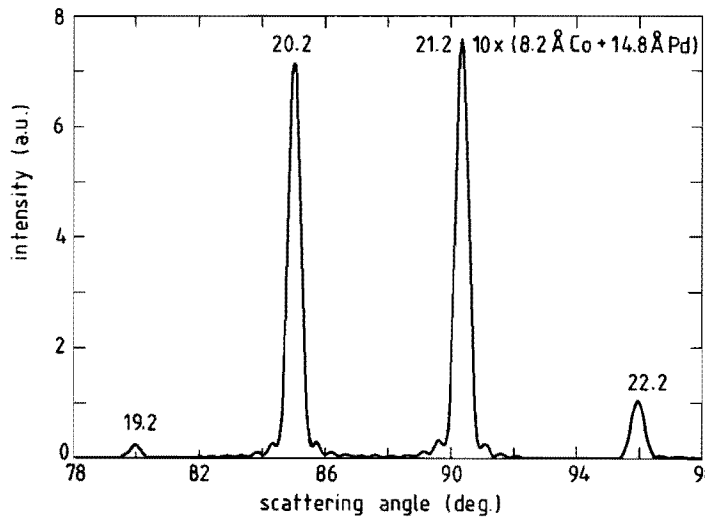

Fig. 3.6 *The diffractogram of the rectangular, incommensurable* Pd/Co *superlattice in the second order reflection range is similar to that in* Fig. 3.3(b) *and can be analyzed in the same way.*

which do not have this property. In-between this range and that of Fig. 3.3(b) the same phenomenon as shown in Fig. 3.5 takes place.

Experimentally it is reported that the intensity of the reflections in compositionally modulated films with lattice commensurable wavelengths is much higher than in films with incommensurable wavelengths [17]. This is contradicted by the theoretical description for nearly lattice-matched materials [18] and by the experiments on naturally modulated crystals. In these crystals, such as Na_2CO_3 [19], the modulation length is temperature-dependent and so-called lock-in transitions occur at which the modulation becomes commensurable with the underlying lattice. At these transitions no considerable change in diffracted intensity is observed [20,21]. In Fig. 3.7 the calculated results are shown of the dependence of the intensity of the reflec-

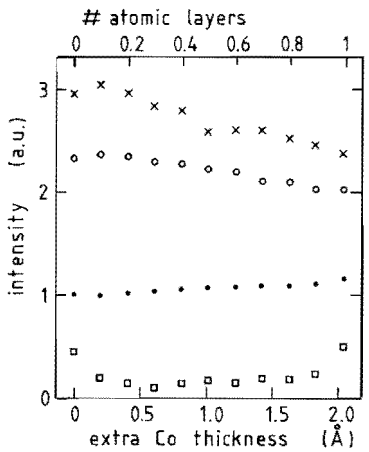

Fig. 3.7 *Intensities of the highest and second highest peaks for multilayers of* 4.5 Å Pd *and* 2.05 Å Co, *increasing up to* 4.1 Å Co (x,□) *and for multilayers of* 22.5 Å Pd *and* 10.25 Å Co, *increasing up to* 12.3 Å Co (○,●).

tions the commensurability of the multilayers in our model. Starting from a certain thickness of the Pd and Co layers, the Co layer thickness is increased in steps of 0.1 atomic layer (0.205 Å). In the figure the intensities of the highest and the next highest peak are indicated. Starting from 4.5 Å Pd (2 atomic layers) and 2.05 Å Co (1 atomic layer) we see that the intensity of the second highest reflection decreases by a factor of 3 as compared with the commensurable situation. When 22.5 Å Pd and 10.25 Å Co are taken no influence of the extra Co thickness on the intensity can be observed.

Conclusion

Incommensurability in artificial superlattices means that an atomic layer with a certain atomic composition is not exactly repeated after the modulation length, irrespective of the lattice mismatch or the composition profile. In a high-angle X-ray diffractogram this yields sets of diffraction peaks which can not be indexed with integers. Within a set of peaks the labels of subsequent peaks differ by 1, but between different sets this is not the case, as can be seen in Fig. 3.5. In our calculation the intensity of the diffraction peaks is not very much different for commensurable or incommensurable superlattices, though this depends on the total thickness of the layers. It is to be noted that in our model the concentration profile is mathematically described, which is not the case in the actual multilayers. Fluctuations in the parameters [11] or contributions from different crystallites [8,9] also add to the X-ray diffraction. Though they can be used to fit the diffractogram in great detail, they do not give

much insight into the mechanisms involved. Once a multilayer is grown, annealing may give diffusion at the interfaces, but the commensurability will remain.

3.2 Transmission electron microscopy

In contrast to XRD, transmission electron microscopy (TEM) can be used to obtain more local information about the structure, since the scattering of electrons is much stronger than of X-rays and electrons can be focussed. Here we will confine ourselves to some specific results of TEM on Pd/Co multilayers.

Specimens are prepared in two ways: 1) so that the incident electron beam is perpendicular to the film (plan-view TEM) and 2) so that the electron beam is parallel to the film (cross-sectional view TEM). In both cases the thickness of the material the electrons have to cross should match the energy of the electrons. In our microscope (Philips EM301) this is 300 keV, which means that about 500 Å metal films can be used. The preparation of the film as a specimen for the TEM is quite different in the two cases.

1) For plan-view TEM, a silicon substrate covered with Si_3N_4 is used. The silicon is locally etched away to make the substrate transparent for the electrons. Fig. 3.8 shows two examples of Pd/Co layers prepared by evaporation. The electron diffraction patterns show that 100 Å Co in-between layers Pd has its unstrained hcp or fcc lattice structure, whereas 8.2 Å Co can not be identified in this way. Note

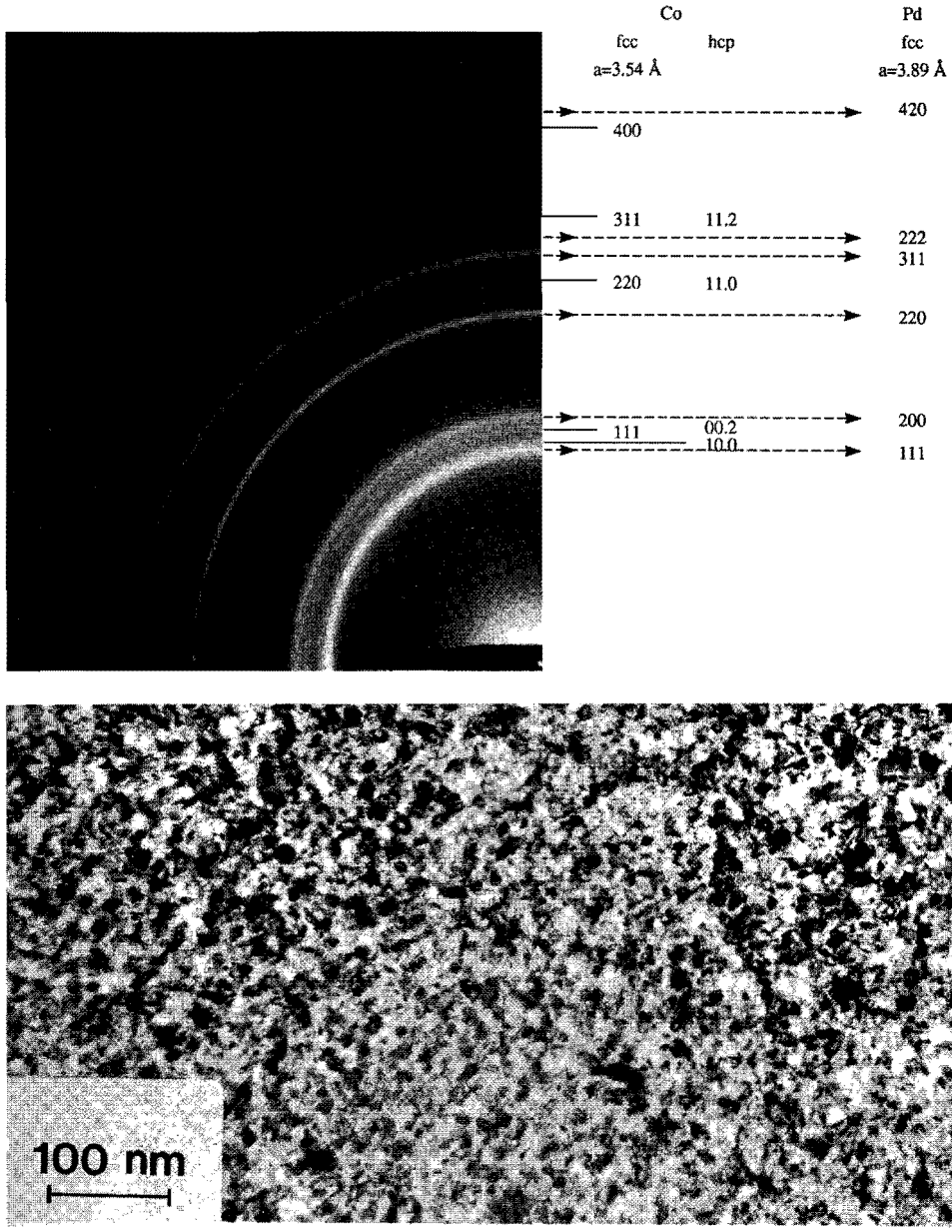

Fig. 3.8(a) *Electron diffraction pattern of a film of* 200 Å Pd + 2*(100 Å Co + 100 Å Pd), *prepared by evaporation on* Si_3N_4. *The diffraction rings are indexed with the lattice constants of the pure elements.* (b) *Bright field image of* (a).

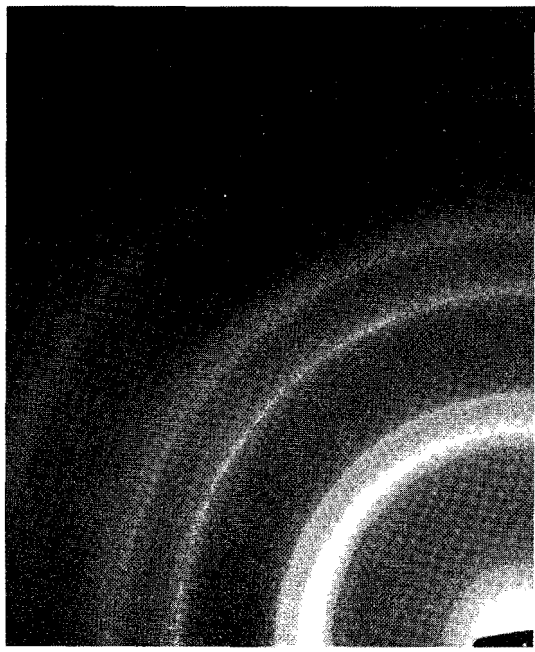

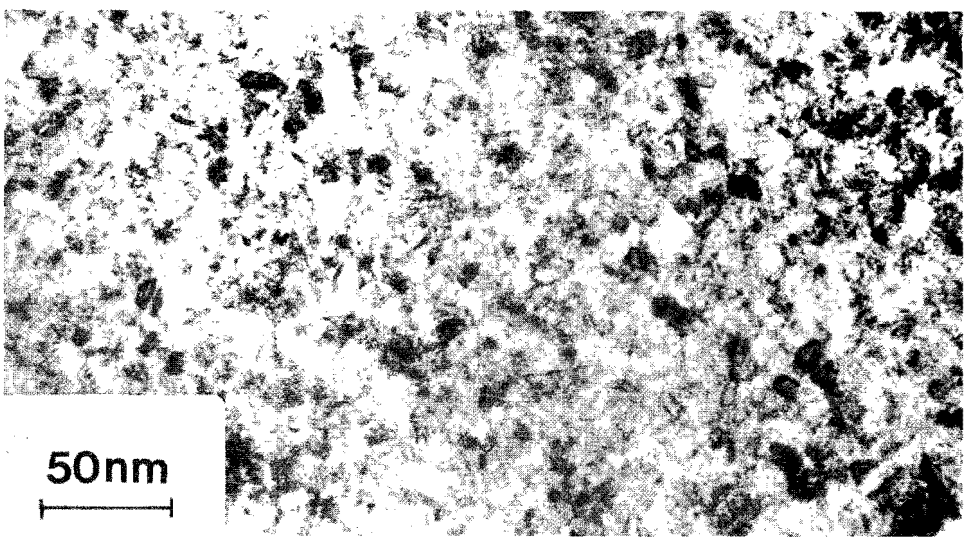

Fig. 3.8(c) *Electron diffraction pattern of a film of* 200 Å Pd + 20*(8 Å Co + 9 Å Pd), *prepared by evaporation on* Si_3N_4. *In this case the rings belonging to pure Co are not visible.* (d) *Bright field image of* (c).

that it is not possible to discern an fcc and an hcp lattice from each other when a large number of stacking faults occur. In both cases the bright field (BF) image shows that the grain size is about 200 Å.

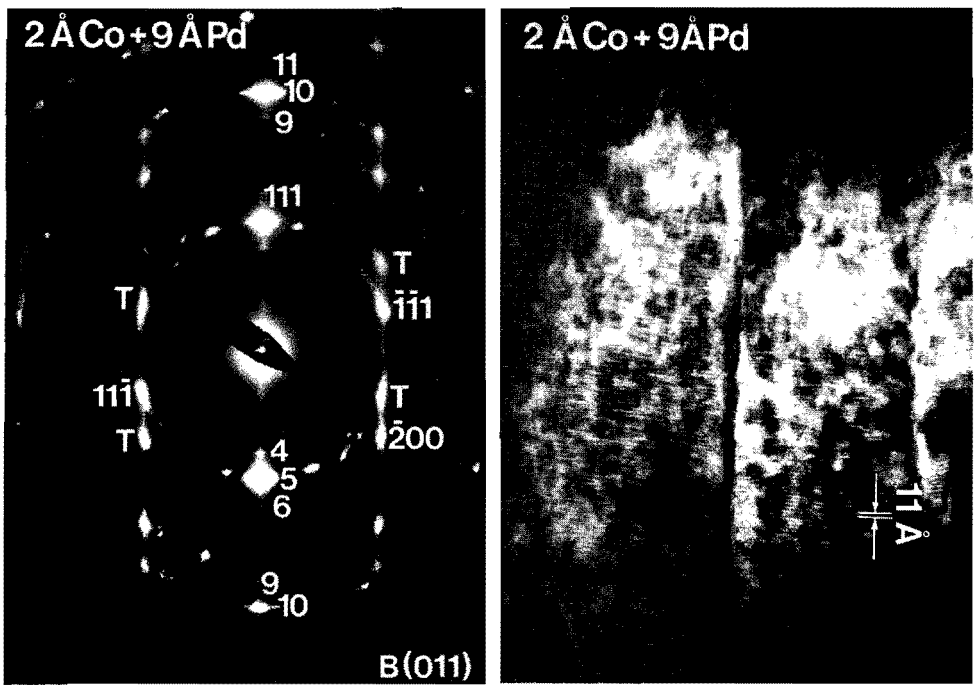

Fig. 3.9(a) *Electron diffraction pattern of a cross-section of the multilayer* 200 Å Pd + 270*(2 Å Co + 9 Å Pd) *prepered by evaporation on* Si. *In the* [111] *direction perpendicular to the film the modulation spots are visible. The other diffraction spots are indexed as originating from an fcc structure, which is heavily twinned* (T). (b) *Dark field image of the film corresponding to the diffractogram* (a).

2) For cross-sectional TEM, a cross-section through the sample of only 500 Å should be made. Two parts of the film are glued onto each other and embedded in an epoxy resin. With a diamond saw a slice is cut which is locally thinned by polishing and ion bombardment. The effect of these thinning techniques is still unclear. In Fig. 3.9 an example of a Pd/Co multilayer cross-section is shown. In the electron diffraction pattern the modulation peaks which are also visible in X-ray diffraction can be recognized. The other diffraction spots can be indexed as an fcc crystal which is heavily twinned. The dark field (DF) image in Fig. 3.9(b) shows that the multilayer containing 2 Å layers is still modulated. From the fact that even in this extreme case the modulation is still visible, we infer that the interfaces between Pd and Co are rather sharp. Also it shows the columnar morphology of the grains in the film.

3.3 Depth profiling with Auger electron spectroscopy

To analyse the composition of the multilayer along the axis normal to the film, surface analysis techniques combined with a surface removing tool can be used. A review of these depth profiling techniques has been given by Hofmann [22].

We have used Auger electron spectroscopy (AES) (PHI model 5500) while sputtering with an Ar^+ beam to probe the composition profile of several multilayers. In Fig. 3.10 a schematic drawing of this technique is given. Fig. 3.11 shows the characteristic dependence of the

atomic concentration as a function of the sputtering time, obtained for a sample consisting of 36*(40 Å Cu + 40 Å Fe). In this figure the peak to peak amplitude of dN/dE (N being the number of electrons with energy E) in a limited region is used to calculate the concentration. Similar profiles were obtained for Pd/Co and Au/Ni multilayers. The decrease of the amplitude of the modulation with time (or depth) can be caused by two effects:

(i) the sputtering process induces mixing of the top layer with deeper layers which causes a broadening of the interface. For this reason the

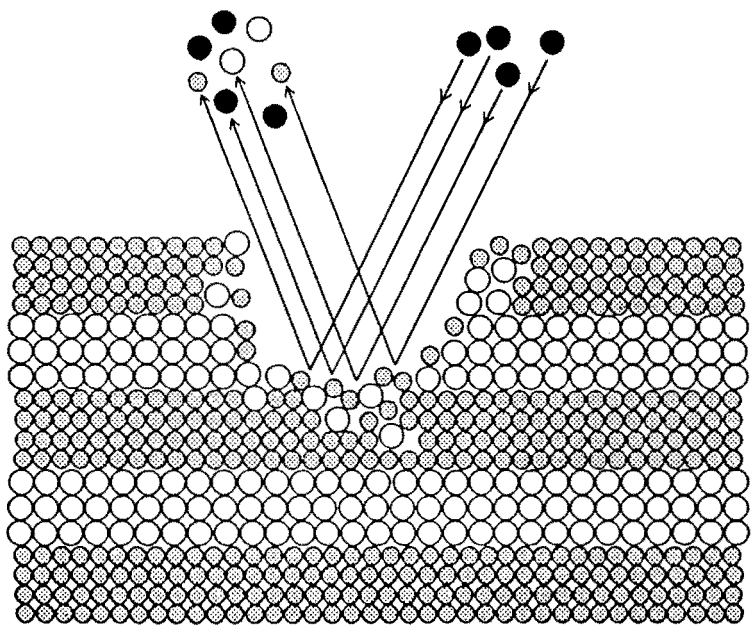

Fig. 3.10 *A schematic drawing of the sputtering proces in depth profiling. Indicated is the atomic mixing that occurs by this.*

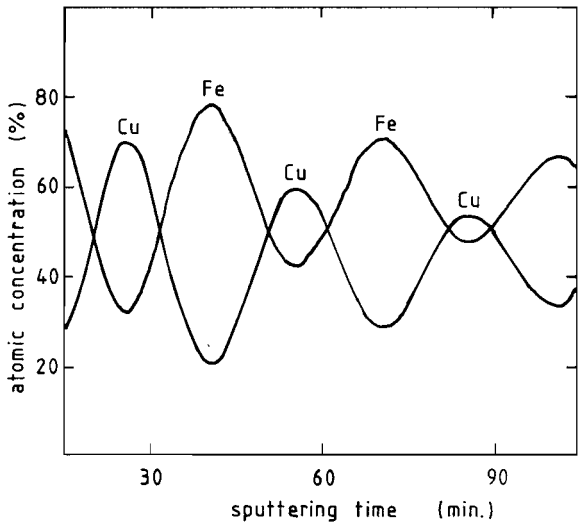

Fig. 3.11 *Amplitude of the Auger signals of* Fe (595 eV) *and* Cu (915 eV) *from a multilayer of* 200 Å Cu + 36*(40 Å Fe + 40 Å Cu) *evaporated on* Si, *expressed as atomic concentration, as function of sputter time.*

energy of the Ar^+ ions should be kept as low as possible. In our case it was 1 keV.

(ii) the statistical character of the sputtering process causes roughening of the surface which increases for deeper layers.

In addition there is of course a limited depth from which the Auger electrons originate, the so-called escape depth [23]. The electron beam (5 kV) had a diameter of 0.2 μm and was positioned in the centre of an area of 2 x 2 cm which was to be sputtered away by the rastered Ar^+ beam.

In the literature it was reported that for Co/Mn the amplitude of the modulation increases instead of decreases with depth [24]. From

that fact it was concluded that Co/Mn multilayers did not grow layer-by-layer but island like. In the combinations of metals we studied, we could only find indications for a good layered structure of all the samples.

After completion of the sputtering a crater is left in the multilayer. At the edges of the crater the different materials can be made visible by their difference in electron scattering coefficient. In Fig. 3.12 this is shown for a Au/Ni multilayer, in which 14 modulations are visible, corresponding to the number of peaks in the Auger signal. This contrast is made from the absorbed current [25] and was,

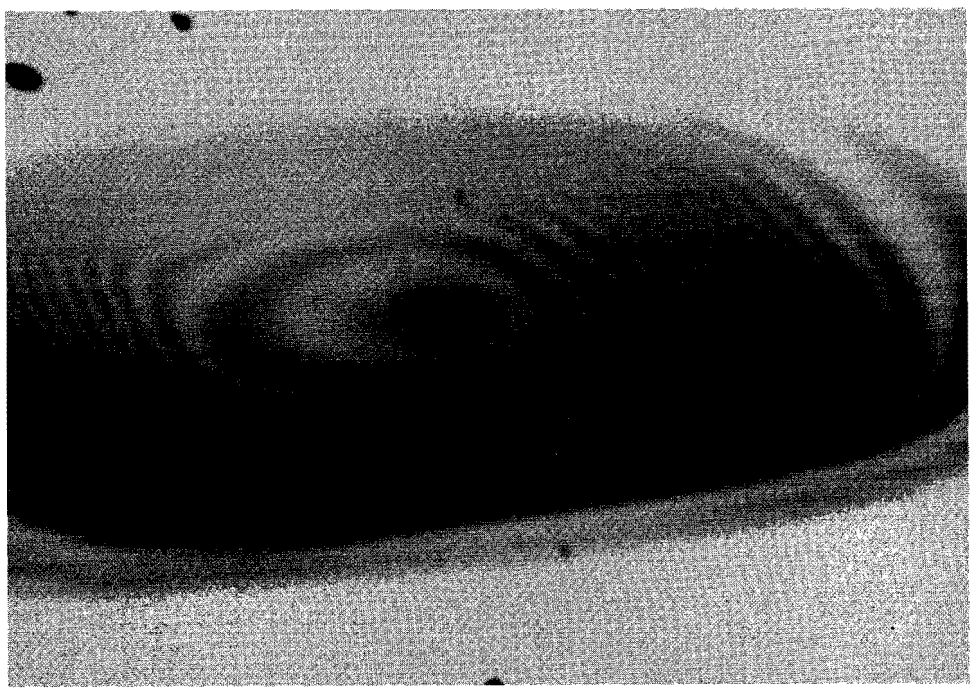

Fig. 3.12 *Absorbed current image from a crater in a multilayer of* 200 Å Au + 60*(25 Å Au + 25 Å Ni), *prepared by ion beam sputtering. The width of the crater is about* 2 cm.

in this case, optimal at a beam voltage of 1.5 kV. Notice the enormous magnification $1/\alpha$ (α is the crater angle) that is obtained. In Fig. 3.12 $\alpha \approx 7 \cdot 10^{-6}$, so that the magnification $1/\alpha \approx 1.4 \cdot 10^{5}$.

In these experiments we found little difference between samples prepared by evaporation and ion beam sputtering. The minimum layer thicknesses which could be detected were 20 Å Cu and 20 Å Fe.

Conclusion

Though Auger depth profiling does not provide a concentration profile on an atomic scale, the technique can be used to probe the modulation in a multilayer in which the individual layers are more than 20 Å. Further the in- or decrease of peak height with depth is an indication for the flatness of the individual layers. In the case of Cu/Fe, Pd/Co and Au/Ni multilayers evaporated and sputtered onto Si and glass substrates, we did not find an island structure.

3.4 Mössbauer study of Cu/Fe composition modulated thin films *)

Cu/Fe composition modulated thin films were prepared by an ion beam sputtering technique in which the modulation is brought about by deflecting the ion beam electrostatically to different targets . The

*) part of this text has been published in the
Journal of Magnetism and Magnetic Materials **51** (1985) 273

combination of Cu and Fe was thought to be interesting for the following reasons:

(i) Although the structure of Fe at room temperature is bcc, several reports claimed to have found that thin Fe layers deposited on Cu are fcc. There exists a considerable controversy about the magnetic ordening of fcc iron films: on one side ferromagnetism [26-29], on the other side antiferromagnetism and above 67 K paramagnetism [30-32].

(ii) Since Cu and Fe do not form solid solutions, chemically sharp interfaces are to be expected due to the absence of interdiffusion. On the other hand, mixing by the sputtering process might cause some diffuseness of the interface.

The Cu/Fe films were characterized by X-ray diffraction, transmission electron microscopy and Auger electron spectroscopy in combination with sputter depth profiling (cf. section 3.3). To study the composition of the interfaces ^{57}Fe conversion electron Mössbauer spectroscopy (CEMS) was applied, as has been done recently by several authors on Fe/Sb [33] and Fe/V multilayers [34].

Experiments

The ^{57}Fe conversion electron Mössbauer spectra were recorded with a conventional constant acceleration spectrometer using a 10 mCi ^{57}Co in Pd source. A proportional counter with a 4% CH_4 in He gas flow was used to detect the conversion electrons. Most of the conversion electrons originate from the outermost 0.2 μm of the sample. The spectrometer was calibrated with a standard α-Fe foil. All measurements were performed at room temperature.

Observed spectra

Fig. 3.13 shows the conversion electron Mössbauer spectra of four different samples (x Cu + y Fe) with $x = y = 40,20,10$ and 6 Å. These layers are repeated up to a total thickness of 0.25 μm. The spectrum for $x = 40$ Å closely resembles that of pure α-Fe with additional peaks. These latter peaks increase in relative intensity with decreasing x. All spectra can roughly be divided into three subspectra:

(i) One "basic" spectrum, resembling that of pure α-Fe. They are supposed to originate from Fe atoms in the middle of the Fe layers having no interaction with the Cu atoms.

(ii) Discrete shoulders at the flanks of the peaks in the basic spectrum. These shoulders indicate the presence of a number of discrete hyperfine fields with values lower than that of pure α-Fe.

(iii) A spectrum originating from Fe atoms which give a paramagnetic contribution, resulting in additional intensity around $v = 0$.

With decreasing x the latter two subspectra increase in intensity at the expense of the basic spectrum. It can be seen in Fig. 3.13 that the relative intensity of lines 2 and 5 changes with decreasing x. The relative intensities of the first three lines is given by $3 : 4\sin^2\vartheta/(1+\cos^2\vartheta) : 1$, in which ϑ is the angle between the direction of the magnetization and the direction of the γ-rays, which is perpendicular to the plane of the film. For $x = 40$ Å the relative intensities of the six lines are about 3 : 4 : 1 : 1 : 4 : 3, which indicates that the direction of the magnetization is parallel to the film plane. For $x = 6$ Å the relative intensity of lines 2 and 5 has decreased considerably, which indicates that the direction of the

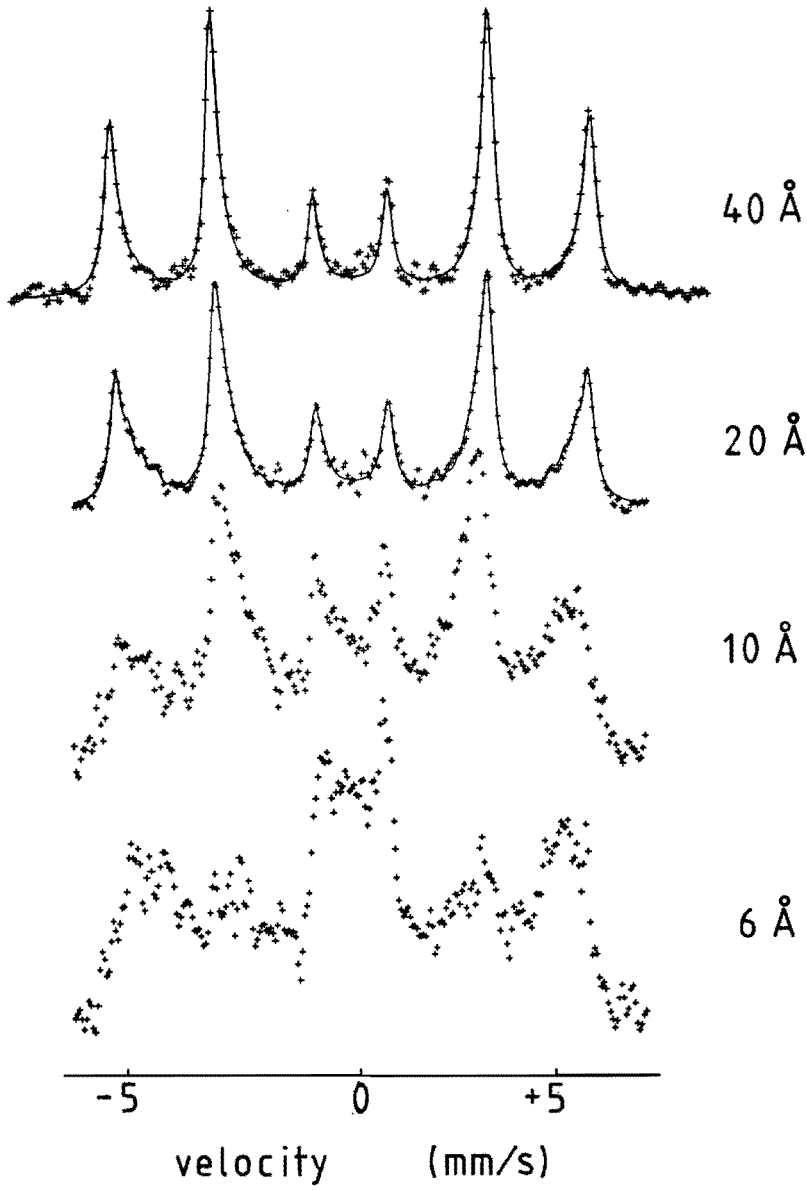

Fig. 3.13 *Conversion electron Mössbauer spectra measured at room temperature for the samples* (x Cu + y Fe) *with* $x = y$ = 40, 20, 10 *and* 6 Å. *For* 40 *and* 20 Å *the result of the calculation is indicated by the drawn line.*

magnetization has rotated away from in-plane to an angle of about (40 ± 10) deg. with the film plane.

Interface model

It is our aim to obtain information about the profile of the Cu/Fe interface from the Mössbauer spectra. This information might be contained in the reduction of the hyperfine field of the Fe atoms owing to the neighbouring Cu atoms. It is well established for iron-rich alloys that the hyperfine field of the Fe atoms can be described by

$$B_{hf} = B_{hf}(0) + n_1 B_1 + n_2 B_2 \qquad (10)$$

Here $B_{hf}(0)$ is the hyperfine field of pure iron, n_1 and n_2 are the number of impurity atoms as nearest neighbour and next nearest neighbour, respectively, and B_1 and B_2 are the corresponding contributions to the hyperfine field. The isomer shift can be expressed in a similar way using IS_1. For a large number of different impurity atoms the values of B_1, B_2 and IS_1 are known [36,37]. However the literature on copper in iron is limited. Cranshaw obtained the following values: B_1 = -1.0 T, B_2 = -0.2 T and IS_1 = 0.015 mm/s [38]. Lauer et al. investigated metastable bcc Fe-Cu alloys produced by simultaneous vapour deposition of Fe and Cu and measured B_1 = -1.6 T, B_2 = -0.7 T and IS_1 = 0.05 mm/s [39]. We used these latter values as starting values for the analysis of the spectra.

For a large number of different compositions in each atomic plane of the Cu/Fe interface we have calculated the relative probabilities

for all configurations Fe(n_1,n_2) with n_1 varying between 0 and 8 and n_2 varying between 0 and 6. With this probability distribution the Mössbauer spectra were computed as being the sum of a large number of subspectra, each belonging to an Fe atom with a particular (n_1,n_2) configuration. For these calculations we made use of the following assumptions:

(i) The electron diffraction studies on (x Cu + y Fe) for $x = y > 6$ Å have shown that most of the Fe atoms are ordered in the bcc structure. For $x = y = 4$ Å only fcc rings are observed. It has been observed that thin Fe films on Cu(111) are ordered in the fcc structure [26-32]. We therefore assume that the first one or two Fe layers on top of the Cu layers are ordered in the fcc structure. In this way we make a distinction between the "bottom" interface, where some of the Fe atoms are in the fcc structure, and the "top" interface, where all the Fe atoms are ordered in the bcc structure. Shinjo et al. also made a distinction between the two types of interfaces in Fe/Sb multilayers [33]. In our case the contribution of the Fe atoms ordered in the fcc structure in the "bottom" interface is assumed to be paramagnetic at room temperature.

(ii) Within each atomic plane near the Cu/Fe interface the Fe and Cu atoms are randomly distributed.

(iii) For simplicity the composition profiles are symmetric with respect to the equiatomic composition.

In our calculation we used the following parameters: B_1, B_2, IS_1, the line width of the individual subspectra and the composition profile. A good fit was obtained without taking a quadrupole splitting

into consideration. This seems reasonable, since for thin Fe films on Cu often no quadrupole splitting has been observed [30,31,40,41], although for very thin films [40] and small Fe precipitates in Cu [42] an additional quadrupole split doublet was noted. By comparing the calculated spectra with the observed spectra we obtained a good estimate of the composition profile of the Cu/Fe interfaces. The calculated spectra giving the best agreement with the observed ones for $x = y$ = 40 Å and 20 Å are shown in Fig. 3.13. A resonable fit was also obtained for 10 Å. For $x = y$ = 6 Å we did not calculate the spectrum, since we doubt whether this sample still has a multilayer structure. It is possible that the film has grown with an island structure.

Results

The following results were obtained from the comparison of our model calculations with the observed spectra:

(i) The interfaces between the Fe and Cu layers seem to extend over three atomic planes , with compositions in the plane : 80 % Cu-20 % Fe atoms, 50 % Cu-50 % Fe and 20 % Cu-80 % Fe.

(ii) The assumption that the "bottom" interface consists of only one or two planes of Fe atoms in the fcc structure might be correct since it gives a good fit of the observed spectra. Assuming all the iron atoms to be in the bcc structure yielded a somewhat worse fit. The spectrum for $x = y$ = 6 Å confirms this, since it appears from this spectrum that in this case about 50% of the Fe atoms is ferromagnetic. This is in contrast with the observations of Gradmann and Tillmanns, who studied thin Fe films on Cu(111) [43]. For a thickness of less

than 8 Å they found fcc iron to be totally paramagnetic at room temperature. They observed that the thickness at which bcc iron appears is strongly influenced by the substrate temperature during evaporation.

(iii) As mentioned earlier, it appears that for $x = y = 6$ Å the magnetization has rotated away from the in-plane direction. Our magnetization measurements in fields parallel and perpendicular to the film plane also revealed a decreasing preference for in-plane magnetization with decreasing modulation wavelength [35]. Analogous observations have been reported by several authors [40,44]. They assumed that for thin films the surface anisotropy becomes larger than the shape anisotropy, which causes the magnetization to rotate out of plane. However, it cannot be excluded that for very thin films the continuiy of the layer is broken down to an island structure, which gives rise to an increased superparamagnetic relaxation [45].

(iv) The hyperfine field of the Fe atoms in the middle of the Fe layers is 31.6 T, which is in good agreement with the value of 31.5 T [40], measured by Keune et al. for a thin film of 30 Å Fe on Cu. These values are somewhat smaller than the value of 33.1 T for bulk α-iron.

(v) The values of B_1, B_2 and IS_1 are -1.6 T, -0.1 T and 0.014 mm/s, respectively, which are in reasonable agreement with literature values [39]. The value of B_1 is in fact only correct for iron-rich Fe-Cu alloys. For $n_1 > 4$ we used increasing values of $|B_1|$, resulting in zero hyperfine field for Fe atoms which are completely surrounded by more than six Cu atoms.

(vi) The line width of the basic Fe spectrum is 0.60 mm/s, which is

much larger than the line width for pure α-iron (0.25 mm/s). This excess line width is probably due to the simplication of taking just one sextet for those Fe atoms that have no Cu atoms as nearest neighbour or next nearest neighbour. Small differences in the surrounding of these Fe atoms will result in a small distribution of hyperfine fields around the value of $B_{hf}(0)$ = 31.6 T, which will cause some line broadening.

(vii) The line width of the other subspectra originating from Fe atoms with $n_1 \neq 0$ and/or $n_2 \neq 0$ is 0.28 mm/s and is very close to the value of pure α-iron. Our value is much smaller than the one obtained by Jaggi et al. for Fe/V multilayers [34].

Conclusion

From the CEMS spectra we have found that most of the Fe nuclei in the multilayers experience a hyperfine field close to the value in bulk α-iron. A small part of the Fe nuclei experience smaller hyperfine fields owing to neighbouring Cu atoms. Concluding, a model in which the interface extends over three atomic planes, can satisfactorily explain our results for Cu/Fe multilayers.

3.5 Other techniques

Rutherford backscattering (RBS) is another often used technique to measure a composition profile [46]. Fig. 3.14 shows an example for Au/Ni layers prepared by ion beam sputtering. In this case the angle

between the incident 0.5 MeV He^{2+} beam and the detector was 170 deg. and the angle between the film and the incident beam was varied. Though the resolution is limited to about 50 Å, it is clear that the Au and Ni layers are not pure, but mixed with each other. A rough estimate is that in the Au layers there is at least 50 at.% Ni and in the Ni layers there is at least 20 at.% Au.

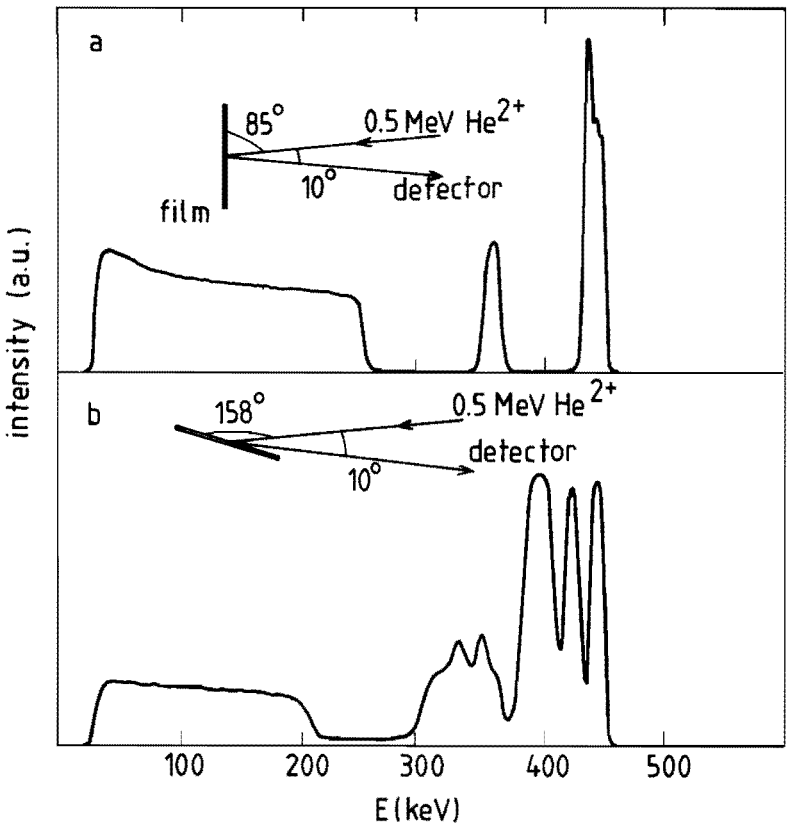

Fig. 3.14 *RBS spectrum of* 2×(100 Å Au + 100 Å Ni) *prepared by ion beam sputtering on* Si. *The two* Au *and* Ni *layers can clearly be separated, but the area in-between the two peaks indicate that there is about* 50 at.% Ni *in the* Au *layers and* 20 at.% Au *in the* Ni *layers.*

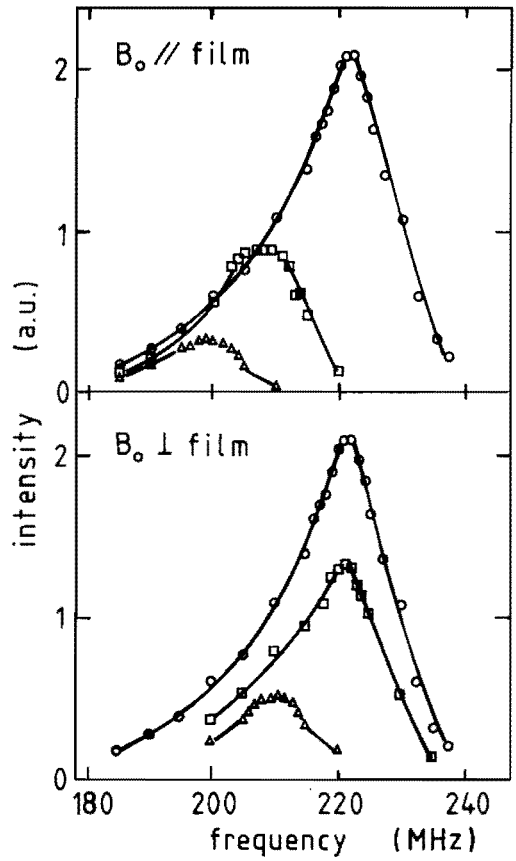

Fig. 3.15 *NMR spectra of* 63*(20 Å Co + 27 Å Pd) *at a temperature of* 4.2 K *with the magnetic field* B_o *parallel and perpendicular to the film* (o B_o = 0 *T*, □ B_o = 1 *T*, Δ B_o = 2 *T*).

Nuclear magnetic resonance (NMR) is used to measure the hyperfine field at the Co nuclei in Pd/Co multilayers. As with Mössbauer spectroscopy it might be possible to observe an extra structure from Co atoms at the interfaces. Resonance signals appear in the same region of frequencies as for pure Co, but unfortunately they are broad (Fig. 3.15) and no extra structure was observed. Still, interesting experi-

ments can be done by applying a magnetic field in various orientations relative to the film. This causes a shift of the resonance line and the preferential orientation of some or all of the Co atomic magnetic moments can be observed [47].

references

[1] B.D. Cullity, "Elements of X-Ray Diffraction" (2nd ed.), Addison-Wesley, Reading (Mass.) (1978)

[2] A. Guinier, "X-Ray Diffraction in Crystals, Imperfect Crystals, and Amorphous Bodies", Freeman, San Francisco (1963)

[3] D.B. McWhan in "Synthetic Modulated Structures", Ed. L.L. Chang and B.C. Giessen, Academic Press, Orlando (1985)

[4] A.M. Kadin and J.E. Keem, Scripta Metallurgica **20** (1986) 443

[5] W.J. Bartels in "Thin-Film Growth Techniques for Low-Dimensional Structures", Ed. R.F.C. Farrow and P.J. Dobson, Plenum Press, London (1987)

[6] I.K. Schuller, Phys. Rev. Lett. **44** (1980) 1597

[7] K.E. Meyer, G.P. Felcher, S.K. Sinha, and I.K. Schuller, J. Appl. Phys. **63** (1981) 6608

[8] M. Jałochowski and P. Mikołajczak, J. Phys. F **13** (1983) 1973

[9] Z. Mitura and P. Mikołajczak, J. Phys. F **18** (1988) 183

[10] D.B. McWhan, NATO ASI on Physics, Fabrication and Applications of Multilayered Structures, Ile de Bendor 1987

[11] W. Sevenhans, M. Gijs, Y. Bruynseraede, H. Homma, and I.K. Schuller, Phys. Rev. B **34** (1986) 5955

[12] R.W. James, "The Optical Principles of the Diffraction of X-Rays", Bell, London (1962)

[13] International Tables for X-Ray Crystallography vol. IV, The Kynoch Press, Birmingham (1974)

[14] "Metals Reference Book", Ed. C.J. Smithells, Butterworths, London (1976)

[15] B. Window, J. Appl. Phys. **63** (1988) 1080

[16] P. Bisanti, M.B. Brodsky, G.P. Felcher, M. Grimsditch, and L.R. Sill, Phys. Rev. B **35** (1987) 7813

[17] N.K. Flevaris, D. Baral, J.E. Hilliard, and J.B. Ketterson, Appl. Phys. Lett. **38** (1981) 992

[18] P. Auvray, M Baudet, and A. Regreny, J. Appl. Phys. **62** (1987) 456

[19] E. Brouns, J.W. Visser, and P.M. de Wolff, Acta Cryst. **17** (1964) 614

[20] K. Fujiwara, J. Phys. Soc. Jpn **12** (1957) 7

[21] R. Brouwer, "Incommensurability in crystal structures", Ph.D. Thesis, Groningen (1978)

[22] S. Hofmann, Surf. and Interf. Anal. **2** (1980) 148

[23] M.P. Seah, Surf. Sci. **32** (1972) 703

[24] R. Krishnan, H. Sakakima, J.F. Crochran, B. Heinrich, K. Myrtle, R.W. Qiao, and C.E. Patton, J. Magn. Magn. Mater. **67** (1987) 88

[25] D.E. Newbury in "Scanning electron microscopy", Ed. Om Johari, Chicago (1977)

[26] J.G. Wright, Phil. Mag. **24** (1971) 217

[27] U. Gradmann, W. Kümmerle, and P. Tillmanns, Thin Solid Films **34** (1976) 249

[28] W. Kümmerle and U. Gradmann, Solid State Comm. **24** (1977) 33

[29] U. Gradmann and H.O. Isbert, J. Magn. Magn. Mater. **35** (1983) 53

[30] W. Keune, R. Halbauer, U. Conser, J. Lauer, and D.L. Williamson, J. Magn. Magn. Mater. **6** (1977) 192

[31] W. Becker, H.-D. Pfannes, and W. Keune, J. Magn. Magn. Mater. **35** (1983) 53

[32] R. Halbauer and U. Conser, J. Magn. Magn. Mater. **35** (1983) 55

[33] T. Shinjo, N. Hosoito, K. Kawaguchi, T. Takada, Y. Endoh, Y. Ajiro, and J. Friedt, J. Phys. Soc. Japan **52** (1983) 3154

[34] N.K. Jaggi, L.H. Schwartz, H.K. Wong, and J.B. Ketterson, J. Magn. Magn. Mat. **49** (1985) 1

[35] H.J.G. Draaisma, H.M. van Noort, and F.J.A. den Broeder, Thin Solid Films **126** (1985) 117

[36] G.K. Wertheim, V. Jaccarino, J.H. Wernick, and D.N.E. Buchanan, Phys. Rev. Lett. **12** (1964) 24

[37] F. van der Woude and G. Sawatzky, Phys. Rep. **12** C (1974) 335

[38] T.E. Cranshaw, Physica **86-88** B (1977) 443

[39] J. Lauer, W. Keune, U. Gonser, and D.L. Williamson, J. Magn. Magn. Mater. **7** (1978) 75

[40] W. Keune, J. Lauer, U. Gonser, and D.L. Williamson, J. de Phys. Coll. **40** (1979) C2-69

[41] W. Wiartalla, W. Becker, W. Keune, and H.-D. Pfannes, J. de Phys. Coll. **45** (1984) C5-461

[42] D.L. Williamson, S. Nasu, and U. Gonser, Acta Met. **24** (1976) 1003

[43] U. Gradmann and P.Tillmans, Phys. Stat. Sol. (a) **44** (1977) 539

[44] T. Shinjo, S. Hine, and T. Takada, J. de Phys. Coll. **40** (1979) C2-86

[45] G. Bayreuther and G. Lugert, J. Magn. Magn. Mater. **35** (1983) 50

[46] W.-K. Chu, J.W. Mayer, and M.-A. Nicolet, "Backscattering Spectrometry", Academic Press, New York (1978)

[47] H.A.M. de Gronckel, Ph.D. Thesis, Eindhoven (1989)

Chapter 4 MAGNETIC MEASUREMENTS

The determination of the magnetic properties of thin ferromagnetic films requires sensitive magnetometric methods, because the amount of material is limited. Further, the contribution of the substrate and sample holder can easily be of the same order of magnitude as the magnetic moment of the film. In this chapter we describe the methods that were available to perform magnetic measurements, illustrated with some typical examples.

4.1 Vibrating sample magnetometry

In a vibrating sample magnetometer (VSM) a sample is attached to a rod and positioned between a poles of an electromagnet. Coils around the moving sample pick up the changing magnetic flux resulting in an induction voltage proportional to the component of the magnetic moment along the direction of the magnetic field [1]. Fig. 4.1 shows the experimental set-up that is used in this study. The movement of the rod and sample is provided for by a motional feedback speaker in which a piezo-electrical element is employed to control the movement of the conus. The speaker is usually operated at 80 Hz. A configuration of 8

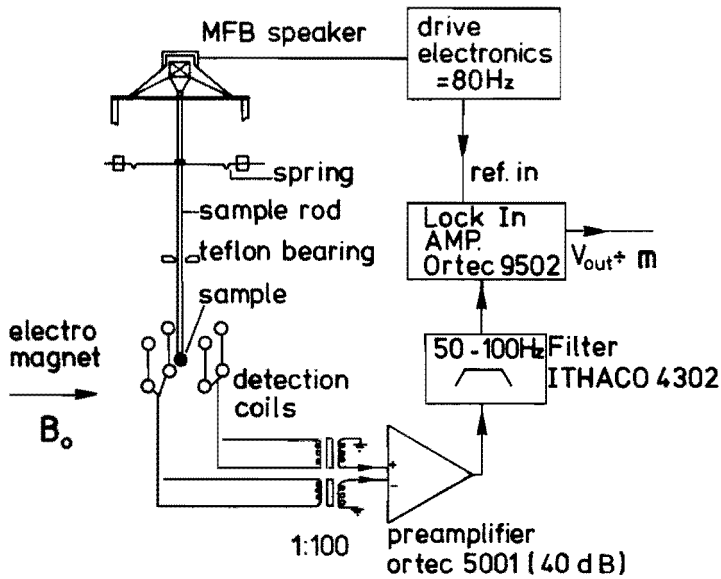

Fig. 4.1 *Diagram of the vibrating sample magnetometer as used in this study.*

pick-up coils is used to have a relatively large volume in which the sample can be positioned. The usual dimensions of our samples are 4x12 mm.

Two series of measurements are made: one with the field direction perpendicular to the film and one with the field parallel to the film (along the 4 mm axis). The field range is -1.6 T to 1.6 T. A characteristic result for a film of 2500 Å Co on glass is shown in Fig. 4.2. By extrapolation of the high field data we find at the external field $B_o = 0$ T the spontaneous magnetic moment at room temperature. The contribution of the sample holder and substrate is $-0.34 \cdot 10^{-6}$ Am^2/T. The minimum magnetic moment that can be measured with this magnetometer is about $1.0 \cdot 10^{-6}$ Am^2.

The total magnetic energy, E, per volume unit of the sample is

$$E = \frac{1}{V} \int_0^m \vec{B}_o \cdot d\vec{m} \qquad (1)$$

in which $\vec{m}$ is the magnetic moment of the sample and $\vec{B}_o$ the external magnetic field [2]. Of course, in principle this definition can only be used when there is no hysteresis, but in practice the magnetization curves in increasing and decreasing field can be averaged. This may introduce an error, but this is never larger than the hysteresis. Thus the energy E can be determined from the area between the magnetization

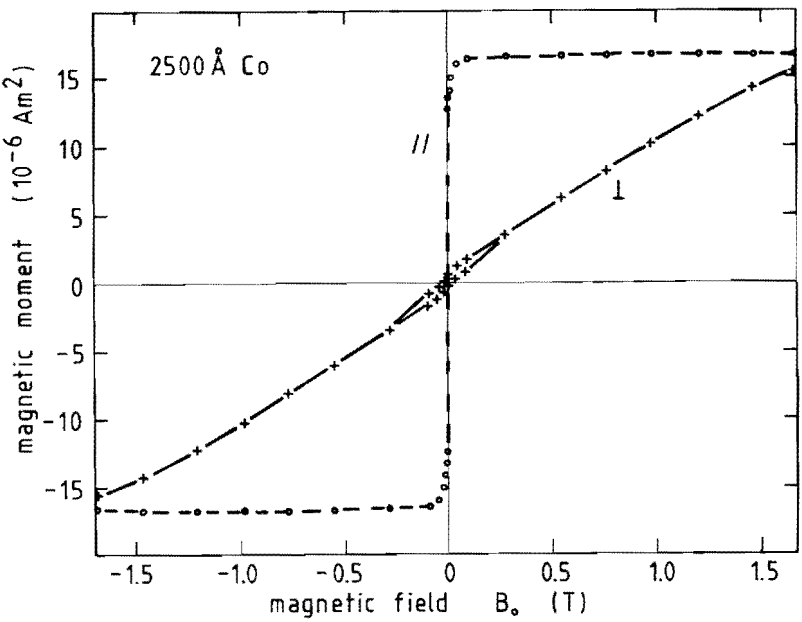

Fig. 4.2 *VSM measurement of a thin film of 2500 Å Co sputtered on glass. The saturation magnetization, $\mu_o M_s$, is 1.74 T, which equals, within the experimental error, the bulk value of Co.*

curve and the axis along which the magnetic moment is plotted, in Fig. 4.2 the vertical axis. The difference in energy between the saturated states in the directions perpendicular and parallel to the film plane can be called the total anisotropy. This includes the magnetostatic energy which is due to the shape of the sample, the demagnetization energy. For a thin film in which the magnetization $\vec{M}$ makes an angle θ with the direction perpendicular to the film, this energy can be written as:

$$E_D = -\frac{1}{2}\mu_o M^2 \sin^2\theta \ . \qquad (2)$$

When there is rotational symmetry around the axis perpendicular to the film, it is possible to expand the total anisotropy as a series of even powers of sin θ :

$$E(\theta) = K_1 \sin^2\theta + K_2 \sin^4\theta + .. \qquad (3)$$

in which K_1 includes $-\frac{1}{2}\mu_o M^2$ (eq. (2)). The anisotropy that is measured by taking the area between the magnetization curves with the field perpendicular and parallel to the film is then:

$$K = K_1 + K_2 + \ldots \ . \qquad (4)$$

Mostly K_1 is the dominating term. Note that the sign of the anisotropy is such that when $K > 0$ the preferential direction for the magnetization is perpendicular to the film plane.

4.2 Faraday balance

Another way to measure the magnetic moment of a sample is the determination of the force exerted on a sample by a magnetic field gradient

$$\vec{F} = \vec{\nabla} (\vec{m} \cdot \vec{B}_o) \quad . \tag{5}$$

An apparatus based on this principle is called a Faraday balance (FB). In our set-up the gradient is provided by extra coils, so that the gradient can be reversed to obtain a greater sensitivity for the magnetic part of the force. The sample is mounted in a holder between the poles of an electromagnet with a field range of 0 - 1.5 T. Because the

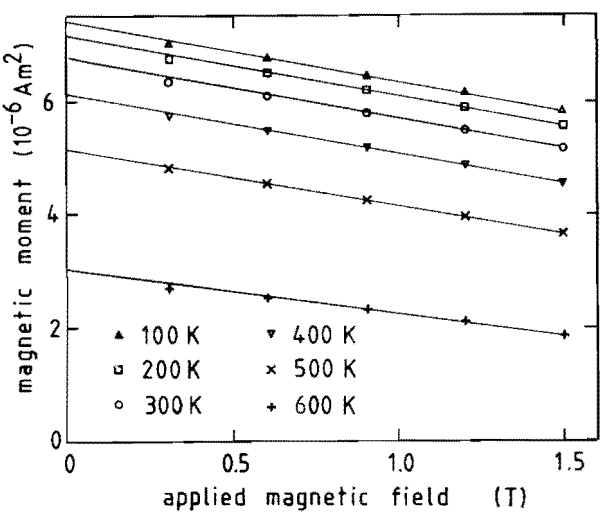

Fig. 4.3 *Faraday balance measurement of the magnetic moment of a multilayer consisting of* 170×(13.5 Å Pd + 4.1 Å Co) *as function of field and temperature. The lines give the extrapolation to zero field.*

sample can rotate freely, the measurement can only be done with the field in one direction relative to the sample, i.e. the easiest magnetization direction for the sample. Between 77 and 1000 K a sensitivity of 10^{-8} Am^2 can be obtained with a gradient of 1 T/m, which means a field difference of 0.01 T over the sample. In Fig. 4.3 a characteristic measurement of the magnetic moment as a function of field and temperature is shown. The diamagnetic contribution of the substrate and sample holder is eliminated by extrapolation to zero field. In this way we obtain the magnetization in zero field as a function of temperature.

4.3 Torque measurement

The torque exerted on a magnetic moment in a homogeneous magnetic field is a suitable way to determine the anisotropy of a ferromagnetic sample [3]. Diamagnetic or paramagnetic contributions play no role since that part of the magnetic moment is collinear with the field. The torque from the field on the magnetic moment is in equilibrium with the torque from the sample on the magnetic moment. In our experimental set-up (TRT-2 from TOEI Kogyo, Tokyo) the last one is provided by a galvanometer on top of a rod to which the sample is attached. The electromagnet has a range from 0 to 1.75 T and can rotate over 360 deg.. When the magnetization is saturated, the torque T is given by

$$T = B_o\, m\, \sin(\phi-\theta) \ , \qquad (6)$$

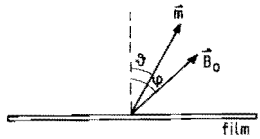

Fig. 4.4 *Definition of the angles θ and φ relative to the film.*

with ϕ and θ as indicated in Fig. 4.4; m is the saturated magnetic moment and B_o the external field. It also equals

$$T = -\int dV \frac{\partial E}{\partial \theta} = -2k_1 \sin\theta\cos\theta - 4k_2 \sin^3\theta\cos\theta \qquad (7)$$

with k_1 and k_2 as the anisotropy constants introduced in equation (3) integrated over the volume.

Given $\frac{k}{m}1$, $\frac{k}{m}2$ and B_o, $\frac{T}{m}$ can be calculated from (7) and ϕ follows from (6) for every angle θ. In Fig. 4.5 a set of torque curves as calculated from these equations is given. Note that, since this model assumes the magnetic moment of the sample always to be saturated, the top of the torque curve has the same value for every field. When this is not the case in the experimental situation, the interpretation as sketched above can not be used. The best way to extract the material parameters from the measured torque curves is the determination of the slope of the curves at the zero-crossings [4]. The value of the torque we could measure had to be between $2.5 \cdot 10^{-6}$ and $-1.4 \cdot 10^{-6}$ Nm. This often limited the recording of a full torque curve, but gave an accurate measurement of the slope. For the final determination of the anisotropy constants k_1 and k_2, the value for the magnetic moment from the VSM and FB measurements was used.

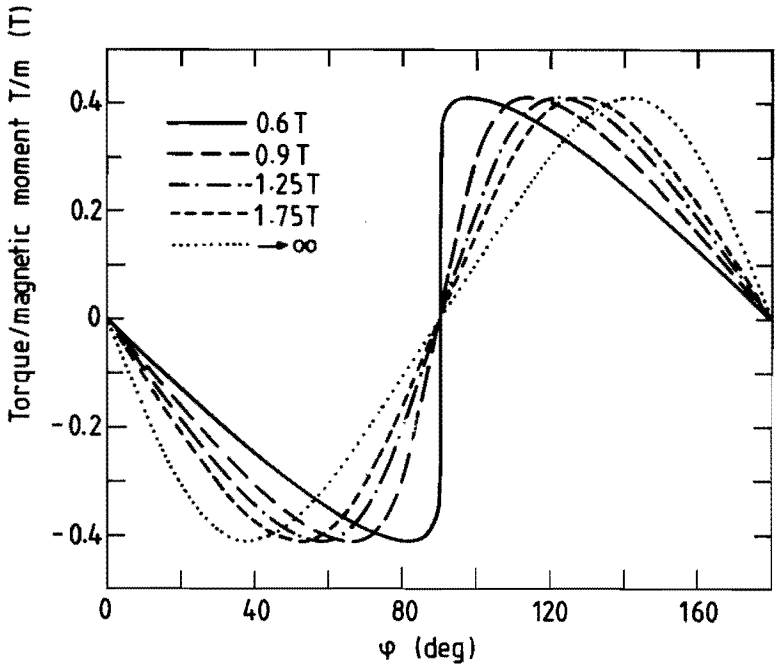

Fig. 4.5 *Torque curves, according to equations* (6) *and* (7) *for* k_1/m = 0.5 *and* $k_2/m = -0.1$.

4.4 Ferromagnetic resonance (FMR)

With FMR an accurate determination of the anisotropy is possible from the value of the magnetic field at which uniform resonance of the magnetization occurs. Further non-uniform resonance in thin films can give information about the spin-wave stiffness. The standard procedure is to expose the ferromagnetic sample to microwave radiation of a fixed frequency. By sweeping the external field in which the sample is positioned, the absorbed microwave power as function of the field is measured. Usually the derivative of this signal is used.

The field at which uniform resonance of the magnetization $\vec{M}$ occurs is conventionally described by the equation of motion [5]

$$\frac{1}{\gamma}\frac{d\vec{M}}{dt} = \vec{M} \times \vec{B}_i \ , \tag{8}$$

in which $\gamma = \frac{g\mu_B}{\hbar}$ is the gyromagnetic ratio and $\vec{B}_i$ the "internal field". In equilibrium

$$\vec{M} \times \vec{B}_i = 0 \tag{9}$$

and the variation $\delta\vec{M}$ fulfills the condition

$$\delta\vec{M} \times \vec{M} = 0 \ . \tag{10}$$

The internal field $\vec{B}_i$ is defined by

$$\vec{B}_i = \vec{B}_o - \frac{\partial E}{\partial \vec{M}} \ , \tag{11}$$

in which $\vec{B}_o$ is the external applied field and E is the energy density of the magnetic sample.

If the energy can be written as

$$E = K \sin^2\theta \tag{12}$$

in which θ is the angle of $\vec{M}$ with the axis perpendicular to the film, it can be shown that the variation $\delta\vec{M}$ with frequency ω is in resonance when

$$(\frac{\omega}{\gamma})^2 = B_o^2 + B_o \frac{2K}{M_s} (2\cos\phi\cos\theta - \sin\phi\sin\theta) + (\frac{2K}{M_s})^2 \cos^2\theta \ , \quad (13)$$

in which ϕ is the angle of the external magnetic field with the normal of the film. For convenience we introduce the anisotropy field B_a

$$B_a = \frac{2\ K}{M_s} \quad (14)$$

and the anisotropy frequency f_a

$$f_a = \frac{g\ \mu_B\ |B_a|}{h} \quad (15)$$

to write the resonance condition as

$$\left[\frac{f}{f_a}\right]^2 = \left[\frac{B_o}{B_a}\right]^2 + \left[\frac{B_o}{B_a}\right](2\cos\phi\cos\theta - \sin\phi\sin\theta) + \cos^2\theta \quad (16)$$

with the frequency $f = \frac{\omega}{2\pi}$, as usual.

The relation between θ and ϕ is, as in section 4.3, given by

$$2\ (\frac{B_o}{B_a})\ \sin(\phi-\theta) + \sin 2\theta = 0 \ . \quad (17)$$

Table 4.1 *Resonance conditions for some special orientations of the external magnetic field* B_o.

	B_o // film (φ = 90 deg.)	B_o ⊥ film (φ = 0 deg.)
$K < 0$	$(\frac{\omega}{\gamma})^2 = B_o(B_o - B_a)$	$B_o \leq \lvert B_a \rvert : \omega = 0$ $B_o > B_a : \frac{\omega}{\gamma} = B_o + B_a$
$K > 0$	$B_o \leq B_a : (\frac{\omega}{\gamma})^2 = B_a^2 - B_o^2$ $B_o > B_a : (\frac{\omega}{\gamma})^2 = B_o(B_o - B_a)$	$\frac{\omega}{\gamma} = B_o - B_a$

In Table 4.1 the resonance conditions for ϕ = 0 deg. (field perpendicular to the film) and ϕ = 90 deg. (field parallel to the film) are summarized. In Fig. 4.6 resonance diagrams for different signs of the anisotropy constant K show at which combination of B_o, ϕ and f resonance can be expected according to this formulation. Usually f is fixed and the variation of B_o with the angle ϕ is measured. In Fig. 4.7 the calculated rotation diagrams for positive and negative values of K are shown for the frequency $f = 1.5\ f_a$.

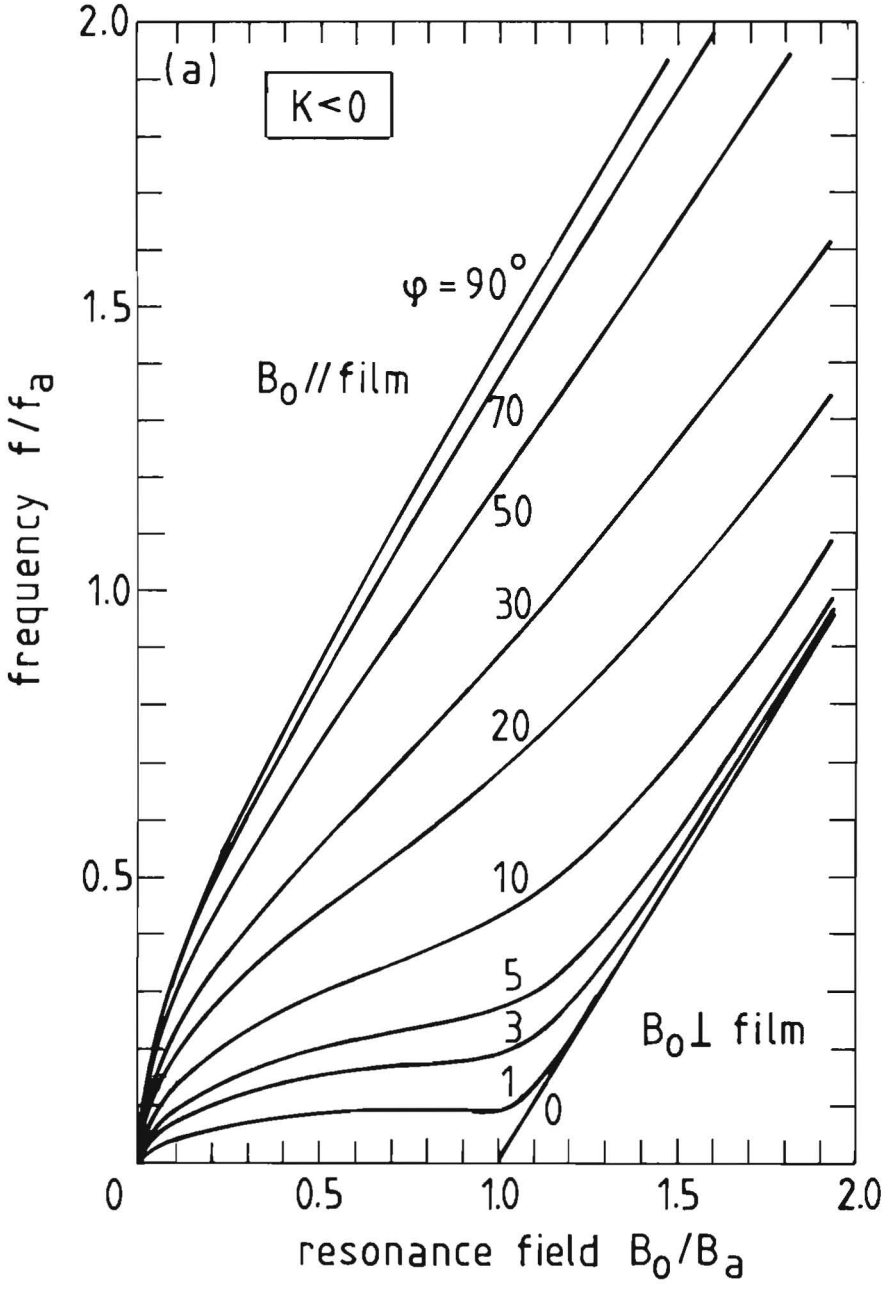

Fig. 4.6(a) *Resonance diagram in the case the uniaxial anisotropy* $K < 0$ *(preferential direction in the plane of the film).*

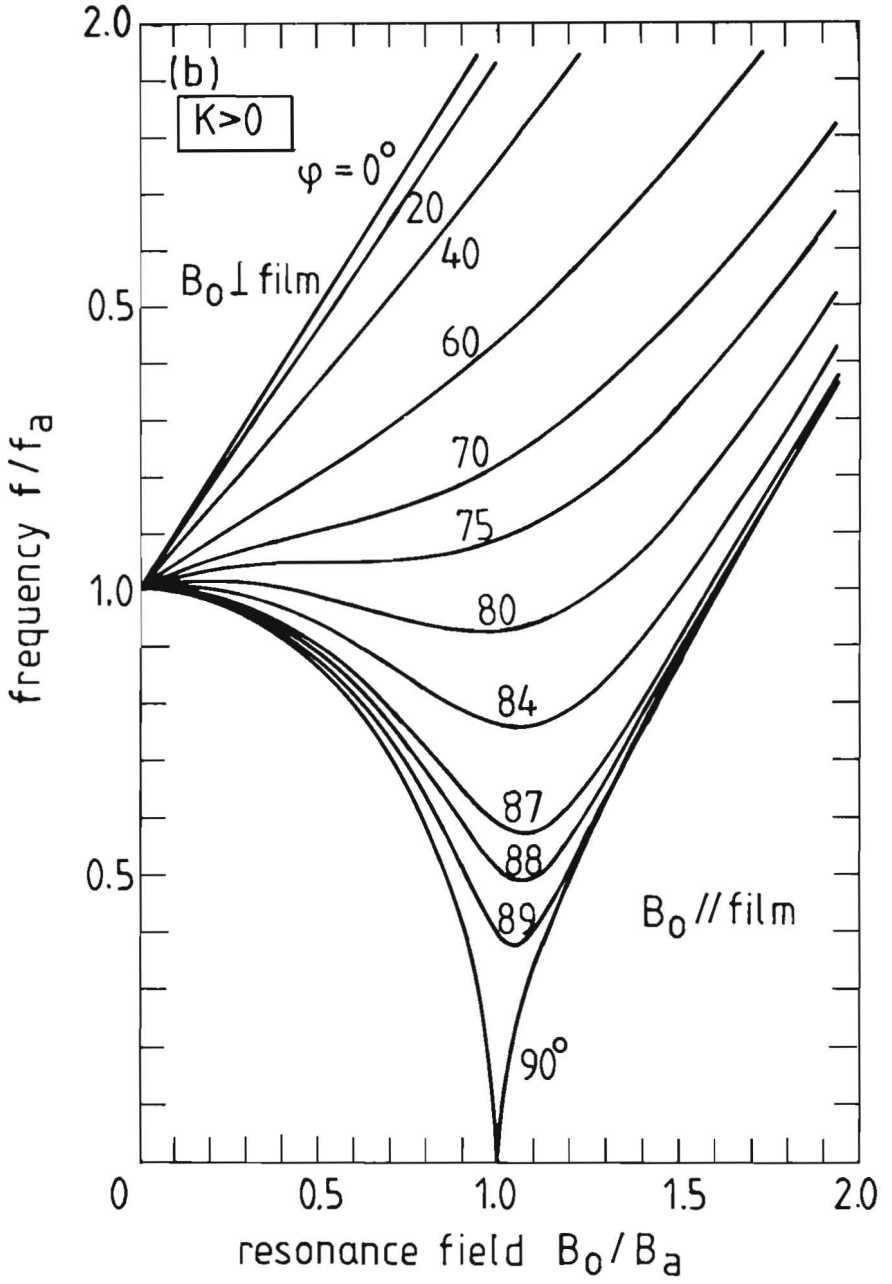

Fig. 4.6(b) *Resonance diagram in the case the uniaxial anisotropy* $K > 0$ *(preferential direction perpendicular to the plane of the film).*

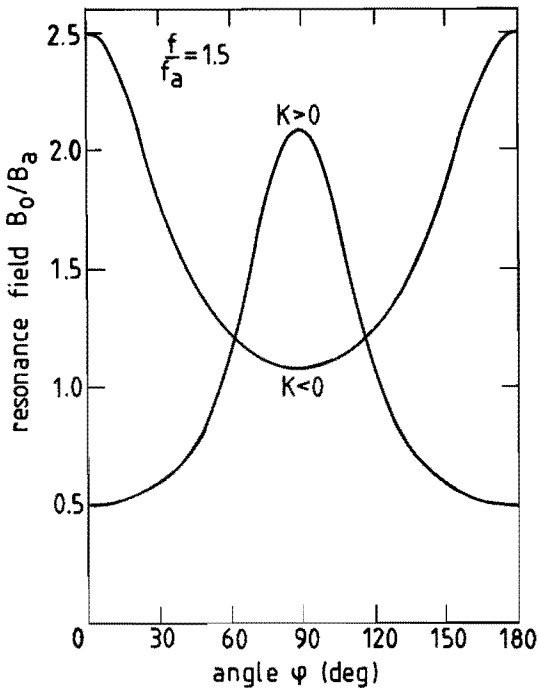

Fig. 4.7 *Rotation diagram for the fixed frequency* $f = 1.5\ f_a$.

references

[1] S. Foner, Rev. Sci. Instr. **30** (1959) 548
S. Foner, IEEE Trans. on Magn. MAG-**17** (1981) 3358

[2] J.D. Jackson, "Classical Electrodynamics" (2nd ed.), John Wiley, New York (1975)

[3] H. Zijlstra, "Experimental Methods in Magnetism" vol. 2, North-Holland, Amsterdam (1967)
R.F. Pearson in "Experimental Magnetism" vol. 1, Ed. G.M. Kalvius and R.S. Tebble, John Wiley, Chichester (1979)

[4] J. Burd, M. Huq, and E.W. Lee, J. Magn. Magn. Mater. **5** (1977) 135

[5] A.H. Morrish, "The Physical Principles of Magnetism", John Wiley, New York (1965)

Chapter 5 MAGNETIC PROPERTIES OF Pd/Co MULTILAYERS

In this chapter results of the study of the magnetic properties of Pd/Co multilayers prepared by evaporation are discussed. Some of these results have already been published or submitted for publication and are presented here in essentially the same form. Consequently, some redundancy may appear in some of the sections, but as an advantage the sections can be read rather independently.

5.1 Magnetic interface anisotropy in Pd/Co and Pd/Fe multilayers *)

Abstract

Pd/Co and Pd/Fe multilayer thin films containing ultra thin (2-12 Å) Co and Fe layers were prepared by vapour deposition in ultra high vacuum. Their magnetization was measured at room temperature in fields parallel and perpendicular to the film plane. The Pd/Co multilayers show a transition of the preferred magnetization direction from lying in the film plane towards lying along the film normal when decreasing the Co layer thickness below 8 Å. The Pd/Fe multilayers are preferably magne-

*) part of this text has been published in the Journal of Magnetism and Magnetic Materials **66** (1987) 351

tized in the film plane, although the anisotropy decreases with lower Fe layer thickness. The magnetic anisotropy of both types of films can be interpreted by assuming an interface contribution which favours a perpendicular magnetization, and a volume contribution which favours an in-plane magnetization. The magnitude of the volume contribution is discussed in terms of magnetostatic, magnetocrystalline and magnetoelastic anisotropies, and equals, surprisingly, the anisotropy of the ferromagnetic elements in bulk thin film form in both cases.

Introduction

Interest in magnetic anisotropy in thin films is stimulated by the possible application of these films as magnetic recording media in which a higher information density is pursued (see section 1.3). Magnetic thin films tend to be magnetized in the film plane to minimize the magnetostatic energy. To orient the preferred direction for the magnetization perpendicular to the film, intrinsic anisotropy is needed to overcome the shape anisotropy. In Co-Cr and $BaFe_{12}O_{19}$ with the hexagonal c-axis perpendicular to the film this anisotropy is provided by crystal anisotropy [1,2]; in sputtered amorphous Gd-Co thin films the anisotropy is attributed to pair-ordening in the film [3].

In multilayer materials the broken symmetry at the interface may cause additional anisotropy energy. This was first pointed out by Néel [4] for the surface of a ferromagnetic material and was called magnetic surface anisotropy. Gradmann has reported experimental values from $-0.5 \cdot 10^{-3}$ to $+0.5 \cdot 10^{-3}$ J/m^2 for this surface anisotropy for interfaces of various materials [5,6]. In the present case a ferromagnetic layer

(Co, Fe; 2-12 Å) is alternated by a non-ferromagnetic layer (Pd). These multilayer films form suitable samples to determine experimentally the interface anisotropy using standard magnetometry.

Preparation

The multilayers were prepared by electron beam evaporation in UHV on silicon substrates at room temperature, as described in section 2.4, with an evaporation rate of 1 Å/s. The depositions were started with a base layer of 200 Å Pd on which the multilayers with individual layer thicknesses as indicated in Fig. 5.1 were grown; the total thickness of the multilayers was about 3000 Å. From X-ray diffraction (XRD) with the scattering vector perpendicular to the film plane the modulation length

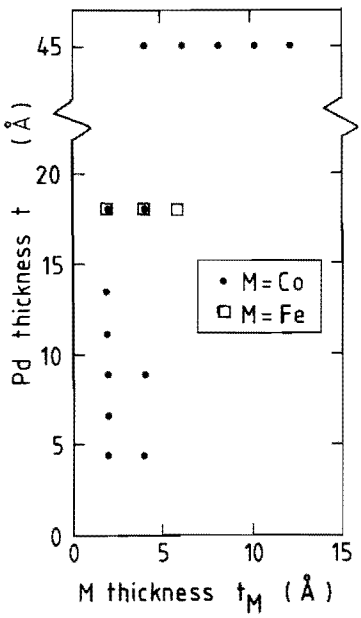

Fig. 5.1 *Overview of the individual layer thicknesses of the* Pd/Co *and* Pd/Fe *multilayers.*

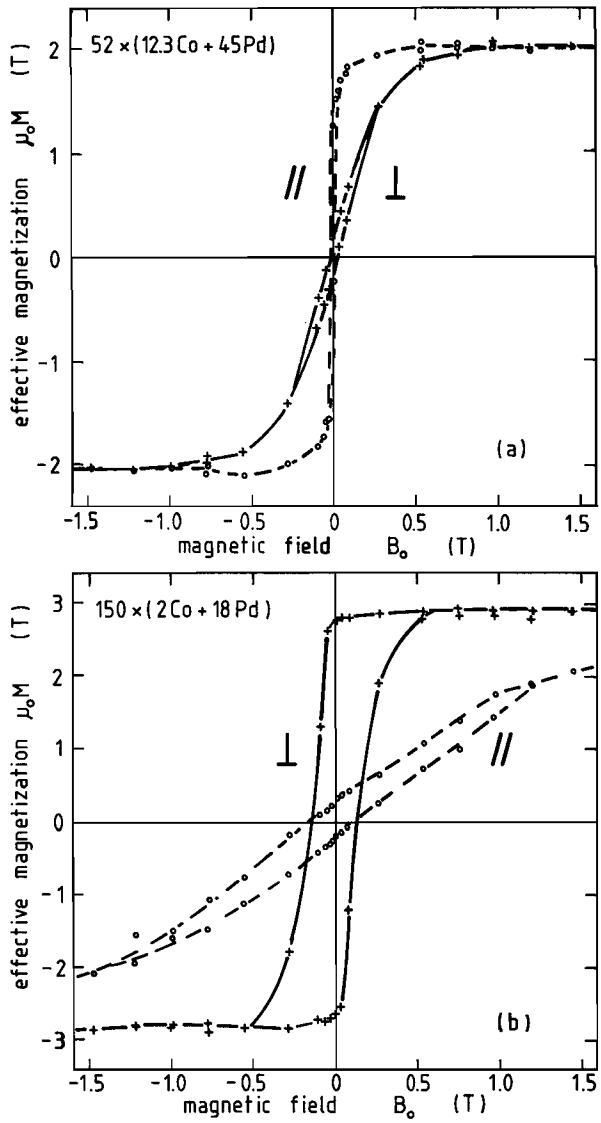

Fig. 5.2 *Magnetization curves at room temperature in a magnetic field parallel to the film (dashed curve) and perpendicular to it (drawn curve)* (a) 52*(12.3 Å Co + 45 Å Pd); (b) 150*(2 Å Co + 18 Å Pd). *Note the increase of the coercive field in the perpendicular curve of case* (b) *and the high remanent magnetization.*

was determined (cf. section 3.1). Chemical analysis of a representative number of films showed that the desired amount of Co and Fe was present whereas the mass of Pd was 10–20 % higher than expected (cf. section 2.4).

For pure Pd these deposition conditions led to a polycrystalline film with a $[111]_{fcc}$ fibre texture. The multilayer reflections were found in the neighbourhood of the peak belonging to this texture of Pd, so we consider the multilayer structure as an alternating stacking of closest packed planes of Pd and Co. In this orientation a Co layer thickness of 2.05 Å is assumed to be equivalent to one monolayer; also for Pd/Co multilayers with Co monolayers, we observed multilayer reflections when the Pd thickness was 6.7 Å or higher. Transmission electron microscopy of cross-sections also proved the periodic structure, even for multilayers containing 2 Å Co (cf. section 3.2). In the case of Pd/Fe multilayers with ultra-thin Fe layers XRD also gave clear multilayer peaks. So far we do not have conclusive results whether the Fe layers are pseudomorph with the Pd(111) layers, resulting in γ-Fe (fcc), or have the α-Fe (bcc) (110) orientation. The growth of γ-Fe would agree with the result for Fe on Cu(111) [7,8] and Fe on CuAu(111) [9].

Magnetic measurements

The magnetic moment of the samples was measured at room temperature with a vibrating sample magnetometer applying magnetic fields up to 1.7 T both parallel and perpendicular to the film plane (see section 4.1). In Fig. 5.2 two typical results are shown, one for the Pd/Co multilayer with 12.3 Å Co layers, which is more easily magnetized with the field parallel to the film than perpendicular to it, and a second one

for the Pd/Co multilayer with 2 Å Co layers, which is more easily magnetized with the field perpendicular to the film. The transition from the one into the other takes place gradually with the decrease of the Co layer thickness. Noteworthy is the high remanence and the large coercivity in the perpendicular magnetization curve for the film with 2 Å Co layers which give the hysteresis loop a rectangular shape; this high remanence is independent of the thickness of the Pd layers, as can be seen in Table 5.1, where we have tabulated some of the properties of the Pd/Co multilayers. Recently, Carcia et al. [10] reported the preparation of Pd/Co multilayer thin films by rf-sputtering. They found perpendicular anisotropy in multilayers with Co layers thinner than 8 Å, but they did not decrease the Co thickness below 4.7 Å.

On the vertical axis of the figures the effective magnetization $\mu_o M$ is shown, which is defined as the magnetic moment divided by the total Co volume. The saturation value of the magnetization is found to exceed the saturation magnetization of the bulk ferromagnetic element. This is thought to be caused by the polarization of interfacial Pd atoms. The effective anisotropy, K, is defined as the area between the perpendicular and the parallel magnetization curve per unit Co volume, as discussed in section 4.1. K is taken positive when the magnetization is preferably oriented perpendicular to the film. If we denote K_s as the anisotropy originating from the interface per unit area and K_v as the contribution to the anisotropy per volume unit Co, K can phenomenologically be described as

$$K = \frac{2K_s}{t_{Co}} + K_v \quad . \qquad (1)$$

Table 5.1 *Properties of the Pd/Co-multilayers:* t_{Co} *and* t_{Pd} *are the thicknesses of the layers, N is the number of repetitions of the two layers,* $\mu_o M_s$ *the saturation magnetization,* $M_r^{\perp}/M_s$ *the relative remanent magnetization in the perpendicular direction and* $\mu_o H_c^{\perp}$ *is the coercivity of the perpendicular loop and K the effective anisotropy energy.*

t_{Co}(Å)	t_{Pd} (Å)	N	$\mu_o M_s$ (T)	$M_r^{\perp}/M_s$	$\mu_o H_c^{\perp}$ (T)	K (10^6 J/m^3)
2	4.5	300	2.77	0.93	0.245	2.13
2	6.7	250	3.05	0.96	0.25	2.32
2	9	200	3.03	0.97	0.225	2.33
2	11.2	200	2.81	0.94	0.245	2.58
2	13.5	150	2.66	0.96	0.215	2.52
2	18	150	2.80	0.96	0.16	2.30
4	4.5	250	2.36	0.12	0.08	0.87
4	9	150	2.69	0.20	0.095	1.2
4	18	100	2.70	0.35	0.09	0.6
4.1	45	61	1.99	0.45	0.06	0.5
6.2	45	59	1.96	0.27	0.04	0.14
8.2	45	56	2.02	0.13	0.045	-0.04
10.2	45	34	2.10	0.07	0.015	-0.23
12.3	45	52	2.02	0.09	0.020	-0.31

Here t_{Co} denotes the Co layer thickness and the factor of 2 arises from the two interfaces of each Co layer. The volume anisotropy K_v consists of magnetostatic or demagnetization energy, magnetocrystalline anisotropy and magnetoelastic energy. The same analysis can be made for the Fe layers. In Fig. 5.3 the anisotropy is shown as function of the thickness of the Co and Fe layers. In both cases the effective anisotropy is well described by equation (1).

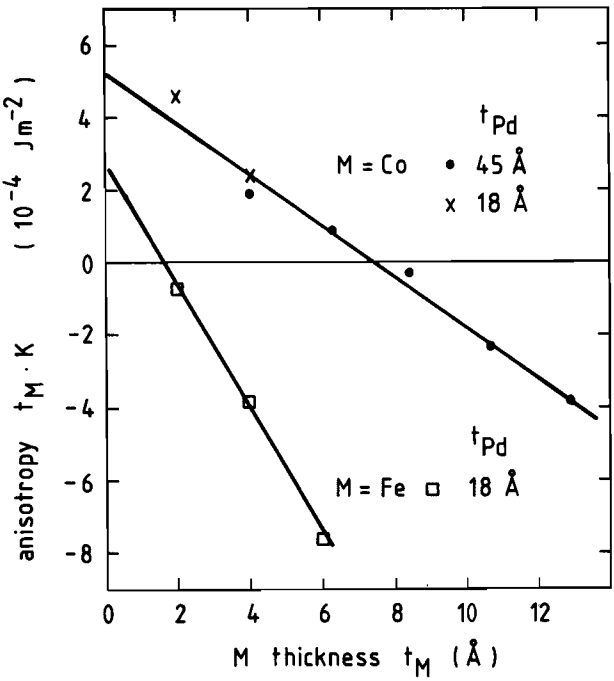

Fig. 5.3 *Effective anisotropy K times the layer thickness of the ferromagnetic element* t_M *, as function of* t_M *for multilayers with a fixed Pd thickness. The lines are the least square fits; the interceptions with the vertical axis yield the interface anisotropies and the slopes give the volume anisotropies.*

Discussion

For the Pd/Co multilayers the transition from perpendicular to in-plane anisotropy takes place at the Co thickness of 7.2 Å as can be seen by the change in sign of K. The measurements yield an interface contribution $K_s = 0.26 \cdot 10^{-3}$ J/m^2 and a volume contribution $K_v = -0.72 \cdot 10^6$ J/m^3. For a pure Co film with the hexagonal axis perpendicular to the film, the demagnetization energy would be $K_D = -\frac{1}{2}\mu_o M^2 = -1.23 \cdot 10^6$ J/m^3 and

the magnetocrystalline energy $K_1 = 0.41 \cdot 10^6$ J/m^3, $K_2 = 0.10 \cdot 10^6$ J/m^3 [11]. This would result in a volume contribution $K_D + K_1 + K_2 = -0.72 \cdot 10^6$ J/m^3, which equals exactly the value we determined for K_v in the Pd/Co multilayers. This is surprising since in the multilayers magnetoelastic energy can also contribute to the volume anisotropy when the Co layers are strained due to the lattice mismatch with Pd (9.1%). A rough estimate with a magnetostriction constant $\lambda = 10^{-5}$ and an elastic modulus $E = 2 \cdot 10^{11}$ N/m^2 yields a magneto-elastic anisotropy $K_\lambda = 0.3 \cdot 10^6$ J/m^3. Furthermore, the magnetocrystalline anisotropy is strongly dependent on the structure and is hard to estimate for the Co layers in these multilayers. The abovementioned agreement may therefore be fortuitous.

The Pd/Fe multilayers also prove to be ferromagnetic and the same analysis of the data yields $K_s = 0.14 \cdot 10^{-3}$ J/m^2 and $K_v = -1.73 \cdot 10^6$ J/m^3. Although in this case too the interface contribution is positive, it is apparently too small to induce a transition to a perpendicularly oriented magnetic state in the present range of the thickness of the layers. A comparison of these values with those of the bulk material, as we performed for the Pd/Co multilayers, is not quite possible since we do not know the structure of the Fe layers. For a pure α-Fe film the demagnetization energy would be $K_D = -1.83 \cdot 10^6$ J/m^3 while the magnetocrystalline anisotropy can be neglected and a possible magnetoelastic contribution may be rather small because of a low magnetostriction constant of α-Fe. For γ-Fe these data seem to be unknown.

With respect to the magnetic state of γ-Fe, controversial results have been reported. Antiferromagnetism was found for Fe on Cu(111) [7], while others found ferromagnetism both on Cu(111) and on CuAu(111)

[8,9]. If in our case γ-Fe is present in the Pd/Fe multilayers, our results support the latter view. Although the magnetization of the Fe layers is higher than that of bulk α-Fe, no definite conclusion can be drawn from it since it may be caused by polarization of the Pd atoms.

Carcia et al. [10] performed a similar analysis for Pd/Co multilayers which were made by rf-sputtering: they found $K_s = 0.16 \cdot 10^3$ J/m^2 and $K_v = -0.37 \cdot 10^6$ J/m^3. The lower value of K_s may be due to diffuse interfaces in the sputtered films, but the reason for the different K_v is unclear.

Conclusion

We found that in both Pd/Co and Pd/Fe multilayers the anisotropy at the interface tends to orient the magnetization perpendicular to the film. In the case of Pd/Co this leads to a perpendicular anisotropy for Co layers below a thickness of 7.2 Å. The Co layers can even be made as thin as 2 Å in which case the anisotropy leads to an almost rectangular perpendicular magnetization loop with high remanence. The volume contribution to the anisotropy is very close to the bulk value of a thin film, which is rather surprising for these very thin layers.

5.2 Magnetization in Pd/Co multilayers

The magnetic moment of thin layers of 3d elements has become of theoretical interest since it can be found directly from band structure calculations [12]. Especially for the bcc metals V, Cr and Fe on Ag(100) and Au(100) the calculated ground state shows an enhanced magnetic mo-

ment for the outer atomic layers of the 3d transition element, whereas the magnetic moment of inner atomic layers tends more to the bulk value [13]. Also a small induced moment on the outer atomic layers of Ag and Au is found, which in the case of Cr on Au amounts to 0.14 μ_B (μ_B is the Bohr magneton).

From the magnetization measurements we only obtain an average atomic moment which we usually attribute completely to the magnetic element. In Fig. 5.4 the saturation magnetization of Pd/Co multilayers, which is obtained by dividing the magnetic moment by the Co volume, is shown as function of the Co thickness. At room temperature the magnetization of pure Co is 1.76 T, which means that in the multilayers an enhancement is

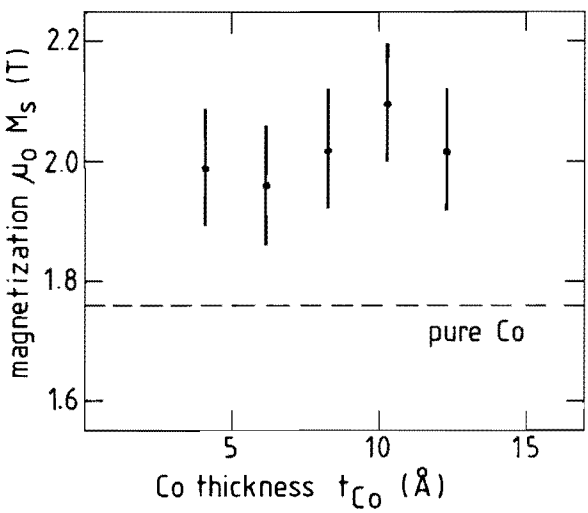

Fig. 5.4 *Saturation magnetization* $\mu_o M_s$, *calculated per volume unit* Co, *at* 20 °C *of multilayers consisting of* t_{Co} Co + 45 Å Pd, *as a function of* Co *layer thickness* t_{Co}. *As a reference, the magnetization of a pure* Co *film (when the thickness is large enough) at this temperature is indicated* (1.76 T).

observed. Table 5.2 gives an overview of the magnetization for various thickness combinations. For multilayers with 2 Å Co the enhancement is very strong, but it depends on the Pd thickness.

Table 5.2 *Saturation magnetization* $\mu_o M_s$ (T) *at room temperature for* Pd/Co *multilayers prepared by e-beam evaporation for different layer thicknesses of* Pd *and* Co, t_{Pd} *and* t_{Co} (Å).

t_{Pd} (Å)	$\mu_o M_s$ (T)					
	t_{Co}=2.0Å	t_{Co}=4.1Å	t_{Co}=6.1Å	t_{Co}=8.2Å	t_{Co}=10.2Å	t_{Co}=12.3Å
2.25	1.97					
4.5	2.77	2.36				
6.75	3.05	2.58				
9.0	3.03	2.69				
11.25	2.81					
13.5	2.73	2.54	2.58	2.20		1.96
18.0	2.80	2.70				
27.0	2.61	2.29	2.45	2.03	2.50	2.11
45.0		1.99	1.96	2.02	2.10	2.02

In Pd-Co alloys also enhancement of the magnetic moment per Co atom is found, which can be described by assuming a contribution of $0.5\mu_B$ per nearest neighbour (to a Co atom) Pd atom [14]. In diluted Pd-Co alloys, which show giant moment behaviour, the Co moment induces a small moment on surrounding Pd atoms via a strong, parallel, itinerant electron polarization extending for about 10 Å [15]. If we assume that in the multilayers only the Pd atoms which are nearest neighbours to Co atoms contribute to the magnetic moment, the magnetization should be independent

of the Pd thickness. Furthermore a part of the magnetization would depend on $1/t_{Co}$, at least when the magnetic moment of the Co atoms does not depend on the thickness. Neither of these characteristics have been found in the present case.

In another model a range r in the Pd layer is assumed in which a polarization of magnitude M'_{Pd} is induced by the neighbouring Co layer. If the ranges overlap (when the Pd thickness $t_{Pd} < 2r$), a polarization of M''_{Pd} is assumed. For the magnetization calculated per unit volume Co we find

$$\left.\begin{aligned} M &= M_{Co} + \frac{2r}{t_{Co}} M'_{Pd} && t_{Pd} > 2r \\ M &= M_{Co} + \frac{t_{Pd}}{t_{Co}} (2M'_{Pd} - M''_{Pd}) + \frac{2r}{t_{Co}} (M''_{Pd} - M'_{Pd}) && r < t_{Pd} < 2r \\ M &= M_{Co} + \frac{t_{Pd}}{t_{Co}} M''_{Pd} && t_{Pd} < r\ . \end{aligned}\right\} \quad (2)$$

M_{Co} and t_{Co} are the magnetization and thickness of the Co layer. In Fig. 5.5 the Pd thickness dependence is shown along with the data for 2 Å Co. The parameters used for this curve are a range r = 8 Å, $\mu_o M_{Co}$ = 2.4 T, $\mu_o M'_{Pd}$ = 0.03 T and $\mu_o M''_{Pd}$ = 0.16 T. Unfortunately the model is unable to fit the data for other thicknesses of Pd and Co as well.

Temperature dependence

According to spin-wave theory the temperature dependence of the magnetization is linear for a two-dimensional (2D) array of magnetic moments without anisotropy in the limit of low temperature [16]. Such a complete

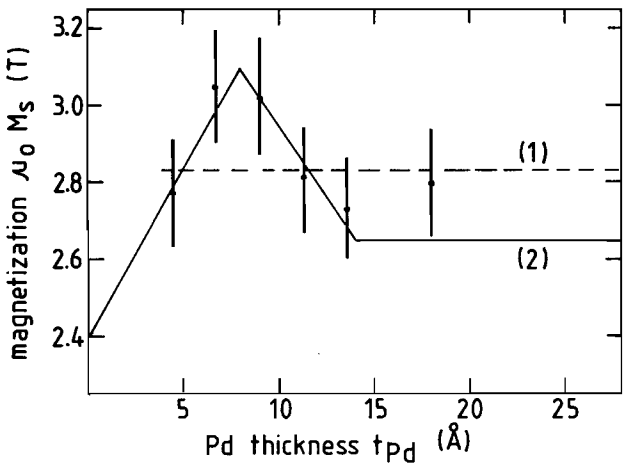

Fig. 5.5 *Saturation magnetization* $\mu_o M_s$ *at* 20 °C *of multilayers of* 2 Å Co + t_{Pd}, *as a function of Pd layer thickness* t_{Pd}. *The data are compared with two models:* (1) *polarization of* 0.6 μ_B *per* Pd *atom (broken line);* (2) *polarization of Pd within a range* r = 8 Å *(full line). Details of these models are dicussed in the text.*

linear dependence has been found in Fe/V multilayers when the thickness of the Fe layers was brought down to 3 atomic layers [17]. With the introduction of anisotropy in a film of N atomic layers Levy and Motchane [18] find

$$\frac{M_N(T)}{M_N(0)} = 1 - \frac{kT}{2\pi AN} \exp\left[-\frac{E}{kT}\right] , \qquad (3)$$

in which A is the spin-wave stiffness, E is the energy gap in the magnon spectrum due to the anisotropy and k is Boltzmann's constant.

The temperature dependence of the magnetization in Pd/Co multilayers is given in Fig. 5.6(a) for a fixed Co thickness (4 Å which is 2 atomic layers) and varying Pd thickness. The maximum temperature used in this measurement is 600 K, because above that temperature interdiffusion destroys the layered structure (see section 5.4). The temperature dependence is clearly affected by the thickness of the Pd layers, which indicates that there is some kind of long range interaction across these layers. From the fact that for 27 Å Pd and 45 Å Pd the same curves are obtained, it may be inferred that this interaction across the Pd layers is effectively reduced to zero, so that the range of the interaction is between 13.5 and 27 Å. This same range is also found in light scattering experiments on Co/Pd/Co sandwiches [19].

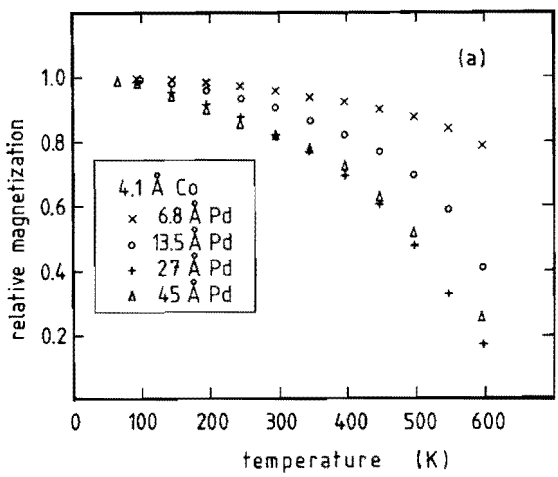

Fig. 5.6(a) *Temperature dependence of the magnetization of multilayers with* 4.1 Å Co *layers and different* Pd *thicknesses. The average composition of these multilayers is, respectively,* 0.45, 0.29, 0.17 *and* 0.11 at.% Co. *The total thickness of each multilayer is* 3000 Å.

If we fit the data with $M(T)/M(0) > 0.6$ to relation (3) we find A/k and E/k as listed in Table 5.3. For pure Co A/k is about 470 K [20]. The dependence of these parameters on the thickness of Pd suggests that the derivation of relation (3) for a single layer should be modified to include the above-mentioned long-range interaction.

Table 5.3 *Spin-wave stiffness A/k and magnon energy gap E/k from relation (3) for the data in* Fig. 5.6(a).

sample	A/k (K)	E/k (K)
4 Å Co + 6.8 Å Pd	180 ± 20	320 ± 30
4 Å Co + 13.5 Å Pd	90 ± 10	280 ± 30
4 Å Co + 27 Å Pd	60 ± 10	250 ± 30
4 Å Co + 45 Å Pd	70 ± 10	200 ± 20

As a reference, Pd-Co alloy thin films with the same range of average composition as the multilayers were prepared by coevaporation. The thickness of these thin films was 3000 Å, the same as the total thickness of the multilayers. The temperature dependence of these films is given in Fig. 5.6(b) which shows a continuous decrease of magnetic order for a given temperature with decreasing concentration of Co.

Conclusion

The enhancement of the magnetization in Pd/Co multilayers is very high, but can not be explained for all thicknesses with simple models. Especially the maximum in the magnetization as a function of Pd thick-

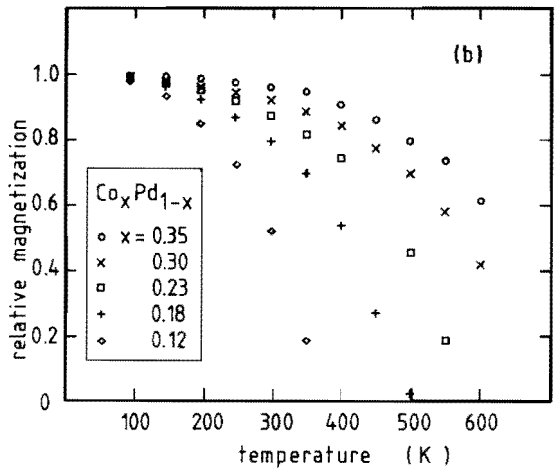

Fig. 5.6(b) *Temperature dependence of the magnetization in* Pd-Co *alloy films showing a continuous decrease of magnetic order when the* Co *concentration decreases.*

ness and fixed Co thickness is interesting but not well understood. The temperature dependence of the Pd/Co multilayers shows that there is an interaction between the Co layers over the Pd layers with a maximum range in the order of 25 Å.

5.3 Analysis of the perpendicular magnetization curves *)

Abstract

In a ferromagnetic thin film with strong perpendicular anisotropy, saturation may be reached at fields lower than the magnetization . This

*) part of this text has been published in the Journal of Applied Physics **62** (1987) 3318

field is calculated for a multilayer with alternating ferromagnetic and nonmagnetic layers assuming that the stripe domains are oriented only up or down along the anisotropy axis. The results are compared with experimental data on Pd/Co multilayers with ultra-thin Co layers. The agreement is very good if we take $\sigma_w = 1 \cdot 10^{-3}$ J/m^2 as the energy of walls between the domains.

Introduction

Multilayer thin films consisting of periodically alternating ferromagnetic and nonmagnetic layers may have interesting new properties. In vapour deposited Pd/Co multilayers high perpendicular anisotropy has been found when the Co layers are very thin (< 8 Å). This anisotropy can be attributed to the interface between Pd and Co (cf. section 5.1). The high remanent magnetization which is found when the Co layers are reduced to 2 Å, may be an important parameter to obtain a high signal-to-noise ratio in magnetic recording [21].

In this section we will examine the shape and properties of the perpendicular magnetization curve of multilayers without taking into account any coercivity effects. This means that the domain walls will be assumed to be completely freely mobile. It is further assumed that for low fields the effect of the coercivity can be approximated by shifting the calculated magnetization curve along the field axis. In this way we expect to obtain a high remanence when the perpendicular field in which the magnetization saturates is smaller than the coercive field. The results of the calculations will be compared with experimental data on Pd/Co multilayers, but will in principle be applicable to any multilayer thin film having perpendicular anisotropy in the ferromagnetic layers.

Perpendicular magnetization curves

Let us consider a multilayer with N bilayers consisting of a ferromagnetic layer of thickness t and a nonmagnetic layer of thickness s. We assume that the perpendicular anisotropy is large enough to orient all (stripe) domains up or down. When this is not the case, closure domains may shortcircuit the magnetic flux. The domain walls are assumed to be infinitely thin and freely mobile resulting in a periodic domain structure as shown in Fig. 5.7. In the z-direction the domains are parallel and in order to obtain a minimum magnetostatic energy the domain walls will be at the same positions in all layers. The magnetization in each domain is the spontaneous magnetization M_s, the width of the domains

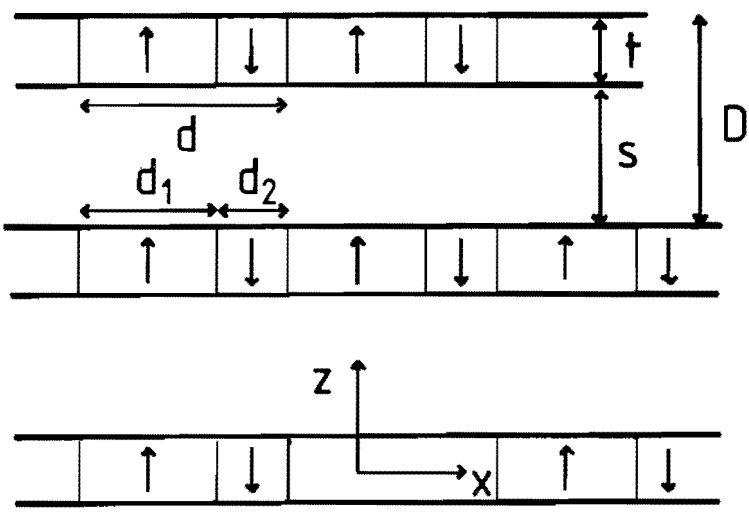

Fig. 5.7 *Model of a domain structure in a multilayer with alternating ferromagnetic and nonmagnetic layers. The domain walls are infinitely thin and freely mobile resulting in a periodic structure. In the perpendicular direction (z) parallel oriented domains will give the lowest magnetostatic energy.*

with upward magnetization is d_1 and with downward magnetization d_2, yielding a net magnetization of

$$\tilde{M} = \frac{d_1 - d_2}{d_1 + d_2} M_s \quad . \tag{4}$$

The magnetic energy of this domain structure contains three terms: the magnetostatic or demagnetizing energy E_d, originating from the poles at the interfaces between the ferromagnetic and nonmagnetic layers, the wall energy E_w of the domain walls between neighbouring domains and the field energy E_h arising from the interaction of the magnetization with the applied magnetic field along the positive z-axis. All the energies are calculated per unit volume of the ferromagnetic material and will be normalized to the maximum magnetostatic energy $\frac{1}{2}\mu_o M_s^2$.

In the appendix at the end of this section we show that the magnetostatic energy can be written as:

$$e_d = \frac{E_d}{\frac{1}{2}\mu_o M_s^2} = m^2 + \sum_{n=1}^{\infty} \frac{4}{(n\pi)^3} \frac{d}{t} \sin^2\left[\tfrac{1}{2}\pi n(m+1)\right] f_n(d)$$

with (5)

$$f_n(d) = 1 - \exp\left[-2\pi\, n\, \frac{t}{d}\right] + \frac{\sinh^2(\pi\, n\, \frac{t}{d})}{\sinh^2(\pi\, n\, \frac{D}{d})} \times \left\{ \frac{1}{N} \left[1-\exp\left[-2\pi n \frac{N\, D}{d}\right]\right] - \left[1-\exp\left[-2\pi n \frac{D}{d}\right]\right] \right\}$$

and with $m = \tilde{M}/M_s$ as relative average magnetization. For $N = 1$ $f_n(d)$ is identical to the expression derived by Kooy and Enz [22] and e_d is independent of s (and D).

Assuming a specific wall energy of σ_w per unit area of a domain wall, we can write:

$$e_w = \frac{E_w}{\frac{1}{2}\mu_o M_s^2} = \frac{2\,\sigma_w}{d\,\frac{1}{2}\mu_o M_s^2} = \frac{2\,\tau}{d}\ , \qquad (6)$$

in which $\tau = \frac{\sigma_w}{\frac{1}{2}\mu_o M_s^2}$ is a length characteristic for the ferromagnetic material under consideration. τ can assume values ranging from a few nanometers to many micrometers.

Finally we have

$$e_h = \frac{E_h}{\frac{1}{2}\mu_o M_s^2} = \frac{-\mu_0 H\,\tilde{M}}{\frac{1}{2}\mu_o M_s^2} = -\,2\,h\,m\ , \qquad (7)$$

where $h = H/M_s$ is the normalized field, applied perpendicular to the film.

The total energy $e = e_d + e_w + e_h$ can be minimized with respect to the domain repetition length d and the magnetization m, which is the same as minimizing with respect to the domain lengths d_1 and d_2:

$$\frac{\partial e}{\partial d} = 0 \quad \rightarrow \quad d = \left\{ \frac{2\,\tau}{\left[\frac{\partial e_d}{\partial d} \right]} \right\}^{\frac{1}{2}} \qquad (8)$$

$$\frac{\partial e}{\partial m} = 0 \quad \rightarrow \quad h = m + \sum_{n=1}^{\infty} \frac{1}{(n\pi)^2} \frac{d}{t} \sin[\pi n(m+1)]\ f_n(d) \qquad (9)$$

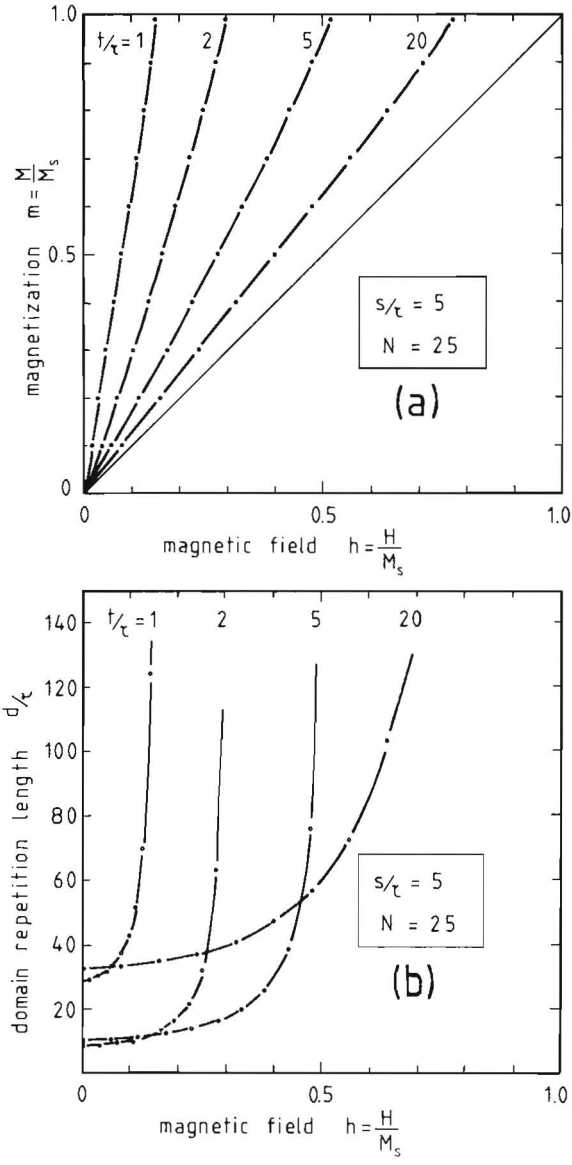

Fig. 5.8(a) *Perpendicular magnetization curves for multilayers with 25 bilayers ($N = 25$), a nonmagnetic layer thickness $s/\tau = 5$, and different ferromagnetic layer thicknesses t/τ; (b) domain repetition length d/τ corresponding to the magnetization curves.*

The calculation procedure is to choose a magnetization m, calculate d from (8) and to find the field at which this magnetization is reached from (9). It is to be noted that all length parameters (t,s,d) can be taken relative to the specific length τ, since only ratios of lengths appear in the formulas. As parameters we have N, t/τ and s/τ which describe the perpendicular magnetization curve completely. The results in this section were obtained by numeric computation of (8) and (9). Much attention was paid to the slow convergence of the series, especially in the case of large d/τ.

In Fig. 5.8 a number of curves, giving combinations of h, m and d/τ, is shown for $N=25$, $s/\tau=5$, and different values of t/τ. The results show a compromise between the opposing tendencies of the individual energy terms: the greater the domain repetition length d/τ, the lower the wall energy will be. The poles of the domains at each side of the nonmagnetic layer also favour a large d/τ, but neighbouring poles of reversed domains do the opposite. If there is no magnetic field, the situation is symmetric, $d_1=d_2$ and d is twice the domain size. The introduction of h along the domain direction increases the size of one kind of domain at the expense of the other, in first instance without seriously affecting the repetition length d as can be seen in Fig. 5.8(b). The minimum of d/τ at $h=0$ for a specific value of the ferromagnetic layer thickness t/τ is also observed for single layers [23]. For $N=1$ the curves are independent of s/τ and completely in accordance with those reported for a single layer by Kooy and Enz [22].

Saturation fields

The concave shape as in Fig. 5.8(a) is obtained for any set of parameters. We will now focus our attention to the magnetic field at which saturation is reached. We will consider the field $h_s = H_s/M_s$ at which $m = 0.99$. Fig. 5.9 shows the increase of h_s with increasing thickness t/τ for a single ferromagnetic layer. In Fig. 5.10 the dependence of h_s on the thickness of the nonmagnetic layers in a multilayer, s/τ, is shown for different N and t/τ. In the limit of large s/τ and arbitrary N we find the same value for h_s as for $N = 1$ because the layers are magnetostatically decoupled. For very small values of s/τ the multilayer behaves magnetically as a single ferromagnetic layer of thickness $N\,t/\tau$. The transition between these two limiting cases takes place for $s/\tau = 1$ to 10.

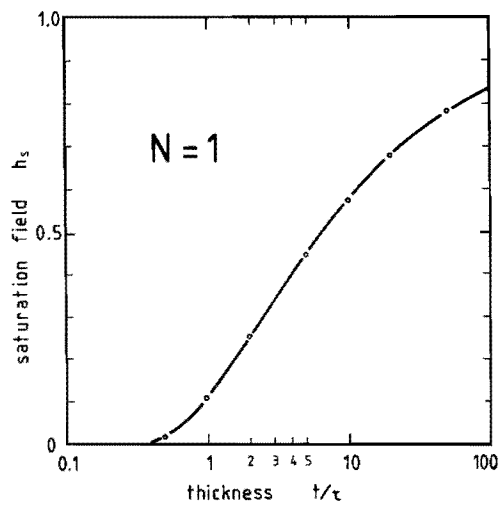

Fig. 5.9 *Saturation field h_s for a single ferromagnetic layer as function of thickness of the layer t/τ. The limiting cases of a multilayer ($s/\tau < 1$ or $s/\tau > 10$) can be treated as a single film.*

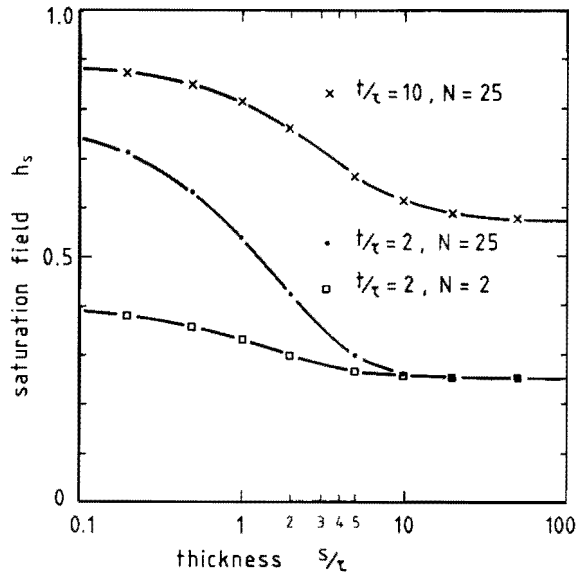

Fig. 5.10 *Saturation field h_s of a multilayer as a function of thickness of the nonmagnetic layers s/τ for different values of the ferromagnetic layer thickness t/τ and the number of bilayers N.*

Comparison with experimental data

The results derived above can be compared with experimental data which have been obtained on vapour deposited Pd/Co multilayers. Only in the cases of 2 Å and 4 Å Co the anisotropy in the Co layers is large enough to ensure that only up and down domains will exist. In Fig. 5.11 we show a number of magnetization curves for multilayers with 4 Å Co and different Pd thicknesses. The determination of the saturation field is somewhat complicated by the observed hysteresis, but the decrease of H_s with increasing Pd thickness is obvious. H_s is estimated by drawing a line through the origin parallel to both branches of the perpendicular magnetization curve; the results are given in Table 5.4. Using for the

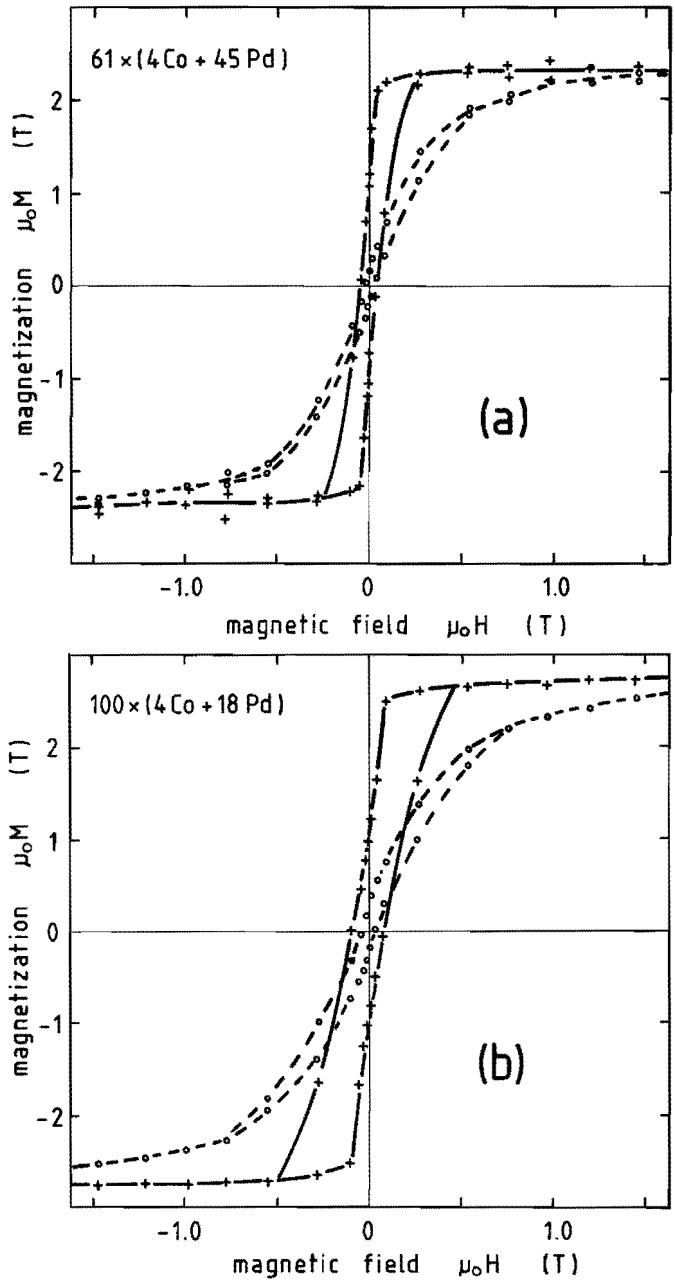

Fig. 5.11 *Magnetization curves of* Pd/Co *multilayers with the field applied in the direction applied perpendicular to the film (solid) and*

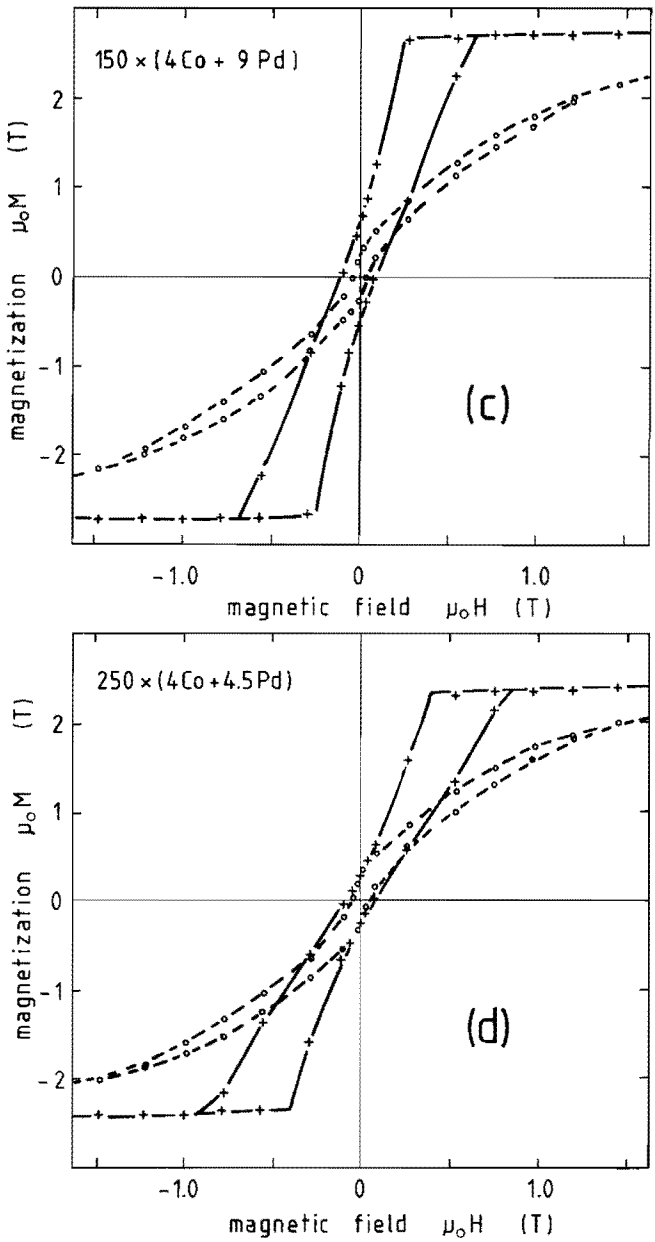

parallel to the film (dashed). The films contain 4 Å Co *layers with different Pd thicknesses:* 45 Å Pd (a), 18 Å Pd (b), 9 Å Pd (c) *and* 4.5 Å Pd (d).

magnetization of the Co layers the same value as for bulk Co, as seems to be justified by previous measurements (cf. section 5.1), we obtain a good agreement for τ = 8 Å, which yields for the energy of a domain wall in these layers $\sigma_w = 1 \cdot 10^{-3}$ J/m^2. Also for multilayers with 2 Å Co layers the comparison is very satisfactory, using the same parameters. It is the low value of H_s combined with a large coercive field which results for these multilayers in a high remanence (0.95-0.99) [21].

Table 5.3 *Comparison of the saturation fields of vapour deposited* Pd/Co *multilayers* $h_s(exp)$, *as estimated from the magnetization curves, with the calculated fields* $h_s(calc)$. *A good agreement is found for* $\mu_o M_s$ = 1.76 T, *as for bulk* Co, *and* τ = 8 Å. *The resulting domain wall energy is* $\sigma_w = 1 \cdot 10^{-3}$ J/m^2.

t_{Co} (Å)	t_{Pd} (Å)	N	$\mu_o H_s$ (T)	h_s(exp)	t/τ	s/τ	h_s(calc)
4	4.5	250	0.69	0.39	0.5	0.56	0.404
4	9	150	0.45	0.26	0.5	1.13	0.254
4	18	100	0.27	0.15	0.5	2.25	0.147
4	45	61	0.12	0.07	0.5	5.63	0.065
2	4.5	300	0.38	0.22	0.25	0.56	0.254
2	6.7	250	0.36	0.20	0.25	0.84	0.186
2	9	200	0.25	0.14	0.25	1.13	0.144
2	11.2	200	0.23	0.13	0.25	1.4	0.121
2	13.5	150	0.20	0.11	0.25	1.69	0.100
2	18	100	0.15	0.09	0.25	2.25	0.079

The direct comparison of a calculated curve with experimental data is complicated by the hysteresis, but they both show the same concave shape. The quantitative agreement between theoretical results and experimental data for this system is somewhat surprising in view of the rather crude approximations we have used. In fact, the actual situation in the Pd/Co multilayers is much more complicated. To explain the observed magnetization, polarization of some of the Pd atoms was introduced (cf. section 5.2), whereas in our model Pd is treated as a vacuum. Furthermore light scattering experiments on Fe/Pd/Fe sandwiches indicate an exchange coupling over Pd layer thicknesses up to 30 Å [24]. Although this additional coupling is not incompatible with our model (since the domains at both sides of a Pd layer are parallel), it might influence the value of the domain wall energy and thus the value of τ.

Conclusion

The effect of the Pd thickness on the magnetization curve of a Pd/Co multilayer with perpendicular anisotropy can be understood both qualitatively and quantitatively by the magnetostatic interaction between the perpendicular domains. By choosing a suitable combination of parameters the saturation field in such multilayers can be reduced, resulting in a high relative remanent magnetization when the coercive field is sufficiently large.

From this model predictions about the domain sizes can be made, in partially magnetized as well as in demagnetized states. It would be very interesting to compare these with observations from direct domain imaging techniques.

Appendix

The magnetostatic energy of domains oriented perpendicular to a thin film or plate has been treated by several authors: Kittel [25] considered a homogeneous ferromagnetic film in the limit of non-interacting sides and in the demagnetized state, in which up and down domains are of equal size. Málek and Kambersky [23] included the interaction between the sides of the plate. Kooy and Enz [22] extended the calculation to magnetized states. Very recently Suna [26] considered the problem of magnetostatic interactions in a multilayer, but only in the demagnetized state. For clarity and to avoid notational problems, we will give a survey of the entire calculation.

To calculate the magnetostatic energy of a domain configuration as shown in Fig. 5.7, we first need the potential φ ($H = -\nabla\varphi$) of a single layer, which satisfies the Laplace equation

$$\nabla^2 \varphi = 0 \ , \tag{10}$$

with the proper boundary conditions. We distinguish between the regions outside the layer ($\varphi_o(x,z)$, $z > \frac{1}{2}t$) and inside the layer ($\varphi_i(x,z)$, $-\frac{1}{2}t \leq z \leq \frac{1}{2}t$). By antisymmetry in z, we have for $z < -\frac{1}{2}t$, $\varphi(x,z) = -\varphi_o(x,-z)$. According to this model we write the magnetization as

$$\left.\begin{array}{rll} M(x,z) = M_s & -\frac{1}{2}d_1 \leq x < \frac{1}{2}d_1 & \wedge \ -\frac{1}{2}t \leq z < \frac{1}{2}t \\ -M_s & \frac{1}{2}d_1 \leq x < \frac{1}{2}d_1 + d_2 & \wedge \ -\frac{1}{2}t \leq z < \frac{1}{2}t \\ 0 & z < -\frac{1}{2}t & \vee \ z > \frac{1}{2}t \ , \end{array}\right\} \tag{11}$$

while it is periodic in x over a distance $d = d_1 + d_2$: $M(x+d,z) = M(x,z)$. Written as a Fourier series this becomes ($-\frac{1}{2}t \leq z \leq \frac{1}{2}t$)

$$M(x,z) = \tilde{M} + \sum_{n=1}^{\infty} \frac{4\,M_s}{\pi\,n} \sin[\tfrac{1}{2}\pi n(m+1)] \cos[2\pi n \frac{x}{d}] \ , \qquad (12)$$

in which $\tilde{M} = \frac{d_1 - d_2}{d} M_s$ is the average magnetization and $m = \tilde{M}/M_s$.

As boundary conditions we now have

$$\left.\begin{aligned} -\frac{\partial \varphi_o}{\partial z}(x,\tfrac{1}{2}t) &= -\frac{\partial \varphi_i}{\partial z}(x,\tfrac{1}{2}t) + M(x,\tfrac{1}{2}t) \\ \varphi_o(x,\tfrac{1}{2}t) &= \varphi_i(x,\tfrac{1}{2}t) \ . \end{aligned}\right] \qquad (13)$$

A general solution of equation (10) taking into account the shape of the (x,z) region to which it should apply, can be written as

$$\varphi(x,z) = A_0 + B_0\, z + \sum_{k=1}^{\infty} \left[A_k \cos(2\pi k \frac{x}{d}) \exp(-2\pi k \frac{z}{d}) + B_k \cos(2\pi k \frac{x}{d}) \exp(2\pi k \frac{z}{d}) \right]. \qquad (14)$$

If we substitute (14) in (13) we obtain

$$\varphi_o(x,z) = \tfrac{1}{2}\tilde{M}\, t + \sum_{k=1}^{\infty} \frac{2M_s\, d}{(\pi k)^2} \sin[\tfrac{1}{2}\pi k(m+1)] \sinh(\pi k \frac{t}{d}) \times \cos(2\pi k \frac{x}{d}) \exp(-2\pi k \frac{z}{d}) \qquad (15a)$$

$$\varphi_i(x,z) = \tilde{M}\, z + \sum_{k=1}^{\infty} \frac{2M_s\, d}{(\pi k)^2} \sin[\tfrac{1}{2}\pi k(m+1)] \exp(-\pi k\, \frac{t}{d}) \times \cos(2\pi k\, \frac{x}{d}) \sinh(2\pi k\, \frac{z}{d}) \quad . \qquad (15b)$$

Now the multilayer problem with parameters as in Fig. 5.7 (p. 103) can be solved. By superposition, the total potential $\varphi_p(x,z)$ in layer p, originating from all the N layers, with $z=0$ in the center of layer p and $\varphi_p(x,0) = 0$ is

$$\varphi_p(x,z) = \sum_{j=1}^{p-1} [\, \varphi_o(x, z+(p-j)D) - \varphi_o(x, (p-j)D) \,] + \varphi_i(x,z) - \sum_{j=p+1}^{N} [\, \varphi_o(x, (j-p)D-z) - \varphi_o(x, (j-p)D) \,] \qquad (16)$$

with the minus sign resulting from the antisymmetry. The corresponding energy density involved for layer p is

$$E_p = \frac{\mu_o}{2\, d\, t} \int_0^d dx\; M(x, \tfrac{1}{2}t) \, [\varphi_p(x, \tfrac{1}{2}t) - \varphi_p(x, -\tfrac{1}{2}t)] \qquad (17)$$

Inserting (15) and (16) and using the Fourier series (12), the only terms that remain after the integration over x are those with $n=k$:

$$E_p = \tfrac{1}{2}\mu_o \left\{ \tilde{M}^2 + \sum_{n=1}^{\infty} \frac{4\, M_s^2}{(\pi n)^3} \frac{d}{t} \sin^2[\tfrac{1}{2}\pi n(m+1)] \left[1 - \exp(-2\pi n\, \frac{t}{d}) - 2\sinh^2(\pi n\, \frac{t}{d}) \left[\frac{\exp(-2\pi n\, \frac{(p-1)D}{d}) + \exp(-2\pi n\, \frac{(N-p)D}{d}) - 2}{1 - \exp(2\pi\, n\, \frac{D}{d})} \right] \right] \right\} . \qquad (18)$$

Normalizing the energy to $\frac{1}{2}\mu_o M_s^2$, the maximum magnetostatic energy, and averaging over all the layers we have

$$e_d = \frac{1}{N} \frac{\sum_{p=1}^{N} E_p}{\frac{1}{2}\mu_o M_s^2} \qquad (19)$$

resulting in expression (5).

5.4 Stability of Pd/Co multilayers *)

Abstract

Polycrystalline Pd/Co multilayers containing Co layers with a thickness of several atomic layers and having perpendicular magnetic anisotropy were subjected to temperature treatments up to 400 °C and to 600 keV Kr^+ bombardment. As a result of the mixing of Pd and Co layers these treatments led to a decrease of the anisotropy, coercivity and remanence. A quantative study of the diffusion by means of X-ray diffraction indicates that the diffusion occurs primarily along grain boundaries, after a short initial relaxation stage. In this latter stage the activation energy of diffusion is 1.1 eV.

*) part of this text has been published in the IEEE Transactions on Magnetics MAG-23 (1987) 3696

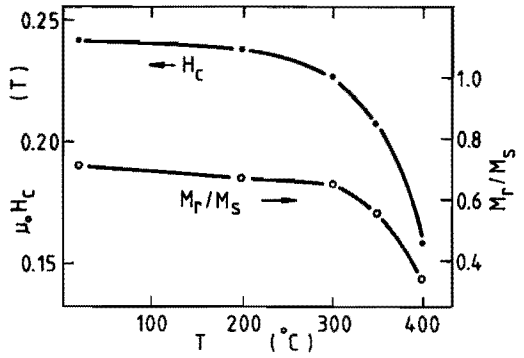

Fig. 5.12 *Coercivity* $\mu_o H_c$ *and remanence* M_r/M_s *for the multilayer* 345×(2 Å Co + 6.7 Å Pd) *as a function of annealing temperature. Each heat treatment lasted* 15 min.

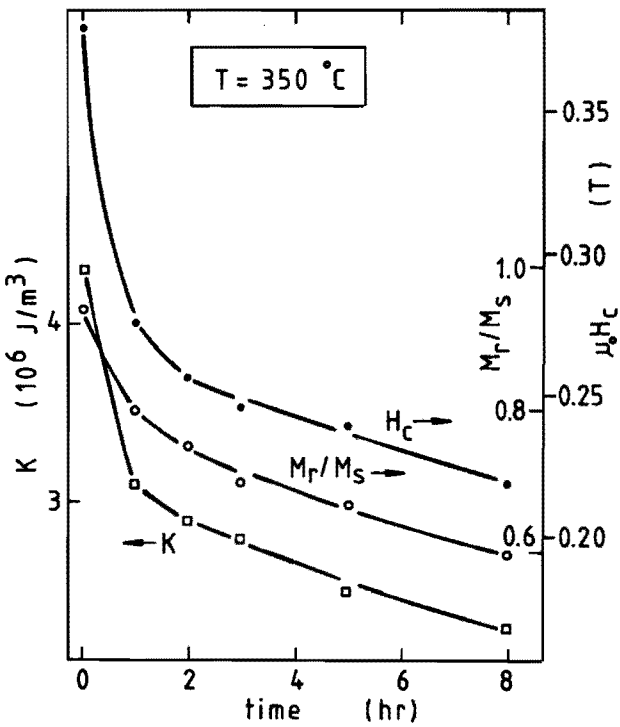

Fig. 5.13 *Anisotropy K, remanence ratio* M_r/M_s *and coercivity* $\mu_o H_c$ *of the multilayer* 275×(2 Å Co + 9 Å Pd) *as a function of annealing time at* 350 °C.

Introduction

In Pd/Co multilayers the easy magnetization direction is perpendicular to the film when the Co thickness is below 8 Å. This is attributed to the magnetic surface anisotropy of the Pd/Co interface. If these interfaces are destroyed it is expected that the perpendicular anisotropy disappears.

The present section deals with the response of coercivity, remanence and anisotropy of Pd/Co multilayers to thermal annealing and ion bombardment. In order to interpret the changes in magnetic properties due to annealing, the diffusion was quantitatively studied by X-ray diffraction (XRD). Diffusion data for the present multilayers are important to describe their thermal stability.

Thermal annealing

In Fig. 5.12 is shown that the coercivity H_c and the remanence to saturation ratio M_r/M_s of a multilayer containing Co monolayers remain surprisingly constant after annealing up to about 300 ^{o}C. At higher temperatures noticeable changes in these properties start to occur. Also the XRD superlattice reflections begin to become weaker after reaching this temperature. This indicates a relatively high thermal stability of these multilayers, with the Co monolayers only starting to dissolve in the Pd matrix at about 300 ^{o}C. The anisotropy changes sign (from out of plane to in-plane) after heating the multilayer for several hours at 400 ^{o}C.

Fig. 5.13 shows the change in H_c and M_r/M_s as a function of annealing time at 350 ^{o}C for a sample consisting of 345*(2Å Co + 6.7Å Pd). Also

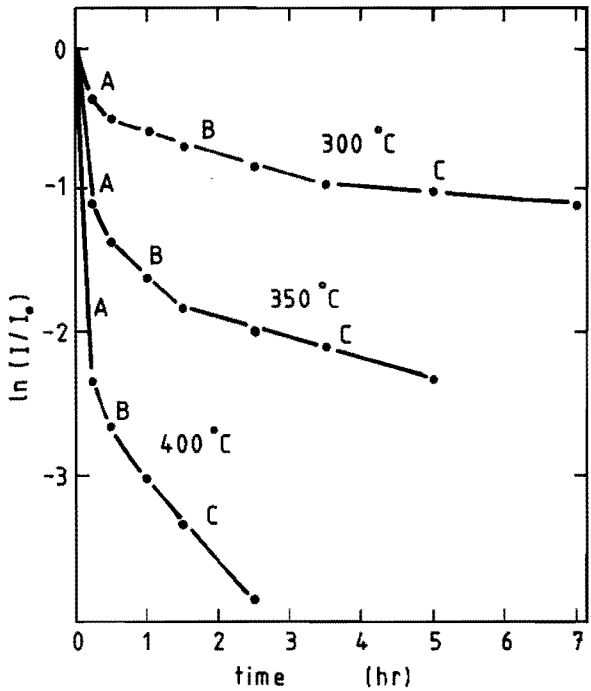

Fig. 5.14 *Decay of the relative XRD satellite intensity I/I_o of the multilayer 200×(4.7 Å Co + 10.6 Å Pd) as a function of diffusion time.*

Table 5.5 *Effective diffusion coefficient $\tilde{D}$ and activation energies E for stages B and C in Fig. 5.14.*

T (°C)	$\tilde{D}$ (m^2/s) stage B	$\tilde{D}$ (m^2/s) stage C
300	$1.6 \cdot 10^{-24}$	$3.1 \cdot 10^{-25}$
350	$3.9 \cdot 10^{-24}$	$1.2 \cdot 10^{-24}$
400	$7.2 \cdot 10^{-24}$	$4.6 \cdot 10^{-24}$
E (eV)	0.5	1.1

plotted is the uniaxial anisotropy K, which is defined as the difference in energy between the parallel and perpendicular saturated state. It is seen that the decrease of H_c is accompanied by a corresponding decrease of M_r/M_s. Indeed, the ratio M_r/H_c remains virtually constant as appears from the non-changing slope of the magnetization curve. The variation in K with time seems fundamental to the change in H_c and M_r/M_s. It is of interest to note that these properties show a rapid initial decrease, followed by a slower change after prolonged heating.

The interdiffusion was examined by measuring the decrease in intensity of the XRD reflections. The diffusion constant $\tilde{D}$ for a sinusoidal modulation with wavelength D can be obtained from

$$\tilde{D} = - \frac{D^2}{8\pi^2} \frac{\mathrm{d}\ \ln(I/I_o)}{\mathrm{d}\ t} \quad . \tag{20}$$

I is the intensity after time t and I_o the initial intensity [27]. In the present study we used the relative intensity of the three strongest reflections.

Fig. 5.14 shows the results for three different temperatures. It is seen that the mixing process can be divided into a rapid intitial stage A, a transition stage B and a final stage C. The initial stage A may be explained by fast diffusion accompanying structural relaxation and recrystallization. Such an initial effect is commonly observed in modulated thin films [28]. For stages B and C diffusion constants and activation energies have been evaluated, as given in Table 5.5. For Pd-Co lattice diffusion an activation energy of about 2.3 eV has been reported

[29], while for diffusion of Au along Pd grain boundaries an activation energy of 0.9 eV has been found [30]. From this we conclude that stage C (E = 1.1 eV) is connected with grain boundary diffusion.

Ion bombardment

A sample of 275*(2Å Co + 6.7Å Pd) has been irradiated with 600 keV Kr^+ at 20 °C in a vacuum of 10^{-6} Torr. The energy and the ion species were chosen so that a maximum of the radiation damage could be expected in the centre part of the multilayer. Higher doses result in a broadening of the damage profile.

Fig. 5.15 shows that H_c, M_r/M_s and K start to decrease after a dose ϕ = 10^{13} Kr^+/cm^2. Until after a dose of ϕ = 10^{15} Kr^+/cm^2 the film has an easy plane anisotropy. At that stage XRD did not reveal superlattice reflections anymore, but only those of a disordered alloy. Therefore the drop in K by irradiation is due to ion beam induced mixing of Pd and Co.

These results are of interest in view of our experience that Pd/Co multilayers prepared by ion beam sputtering with 1.5 keV Ar^+ ions have always an easy-plane anisotropy irrespective of the Co thickness. We may explain this by Pd-Co mixing at the interfaces due to bombardment during the deposition with Ar^+ ions that have been reflected from the targets. Although the penetration depth of 1.5 keV Ar^+ is only about 30 Å, the continuous bombardment during deposition leads to a damage which is homogeneously distributed over the whole thickness of the multilayer.

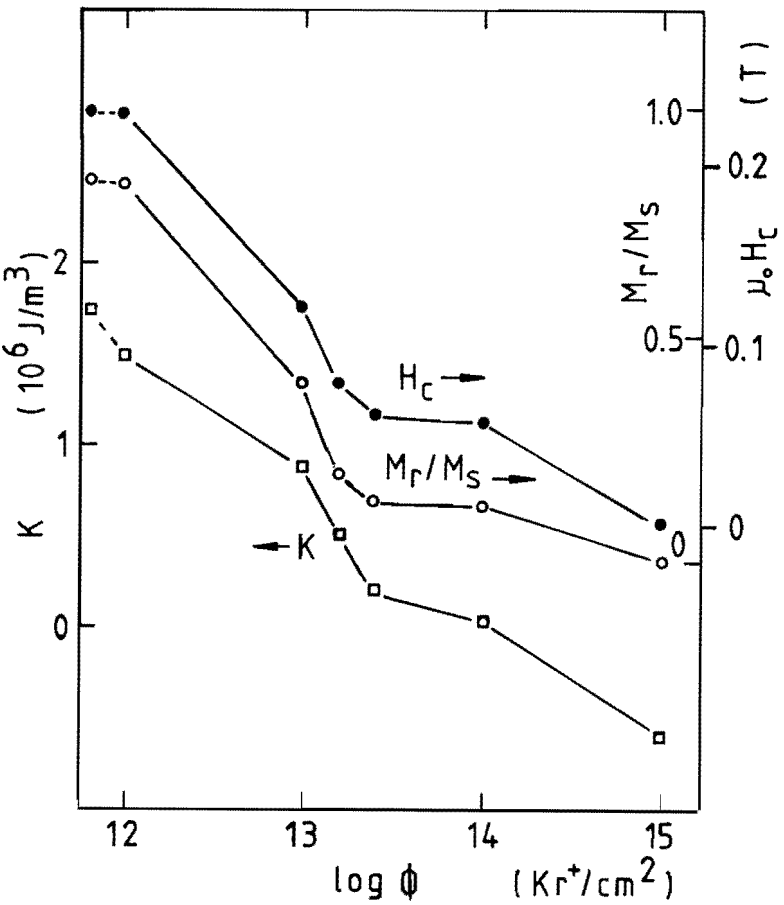

Fig. 5.15 *Anisotropy K, remanence ratio* M_r/M_s *and coercivity* $\mu_o H_c$ *of the multilayer* 345×(2 Å Co + 6.7 Å Pd) *as a function of irradiation dose* ϕ *of* 600 keV Kr^+.

Conclusion

In conclusion, the decrease of the coercivity and the remanence is accompanied by a reduction of the anisotropy, whereas the saturation magnetization M_s slightly increased upon diffusion. In principle, the

perpendicular interface anisotropy can be attributed to an anisotropic Pd-Co distribution. A decrease of this anisotropy is then described by a change of this distribution into a more isotropic one. However, it may be difficult to apply such a model to polycrystalline multilayers, where grain boundary diffusion leads to a mixture of well- and ill-homogenized regions.

In contrast to the Pd-Co system, in which a continuous series of solid solutions can be formed, the combination of Au-Co do not allow the formation of alloys. In that case, annealing of a multilayer system does not lead to diffusion between the layers, but it can lead to segregation of the seperate layers. Au/Co multilayers prepared by ion beam sputtering (cf. section 2.5) with 8 Å Co layers showed a change of the anisotropy from in-plane to out of plane upon annealing at temperatures of 400 ^{o}C [31]. This is the opposite effect of the change observed for the Pd/Co multilayers, where the interfaces become more diffuse.

5.5 The influence of interface roughness on the anisotropy *)

Abstract

The anisotropy values in polycrystalline Pd/Co multilayers with [111] texture as determined from magnetization measurements and torque measurements are compared . It is concluded that the most reliable value is

*) part of this text has been published in the Journal of Applied Physics **63** (1988) 3479

obtained from the first ones. In a pair interaction model for the interface anisotropy it is shown that it is very sensitive to the precise distribution of Co and Pd at the interfaces. From the experimental data we derive a lower bound value of 0.2 meV per Co atom for the energy change with the direction of the magnetic moment.

Introduction

One of the intriguing aspects of magnetic multilayers is the reduced symmetry at the interfaces, which can lead to a considerable contribution to the total anisotropy. In polycrystalline Pd/Co multilayers with [111] texture this leads to a preferred direction for the magnetization perpendicular to the film plane when the Co thickness is below 8 Å (cf. section 5.1). The values for the anisotropy in these multilayers were obtained from the area between the parallel and perpendicular magnetization curves as measured with a vibrating sample magnetomeer (VSM). As has been shown in section 5.1, the anisotropy is independent of the thickness of the Pd layers and can be interpreted as the sum of an interface and a volume contribution of the Co layers. The influence of the Pd layers on the magnetization curves has been described in section 5.3. In this section we present additional measurements on new samples of Pd/Co, prepared by electron beam evaporation, and compare the values for the total anisotropy resulting from torque and magnetization measurements with the values of previous samples (section 5.1) and of Pd/Co multilayers prepared by rf-sputtering [10]. Further we examine the effect of interdiffusion on the anisotropy with a pair interaction model.

Torque measurements

Torque measurements provide a direct way to determine the magnetic anisotropy in ferromagnetic materials [32]. In thin films with rotational symmetry around the axis perpendicular to the film plane, the anisotropy can be written as

$$K(\vartheta) = K_1 \sin^2\vartheta + K_2 \sin^4\vartheta + \ldots \qquad (21)$$

in which ϑ is the angle between the magnetization and the perpendicular axis. K_1 includes the magnetostatic energy (or demagnetization energy) as a negative term, since in multilayers with inhomogeneous magnetization this contribution can not be distinguished from contributions of crystalline and magneto-elastic origin with the same angular dependence. The measurement results in the torque, T, acting on the sample as a function of the angle, φ, between the applied field and the axis normal to the film plane. The most accurate way to interpret the data is to determine the slope of the curve at angles where the torque is zero [33]. It can easily be found that for $\varphi = 0$ this slope can be written as

$$\left[\frac{dT}{d\varphi} \right]_{\varphi=0} = - \left[\frac{1}{2K_1} + \frac{1}{MB_o} \right]^{-1} \qquad (22)$$

in which B_o is the applied magnetic field (in T) and M is the magnetization in the film (in A/m). B_o should be large enough to saturate the sample and keep the angle between the magnetization and the applied field small. When K_1 is positive, the slope will be negative and vice versa.

For a series of Pd/Co multilayers with varying Co thickness we measured the torque curve using a standard torque magnetometer (TRT-2 from Toei Kogyo Co., Japan) in a field B_o = 1.75 T , which was the highest field available. The results, shown in Fig. 5.16, indicate a sign change of the anisotropy for Co layers between 6 and 10 Å in agreement with previous VSM measurements. In Fig. 5.17 the values K_1 found from the slope of the torque curves are compared to the values determined from the area between the magnetization curves with the magnetic field parallel and perpendicular to the film plane. Though the last method measures the total anisotropy $K = K_1 + K_2 + \ldots$, K_1 is often the dominating

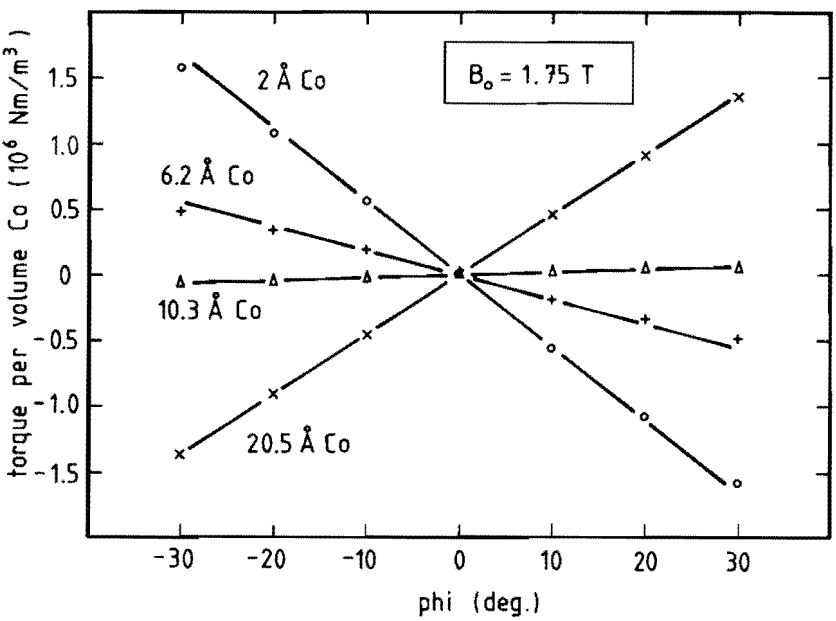

Fig. 5.16 *The torque per unit volume Co as a function of the angle φ between the applied field (B_o = 1.75 T) and the axis perpendicular to the film plane, indicates a sign change of the anisotropy as the Co layers become thinner. From the slope of the tangent at $\varphi = 0$, given by the straight lines, the anisotropy constant K_1 can be calculated.*

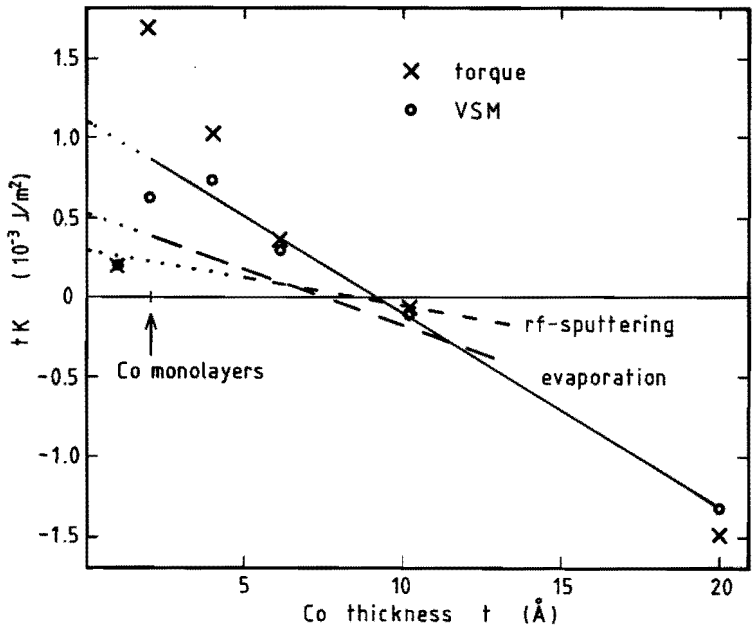

Fig. 5.17 *Anisotropy per area of one Co layer as function of the thickness of the Co layer reveals the interface and volume contribution to the anisotropy. A comparison is made for rf-sputtered samples* [10], *previously vapour deposited samples (cf. section* 5.1) *and the present samples, also prepared by vapour deposition. The data are given for these latter samples. The length of the lines indicates the range of Co thicknesses studied in each series of experiments.*

term. For the samples with Co thickness larger than 6 Å the comparison is quite good, but deviations begin to occur for 4 Å. In the case of 2 Å Co (monolayers) the values differ by a factor of 3. From the magnetization curves we know that 1.75 T is not enough to saturate these samples in another than the perpendicular direction, but if that would be the cause of the deviation we would expect a lower value from the torque

measurement instead of a higher. It is possible however, that the large hysteresis ($\mu_o H_c$ = 0.3 T) in the multilayers with 2 Å Co disturbs the torque measurement and that higher fields are necessary.

Therefore we use the values from the VSM measurements to estimate the interface and volume contribution to the anisotropy. For the present samples we find $K_s = 0.55 \cdot 10^{-3}$ J/m^2 and $K_v = -1.2 \cdot 10^{6}$ J/m^3. Previously we found $K_s = 0.26 \cdot 10^{-3}$ J/m^2 and $K_v = -0.72 \cdot 10^{6}$ J/m^3 (section 5.1), while for rf-sputtered multilayers $K_s = 0.16 \cdot 10^{-3}$ J/m^2 and $K_v = -0.37 \cdot 10^{6}$ J/m^3 were found [10]. It is to be noted that these figures result from a series of samples, which means that the deviations are caused by systematic differences between the series. The present samples were deposited onto a 100 Å Ti layer to improve the sticking to the glass substrate, but this did not seem to affect the structural characteristics as measured by X-ray diffraction. Two features are worth noting: First, the experimental interface anisotropy is not a fixed quantity, but seems to fall in a wide range of possible values. Secondly, when the interface contribution is higher, the volume anisotropy is lower, resulting in a constant value for the Co layer thickness at which the total anisotropy is zero (8 Å).

As an experiment to verify the concept of interface anisotropy, we prepared samples in which the amount of Co was just enough to form half a monolayer (1 Å). The anisotropy should fall down in these samples, because there is no complete interface anymore between Co and Pd. The result is given in Fig. 5.17 at a (virtual) Co thickness of 1 Å and confirms our expectations. In this case the hysteresis is small and the torque and VSM measurement yield the same positive value for the anisotropy.

Finally we prepared Pd-Co alloys by co-evaporation to compare the magnetic properties of the layered films with homogeneous ones. Surprisingly we found some perpendicular anisotropy in these fcc alloys with a maximum of $0.2 \cdot 10^6$ J/m^3 at 20 at.% Co. Though it is much lower than in a comparable multilayer, it may indicate that the alloys are not random, but that some ordening occurs.

These experiments led us to suspect that the local environment of the Co atoms is responsible for the anisotropy in these layers. We examined this somewhat further in a pair interaction model.

Pair interaction model

The influence of the surroundings of an atomic magnetic moment on its preferential direction can phenomenologically be described by the interaction energy $w(r,\varphi)$ between all pairs of atoms, depending on the distance r between the two atoms and the angle φ between the direction of the magnetic moment and the line connecting the pair of atoms [4] (Fig. 5.18). The interaction energy is essentially the result of spin-orbit coupling. The magnetic moments are assumed to be oriented parallel by the isotropic exchange interaction. We expand the interaction w as a

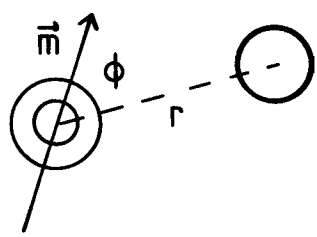

Fig. 5.18(a) *Definition of the parameters as used in the pair interaction model. The magnetic moment is indicated by the vector* $\vec{m}$*, but does not have to be localized.*

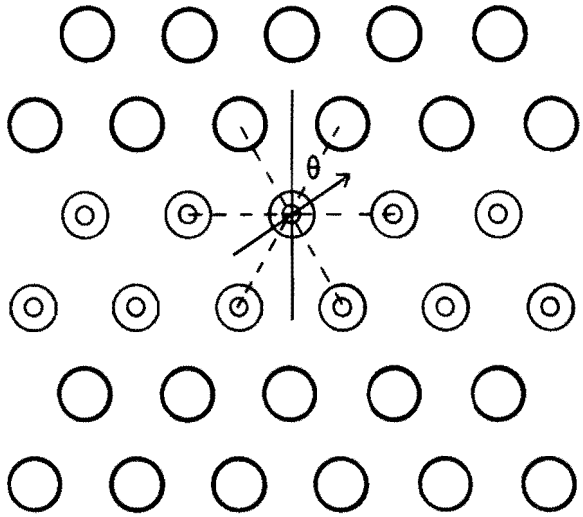

Fig. 5.18(b) *Schematic, two-dimensional drawing of the relative orientation of the atoms at the interface illustrates the anisotropic bonding of the Co atoms at the interface.*

series and consider the first angle dependent term $k(r)\cos^2\varphi$ as the pair energy. Taking only nearest neighbours, the sum over all pairs in the bulk fcc and/or hcp phase is zero, so that to describe the bulk anisotropy more neighbours or more terms in the expansion need to be considered. At the interface in the Pd/Co multilayers however, the nearest neighbours of the Co atoms are partially replaced by Pd so that the (large) contributions no longer cancel. For a (111) interface the anisotropy per Co atom becomes

$$w = \sum_i k_i \cos^2\varphi_i = \frac{3}{4}\left(k_{Co} - 2k_{Pd} \right) \sin^2\vartheta = L \sin^2\vartheta \qquad (23)$$

in which i runs over the nearest neighbours; k_{Co} is the interaction

energy constant between two Co atoms, k_{Pd} that between a Co and Pd atom and ϑ is the angle between the magnetic moment and the axis perpendicular to the interface.

Interdiffusion will lower this interface effect, because it increases the randomness of the Co-Pd bonds. Assuming a concentration c of Co atoms in each atomic (111) plane, randomly distributed over the available sites, we obtain per Co atom an average anisotropy

$$\bar{w} = L \sin^2\vartheta \frac{\sum (2c_j - c_{j-1} - c_{j+1})\, c_j}{\sum c_j} = L' \sin^2\vartheta \ , \qquad (24)$$

in which the summation runs over all (111) planes. When we consider Co monolayers with perfectly sharp interfaces we have the concentrations $\{c\} = \ldots 0,1,0,\ldots$ in consecutive layers, resulting in $L' = 2L$. When more interdiffusion is introduced we obtain for a nominal monolayer e.g. $\ldots 0,0.5,0.5,0,\ldots$ and $L' = 0.5L$. This illustrates the strong dependence of the interface anisotropy on the mixing at the interface. If a is the distance between two Co atoms along the [100] direction, the area per Co atom at the interface is $S = \frac{1}{4} a^2 \sqrt{3}$. Because each layer has two interfaces, the experimental interface anisotropy is now

$$K_s = \frac{L'}{2S} \sum c_j = \frac{2}{3}\sqrt{3}\, \frac{L'}{a^2} \sum c_j \leq \frac{4}{3}\sqrt{3}\, \frac{L}{a^2} \ . \qquad (25)$$

Taking $a = 3.8$ Å and $K_s = 0.55 \cdot 10^{-3}$ J/m^2, this yields $L \geq 0.2$ meV per Co atom.

When the layers are more interdiffused, the magnetization distribu-

tion is more homogeneous, which leads to a lower magnetostatic energy ($\sim M^2$). This causes an increase of K_v and explains the simultaneous change of K_s and K_v as was observed above. In a previous experiment, we observed that the anisotropy collapsed rapidly upon bombardment with a relatively low dose of 600 keV Kr^+ ions (cf. section 5.4). This can be explained by the great sensitivity to the Co distribution in the multilayer.

Conclusion

The magnetic anisotropy energy in Pd/Co multilayers can be measured most directly by magnetization measurements with the field parallel and perpendicular to the film plane. Phenomenologically the interface contribution to this anisotropy and the effect of interdiffusion at the interfaces can be described quite well by the anisotropy in Co-Pd bonds. To obtain a relevant value for the pair interaction an independent measurement of the interdiffusion on atomic scale is necessary, or one should have the ideal case of atomically flat interfaces.

5.6 Contribution of dipole-dipole interaction to the anisotropy *)

Abstract

At the boundary of a ferromagnetic material, the local change in the surroundings of the atomic magnetic moments induces an additional mag-

*) part of this text has been accepted for publication in the Journal of Applied Physics (Oct. 1988)

netic anisotropy. The dipole-dipole interaction, responsible for the shape-dependent demagnetizing field inside the ferromagnet, differs for magnetic moments at the boundary and magnetic moments inside the bulk material. By calculation it is shown that the demagnetization factor for an ultra-thin ferromagnetic film is thickness dependent. However, the anisotropy resulting from the dipole-dipole interaction can be interpreted as a surface and a volume anisotropy which depend on the crystalline structure and orientation of the film, but are independent of the thickness of the film.

Introduction

One of the interesting magnetic properties of thin films is the anisotropy, which determines the preferential orientation of the magnetization. Experimentally it has been found that when the thickness of ferromagnetic films is reduced to several atomic layers, the anisotropy differs considerably from its value in thick films. As the difference depends on the thickness t as $1/t$, it is attributed to the two surfaces of the film and consequently called surface anisotropy [5]. The influence of the surfaces (or interfaces, when in contact with another material) can be large enough to change the preferential orientation of the magnetization from in the plane of the film to perpendicular to the film.

Despite early attempts to determine the surface anisotropy theoretically [34], present calculations seem to be resticted to monolayers [35] and do not include the thickness t. Therefore the dependence of the anisotropy on $1/t$, as quoted above, has not yet been confirmed from first principles.

In this section we want to evaluate the influence of the dipolar interaction on the surface anisotropy. First we will consider the ferromagnetic film as a continuum and secondly as a set of discrete, atomic dipoles, neatly ordered in the film. Using this last approach, the result of the calculation will depend on the crystal structure of the film. Since we will only consider simple ferromagnets, it seems appropriate to concentrate on high-symmetric structures as body centered cubic (bcc), face centered cubic (fcc), hexagonal close packed (hcp) and tetragonal. The structure can have different orientations relative to the film and we will indicate this by the axis that is perpendicular to the plane of the film, e.g. bcc[110] means the film has the bcc structure with the [110] axis perpendicular to the film.

We will assume that the magnitude of the magnetic moment does not depend on its orientation, as is the case for most ferromagnets. The anisotropy can then be calculated as the energy difference between two magnetic saturated states, one with the magnetization parallel to the plane of the film and the other one with the magnetization perpendicular to the plane of the film. Further it will be assumed that the magnitude of the magnetic moment does not depend on the thickness of the film or its position in the film.

Apart from saturated states, domain structures in these ultra-thin films are of interest. We will not consider these, but refer to a recent paper by Yafet et al.[36], which theoretically treats them for a ferromagnetic monolayer and to section 5.3 for domain configurations in a multilayer.

Continuum approach

Neglecting the discrete nature of matter, magnetization can be treated as a field $\vec{M}(\vec{r})$, which obeys the currentless Maxwell equations. At interfaces between two regions with different magnetization we have the usual boundary conditions: the normal component of $\vec{B}$ and the tangential component of $\vec{H}$ should be continuous. The magnetostatic energy is the total energy difference between the situation in which the sample has a given magnetization distribution to the situation in which there is no sample at all [37]. This involves both the magnetic field inside and outside the sample, but by taking the appropriate expressions for the energy, the volume of integration can be limited to the sample volume. When a field $\vec{M}$ is given, the solutions for $\vec{B}$ and $\vec{H}$ are often formulated with the use of the magnetic potential Ψ, defined by $\vec{H} = -\nabla\Psi$. The function Ψ is a solution of Laplace's equation $\nabla^2\Psi = 0$. In this formulation the average magnetostatic energy density can be expressed as [11]

$$E = -\frac{\mu_o}{2V}\int dV\ \vec{M}\cdot\vec{H} = \frac{\mu_o}{2V}\int dV\ (-\nabla\cdot\vec{M})\ \Psi \qquad (26)$$

with V for the volume of the sample. In the planar geometry of a thin film we find that, when the magnetization is saturated and ϑ is the angle between the axis normal to the plane of the film and $\vec{M}$, the average energy density becomes

$$E(\vartheta) = \frac{1}{2}\mu_o M_s^2 \cos^2\vartheta \qquad (27)$$

in which M_s is the saturation value of the magnetization. The anisotropy E_a is the difference between the magnetostatic energy for the parallel orientation ($\vartheta = \frac{\pi}{2}$) and the perpendicular orientation ($\vartheta = 0$), which yields

$$E_a = -\frac{1}{2}\mu_o M_s^2 \ . \qquad (28)$$

In this approach the thickness of the film plays no role and therefore no surface contributions proportional to $1/t$ are predicted.

Discrete dipoles

When the thickness of the ferromagnetic film is reduced to a few atomic layers, the assumption that the film can be treated as a magnetic continuum is no longer valid. In that case we treat the magnetic system as a collection of discrete magnetic dipoles, which are regularly arranged on a crystalline lattice. The dipolar energy of a dipole i can then be expressed as

$$\varepsilon_i = -\frac{1}{2}\frac{\mu_o}{4\pi}\sum_{j\neq i}\left[-\frac{\vec{m}^2}{r_{ij}^3} + \frac{3(\vec{m}\cdot\vec{r}_{ij})^2}{r_{ij}^5}\right] . \qquad (29)$$

$\vec{m}$ is the magnetic moment of the dipoles, $\vec{r}_{ij} = \vec{r}_i - \vec{r}_j$ is the relative position of dipoles i and j and $r_{ij} = |\vec{r}_{ij}|$. This dipole-dipole interaction can be interpreted as the energy of the dipole in the field of all the other dipoles:

$$\varepsilon_i = -\frac{1}{2}\vec{m}\cdot\vec{B}_i$$
$$\vec{B}_i = \frac{\mu_o}{4\pi}\sum_{j\neq i}\left[-\frac{\vec{m}}{r_{ij}^3}+\frac{3(\vec{m}\cdot\vec{r}_{ij})\,\vec{r}_{ij}}{r_{ij}^5}\right]. \qquad (30)$$

The factor of $\frac{1}{2}$ results from the fact that every pair of dipoles should only be counted once. The field $\vec{B}_i$ is called the dipole field and can be viewed upon as the sum of the demagnetizing field and the Lorentz field [38]. $\vec{B}_i$ can be written as

$$\vec{B}_i = \mu_o \vec{\vec{d}}_i \vec{m} = \mu_o \vec{\vec{D}}_i \vec{M}_s , \qquad (31)$$

where we have used

$$\vec{M}_s = \frac{\vec{m}}{V_{dip}} , \qquad (32)$$

with V_{dip} for the volume per dipole. For a given dipole i, $\vec{\vec{D}}_i$ is a second rank tensor which depends on the position of the dipole, relative to the other dipoles, but is independent of the dimensions of the sample and the unit cell of the crystallographic lattice. In Cartesian coordinates we can write its components as

$$(\vec{\vec{D}}_i)_{kl} = \frac{V_{dip}}{4\pi}\sum_{j\neq i}\left[-\frac{\delta_{kl}}{r_{ij}^3}+\frac{3\,(\vec{r}_{ij})_k\,(\vec{r}_{ij})_l}{r_{ij}^5}\right] \qquad (33)$$

with $k,l = x,y,z$. Note that $\vec{\vec{D}}_i$ is symmetric for all positions i and also $D_{xx} + D_{yy} + D_{zz} = 0$.

In our case, the dipoles are arranged in an infinitely large thin film. We choose the z-axis perpendicular to the plane of the film. An additional property of $\vec{\mathbf{D}}_i$ is then $(\vec{\mathbf{D}}_i)_{xz} = (\vec{\mathbf{D}}_i)_{yz} = 0$ and $\vec{\mathbf{D}}_i$ is only dependent on the position of the atomic layer in the z-direction. So $\vec{\mathbf{D}}_i$ is determined by three independent parameters: D_{xx}, D_{xy} and D_{zz} for each atomic layer in the film. A further reduction occurs when the atomic layers have more than twofold rotational symmetry. In that case $D_{xy} = 0$ and $D_{xx} = D_{yy}$ and therefore $D_{xx} = -\frac{1}{2} D_{zz}$, so there is only one parameter left.

The ferromagnetic film consists of N atomic layers in the z-direction. The anisotropy $E_a(n)$ contributed by the dipoles in atomic layer n is the difference in energy between the state in which all dipoles point in the x-direction ($\vartheta = \frac{\pi}{2}$) and the state in which they all point in the z-direction ($\vartheta = 0$). From equations (30), (31), and (32) we can derive that

$$E_a(n) = \frac{\varepsilon_i(\vartheta=\frac{\pi}{2}) - \varepsilon_i(\vartheta=0)}{V_{dip}} = -\frac{1}{2}\mu_o M_s^2 (D_{xx} - D_{zz}) , \qquad (34)$$

when dipole i is in layer n. Introducing the reduced anisotropy $k(n)$, we can write in a high-symmetric lattice

$$k(n) = \frac{E_a(n)}{\frac{1}{2}\mu_o M_s^2} = -(D_{xx}-D_{zz}) = \frac{3}{2} D_{zz} . \qquad (35)$$

The actual calculation of D_{zz} has been performed for various films

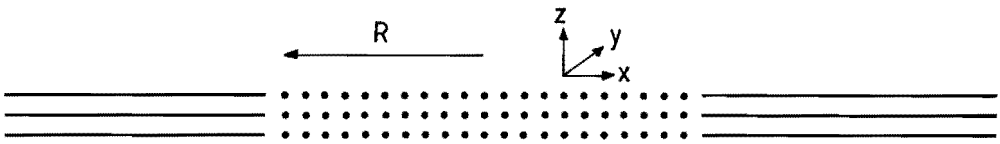

Fig. 5.19 *Magnetic dipoles within a cylinder of radius R are summed in a discrete way, whereas those outside are integrated. R is taken large enough (about 100 times the interatomic distance) to have no influence on the results. The contributions of each atomic layer are summed to obtain the final result.*

consisting of monolayers up to several atomic layers. The dipoles are divided into two sets: those within a cylinder of radius R with its rotation axis perpendicular to the film plane around a dipole in layer n and those outside that cylinder. The contribution to D_{zz} of dipoles from the first set is summed discretely, according to equation (33). The contribution of dipoles from the second set is included by integration. Fig. 5.19 shows this schematically by indicating a dot for a discretely summed dipole and a line for an integrated area. Note that the integrals are absolutely convergent due to the twodimensional configuration of the dipoles. R is chosen large enough to have no influence on the results, which is about 100 atomic distances in the present calculations.

As an example we show in Fig. 5.20 the value of $k(n)$ for a bcc[100] film consisting of $N = 1,\ldots,10$ atomic layers. The value at the outside layers is 23% smaller than at the inside layers, whereas at the second layer $k(n)$ is 2% larger than at the inside. This result is similar to an earlier calculation of the dipole field at the surface of small particles by Christensen et al. [39].

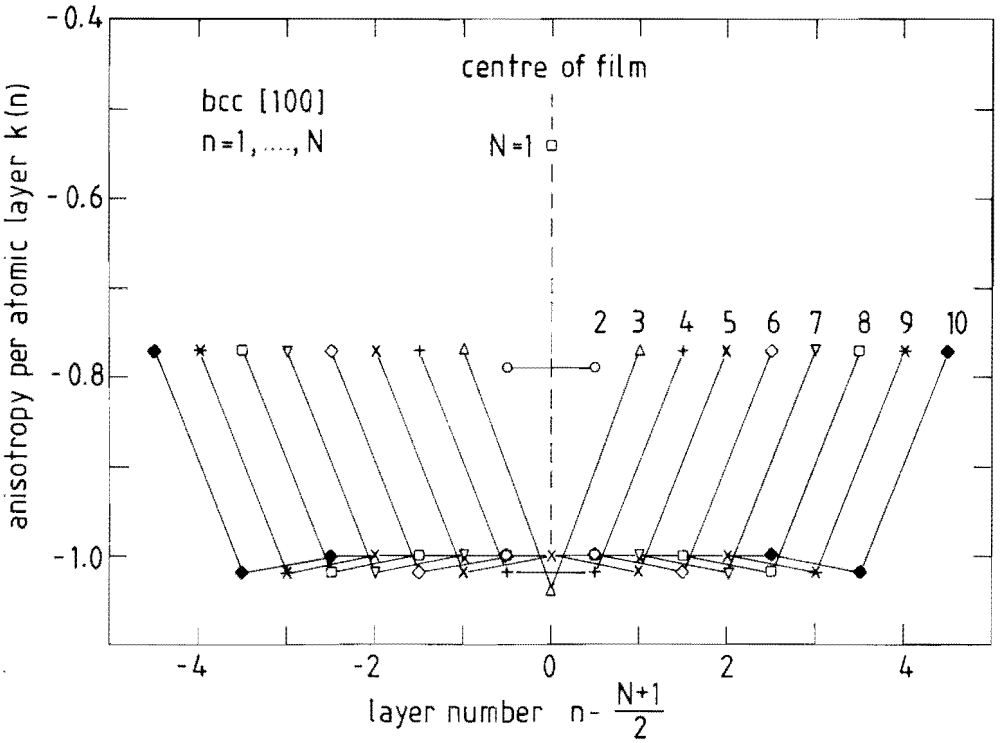

Fig. 5.20 *The anisotropy of a dipole in a ferromagnetic film is dependent on the layer in which the dipole is located. In this figure the anisotropy of a dipole field in a* bcc[100] *film is shown as function of the layer number n (n=1,..,N , where N is the number of atomic layers in the film). The horizontal axis is shifted for different N to keep the centre of the film at the same position.*

The total reduced anisotropy k is the average of the anisotropy of the different layers:

$$k = \frac{1}{N} \sum_{n=1}^{N} k(n) \quad . \tag{36}$$

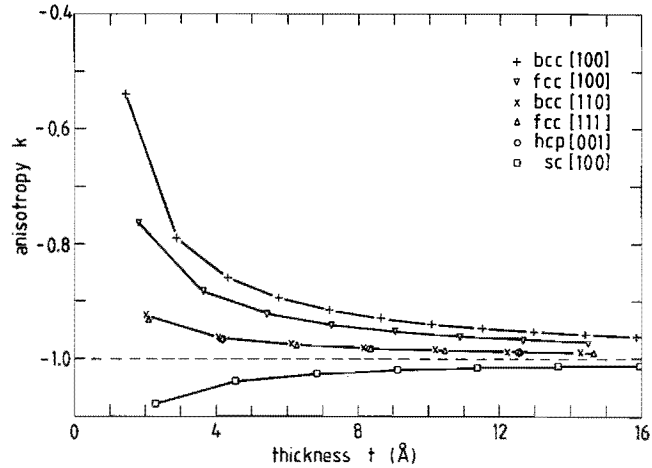

Fig. 5.21(a) *Calculated anisotropy k vs. thickness of the film t for films of various crystalline structures and orientations. Only for large thicknesses the anisotropy tends to its continuum value (k = -1).*

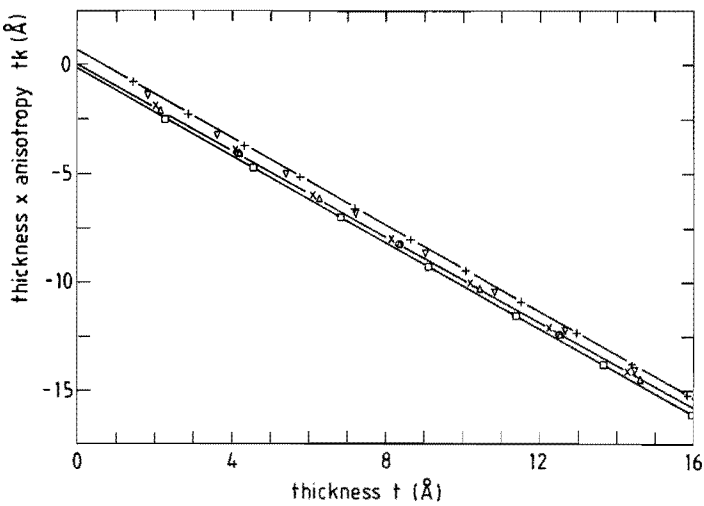

Fig. 5.21(b) *The same data as shown in* Fig. 5.21(a), *plotted as thickness times anisotropy vs. thickness. This shows that the anisotropy resulting from dipole-dipole interactions between the magnetic moments can be separated into a surface and a volume anisotropy, according to equation* (37).

This reduced anisotropy k can partly be considered as an equivalent of the demagnetizing factor, but we will not dwell on this point of view. Note that the definition of k is such that a negative value indicates a preferential direction in the plane of the film and a positive value indicates a perpendicular preferential direction. In this formulation the continuum approach yields $k = -1$.

Results

The calculated results of the reduced anisotropy k for various crystal structures and orientations is shown in Fig. 5.21(a). The value of k is independent of the lattice constant for one and the same structure, but in order to compare different structures, the lattice constants have to be relatively fixed. We have chosen to take the same V_{dip} for all structures (V_{dip} = (2.28 Å)^3), so that the same magnetic moment in different structures leads to the same magnetization. For all high-symmetric structures k approaches the continuum limit $k = -1$ for thick layers. As the thickness is reduced, the total anisotropy deviates appreciably from the continuum value. For monolayers, represented by a thickness of approximately 2 Å, it is of course impossible to define the crystal structure, but it is understood that the same crystallographic net can be taken as for an atomic layer in the complete crystal and the same value for V_{dip}.

As quoted in the introduction, the analysis of experimentally observed anisotropies seems to indicate that a volume and a surface contribution can be distinguished. This observation can be expressed as

$$k\,t = 2k_s\,d + k_v\,t \quad , \tag{37}$$

with t for the thickness of the film and d for the distance between two successive atomic layers in the z-direction. d is introduced only to make k_s dimensionless, just as k and k_v (note $t = N d$). k_v is the contribution proportional to the volume of the film, whereas k_s represents the contribution proportional to the surface of the film. In the spirit of this analysis of experimental data we have treated our calculations accordingly. In Fig. 5.21(b) the product of the thickness t and the anisotropy k have been plotted as function of t. For all cases calculated in Fig. 5.21(a) indeed a linear dependence is found. In Table 5.6 the resulting k_s and k_v as they follow from least square fits for the points in Fig. 5.21(b) are tabulated. For the crystal stuctures considered here, we find $k_v = -1$ which means that there is no contribution from the

Table 5.6 *Least square parameters for the volume (k_v) and surface (k_s) anisotropy in a thin film as a result of the dipole-dipole interaction between the magnetic moments. The values included to obtain this fit are those shown in* Fig. 5.21.

film	k_v	k_s
sc[100]	-0.9999	-0.0393
fcc[111]	-0.9999	0.0344
fcc[100]	-1.0003	0.1178
bcc[110]	-1.0001	0.0383
bcc[100]	-1.0016	0.2187
hcp[001]	-0.9994	0.0338

dipole-dipole interaction to what is usually called the crystalline anisotropy. There is however a contribution from the dipole-dipole interaction to the anisotropy which can be designated as dipole-dipole surface anisotropy. It has to be noted that relation (37) does not exactly fit the calculated values. However, the differences are much smaller (< 1 %) than usual experimental errors, so that this relation can be used fruitfully.

From the reduced value of the anisotropy we can find the actual value via

$$K_s = k_s \, d \, \frac{1}{2} \mu_o \, M_s^2 \, . \qquad (38)$$

To estimate the order of magnitude, let us take Co in fcc[100] orientation. As parameters we take the lattice constant a = 3.55 Å and the magnetization $\mu_o M_s$ = 1.76 T. The volume contribution to the total anisotropy resulting from dipole-dipole interactions is then K_v = - $1.23 \cdot 10^6$ J/m^3 and the surface contribution K_s = $25.7 \cdot 10^{-6}$ J/m^2. In the fcc[111] orientation K_v is the same, but K_s = $8.67 \cdot 10^{-6}$ J/m^2. Experimentally, in polycrystalline Pd/Co multilayers with [111] texture it is found that K_s = $550 \cdot 10^{-6}$ J/m^2 (cf. section 5.5), which is more than an order of magnitude larger. This means that other sources for anisotropy, such as spin-orbit coupling, are more important for the Pd/Co interface.

Of course, this calculation can be performed for other structures as well. As an example to show the influence of a reduction of symmetry in the crystal structures relative to the high-symmetric structures, we have calculated the anisotropy for the tetragonal structure with differ-

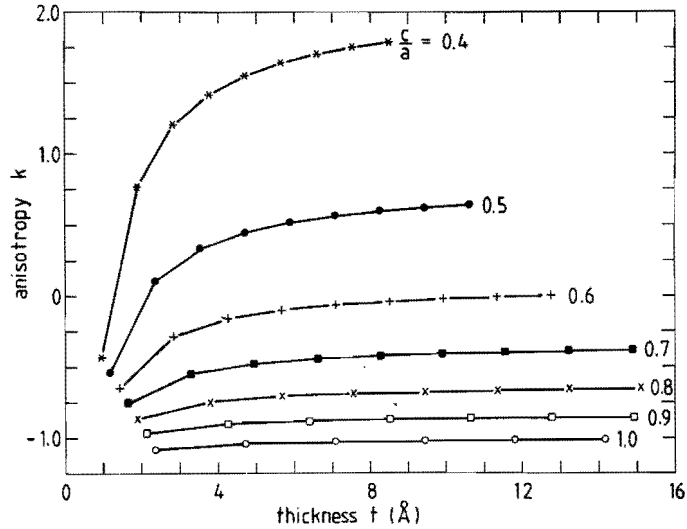

Fig. 5.22(a) *Anisotropy vs. thickness for tetragonal structures with different* $\frac{c}{a}$ *ratios.*

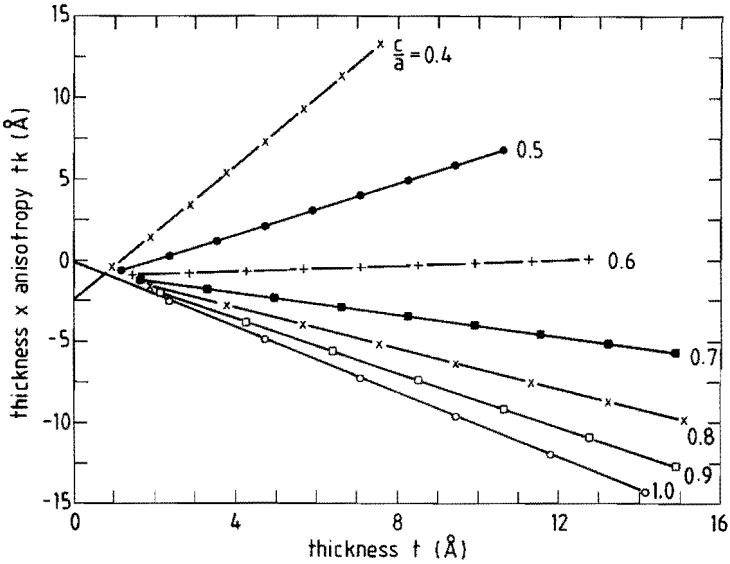

Fig. 5.22(b) *Thickness times anisotropy vs. thickness for tetragonal structures showing that also in this case a distinction between surface and volume anisotropy can be made.*

ent $\frac{c}{a}$ ratios. In Fig. 5.22 and Table 5.7 the results show that again the anisotropy can be divided into an interface and a volume contribution, but now there is a substantial contribution from the dipole-dipole interaction to the crystalline anisotropy. The volume anisotropy k_v even becomes positive for $\frac{c}{a} = 0.6$, which means that the preferential direction for the magnetization becomes perpendicular to the film when the film is thick enough to overcome the surface anisotropy, which is negative in this case. The fact that k_v becomes more positive when the ratio $\frac{c}{a}$ decreases can qualitatively be understood by observing that the magnetic dipole density in the direction of the c-axis increases, which strongly favours the alignment in that direction.

When magnetic layers can be epitaxially grown on materials with larger lattice constants [40], this causes an expansion of the lattice in the plane of the film and a contraction perpendicular to it. With the

Table 5.7 *Volume* (k_v) *and surface* (k_s) *anisotropy for tetragonal structures with different* $\frac{c}{a}$ *ratios, when the dipole-dipole interaction is the only source of anisotropy.*

c/a	k_v	k_s
1.0	-1.000	-0.0392
0.9	-0.834	-0.0685
0.8	-0.624	-0.1196
0.7	-0.337	-0.2102
0.6	0.0913	-0.3725
0.5	0.793	-0.6788
0.4	2.078	-1.2960

mechanism sketched above, this can have a large influence on the magnetic anisotropy energy.

Conclusion

We have shown from first principles that the variation of the anisotropy with the thickness of thin, crystalline, ferromagnetic films can be understood in the case that only discrete dipole-dipole interactions are taken into account. The calculated anisotropy in this case can very well be described by a surface and a volume contribution. In a way this result is somewhat surprising in view of the long range of the dipole-dipole interaction, in contrast to local sources of anisotropy (primarily resulting from spin-orbit coupling). The results justify theanalysis of the experimental anisotropy in ultra-thin films in terms of a surface and volume contribution based on the thickness dependence of the anisotropy. Corrections for the demagnetization, based on the continuum approach, should be avoided, since they are not physically meaningful in this case.

5.7 Ferromagnetic resonance experiments on Pd/Co multilayers *)

Abstract

Ferromagnetic resonance experiments at room temperature were performed on Pd/Co multilayers and Pd/Co/Pd sandwiches as function of layer

*) part of this text has been accepted for publication in the Journal de Physique

thickness at frequencies of 9 and 20 Ghz in order to determine the magnetic anisotropy of these films. From the FMR data it is found that in all cases the anisotropy is decreasing with decreasing Co layer thickness. For the Pd/Co films a switching of the magnetic preferential direction occurs when the layer thickness becomes smaller than 8 Å.

Introduction

A considerable amount of attention has been given in recent years to the research of magnetic multilayers. These new materials exhibit properties which are of interest both from theoretical as technological point of view [40,41]. For multilayered Pd/Co films it has been found that a competition between the surface and volume magnetic anisotropy exists, which results in a reorientation of the magnetization from in-plane to perpendicular to the plane.

It is therefore worthwhile to perform ferromagnetic resonance (FMR) experiments on these multilayers because this technique probes the local behaviour of the magnetic moments, in contrast to magnetization measurements, which samples the overall contribution of the magnetization.

Experimental techniques

The samples were prepared by electron beam evaporation of Co and Pd after deposition of a 100 Å Ti base layer on a rotating glass substrate. The measurements on the multilayers were performed at room temperature in fields up to 1 T at frequencies of 9.5 and 20 Ghz. When necessary with regard to sensitivity, some of the samples were mounted in a TE_{01} mode cavity. For very thin Co layers, where it can be expected that the

Table 5.8 *Results from FMR experiments on Pd/Co/Pd sandwiches.*

t_{Co} (Å)	f (GHz)	$\mu_o H^{//}$ (T)	$\mu_o \Delta H_{pp}$ (mT)	$\mu_o H_a$ (mT)	$t_{Co}K$ (10^{-3} J/m^2)
80	9.56	0.063	6.4	1.48	-8.29
40	9.56	0.075	11.0	1.24	-3.47
20	9.56	0.095	32.0	0.92	-1.29
10	9.41	0.157	74.0	0.48	- 0.336
80	20.51	0.255	16.0	1.52	-8.49
40	20.47	0.291	22.0	1.25	-3.50
20	20.45	0.355	42.0	0.91	-1.27

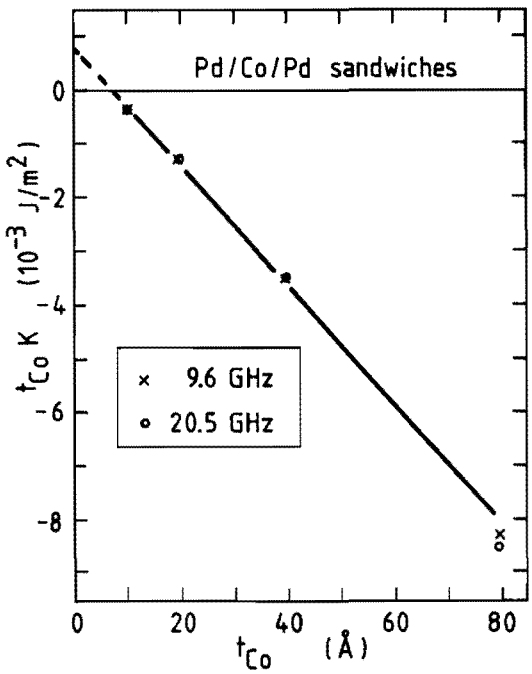

Fig. 5.23 *Anisotropy times Co thickness vs. Co thickness for Pd/Co/Pd sandwiches. The drawn line is a least square fit to the data points.*

resonance fields are high, experiments were performed in a superconducting magnet with a field up to 5 T.

The resonance data were interpreted on the basis of the conventional theory (see section 4.5). The observed experimental data were fitted to equation (16) (p. 80) using a least square error method. In the fitting procedure g was kept fixed and equal to the Co bulk value $g = 2.18$ [20].

Results

1) Pd/Co/Pd sandwiches: these samples are built up from a single Co layer with on both sides a 200 Å Pd layer and can be considered as the limiting case of a multilayer system. The advantages are that signal detoriation due to irregularities in structure in different layers and the possible exchange coupling between layers is eliminated and that contributions to the surface anisotropy originate from only two interfaces Pd/Co.

The experimental data on these sandwiches are shown in Table 5.8. Here t_{Co} is the thickness of the Co-layer, $H^{//}$ the resonance field when the external field is parallel to the plane of the film and ΔH_{pp} is the corresponding linewidth. The last two colums give the anisotropy in terms of $\mu_o H_a = -2K/M_s$ and the anisotropy scaled with regard to the Co layer thickness. The reason for this scaling is that the data can be very well described by the phenomenological relation (cf. section 5.1):

$$t_{Co}K = t_{Co}K_v + 2K_s \ , \qquad (39)$$

as is shown in Fig. 5.23. From this figure it is clear that there is a

change of sign of the anisotropy at $t_{Co} = 7.5$Å, i.e. a reorientation of the direction of the magnetization from in the plane to normal to the plane. From the extrapolation and the slope of the fitted line the values $K_s = (0.35 \pm 0.05) \cdot 10^{-3}$ J/m^2 and $K_v = (-1.08 \pm 0.04) \cdot 10^{6}$ J/m^3 are found. These results are in reasonable agreement with the data from magnetization measurements on Pd/Co multilayer systems.

2) Pd/Co multilayers: experiments were performed on films with $t_{Co} = 2$, 4, 8, 10, 12 and 20 Å. The thickness of the Pd layers varied from 27Å, 36Å to 45Å. Also in this case the experimental data show a rapid increase in linewidth with decreasing Co layer thickness. Since the observed linewidth in these multilayers is considerably larger than for the corresponding Co sandwich structures and since there seems to be

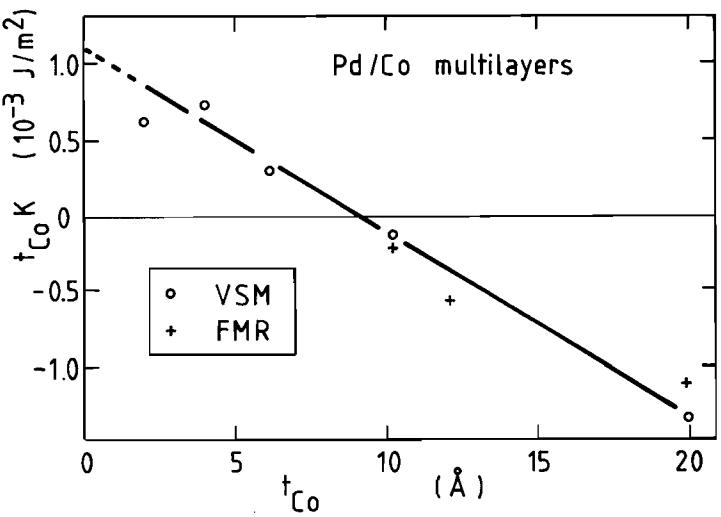

Fig. 5.24 *Anisotropy times Co thickness vs. Co thickness for Pd/Co multilayers. Also are shown data obtained from magnetization measurements (VSM). The drawn line is a least square fit to the data points.*

no relation between linewidth and Pd layer thickness, it seems reasonable to assume that this is caused by structural imperfections. Furthermore, the experimental data show no evidence of any correlation between the observed resonance fields and the Pd layer thickness.

The values for the anisotropy as found from the FMR experiments for $t_{Co} > 8$ Å as well as the data obtained by magnetization measurements are shown in Fig. 5.24. Although there is some scattering of the data, it appears that the overall agreement between FMR data and magnetization data is reasonable.

Measurements on films with $t_{Co} < 8$ Å give some peculiar results in the sense that only relativily narrow and strong signals were observed resembling the signals found in bulk Co films. The intensity of these signal was also strongly dependent on the "magnetic history" of the sample.

These results can be explained by assuming that these multilayers consist of domains in which the magnetization is alternatingly normal to the film plane and in the plane. However, no signals related to the perpendicularly orientated domains were observed. This may be due to the fact that these signals, at least at low frequencies, are very strongly dependent on the orientation of the field (see Fig 4.6(b)).

references

[1] S. Iwasaki and K. Ouchi, IEEE Trans. Magn. MAC-**14** (1978) 849

[2] M. Naoe, S. Hasunuma, Y. Hoshi, and S. Yamanaka, IEEE Trans. Magn. MAC-**17** (1981) 3184

[3] P. Chaudari, J.J. Cuomo, and R.J. Gambino, IBM J. Res. Dev. **17** (1973) 66

[4] M.L. Néel, J. de Phys. et le Rad. **15** (1954) 225

[5] U. Gradmann, J. Magn. Magn. Mater. **54-57** (1986) 733

[6] U. Gradmann, Appl. Phys. **3** (1974) 161

[7] R. Halbauer and U. Conser, J. Magn. Magn. Mater. **35** (1983) 55

[8] W. Kümmerle and U. Gradmann, Solid State Comm. **24** (1977) 33

[9] U. Gradmann and H.O. Isbert, J. Magn. Magn. Mater. **15-18** (1980) 1109

[10] P.F. Carcia, A.D. Meinhaldt, and A. Suna, Appl. Phys. Lett. **47** (1985) 178

[11] S. Chikazumi, "Physics of Magnetism", Krieger, Malabar (Fl.) (1964)

[12] A.J. Freeman, H. Krakauer, S. Ohnishi, D.-S. Wang, M. Weinert, and E. Wimmer, J. Magn. Magn. Mater. **38** (1983) 269

[13] C.L. Fu, A.J. Freeman, and T. Oguchi, Phys. Rev. Lett. **54** (1985) 2700

[14] R. Bozorth, P. Wolff, D. Davies, V. Compton, and J. Wernick, Phys. Rev. **122** (1961) 1157

[15] J.A. Mydosh and G.J. Nieuwenhuys in "Ferromagnetic Materials" vol. 1, Ed. E.P. Wohlfarth, North-Holland, Amsterdam (1980)

[16] M.J. Klein and R.S. Smith, Phys. Rev. **81** (1951) 378

[17] H.K. Wong, H.Q. Yang, J.E. Hilliard, and J.B. Ketterson, J. Appl. Phys. **57** (1985) 3660

[18] J.C. Levy and J.L. Motchane, J. Vac. Sci. Tech. **9** (1972) 721

[19] P. Grünberg (to be published)

[20] E.P. Wohlfarth in "Ferromagnetic materials" vol. 1, Ed. E.P. Wohlfarth, North-Holland, Amsterdam (1980)

[21] F.J.A. den Broeder, H.J.G. Draaisma, H.C. Donkersloot, and W.J.M. de Jonge, J. Appl. Phys. **61** (1987) 4317

[22] C. Kooy and U. Enz, Philips Res. Rep. **15** (1960) 7

[23] Z. Málek and V. Kambersky, Czech. J. Phys. **8** (1958) 416

[24] P. Grünberg, J. Appl. Phys. **57** (1985) 3673

[25] C. Kittel, Phys. Rev. **70** (1946) 965

[26] A. Suna, J. Appl. Phys. **59** (1986) 313

[27] M.P. Rosenblum, F. Spaepen, and D. Turnbull, Appl. Phys. Lett. **37** (1080) 184
H.E. Cook and J.E. Hilliard, J. Appl. Phys. **40** (1969) 2191

[28] G.E. Henein and J.E. Hilliard, J. Appl. Phys. **55** (1984) 2895

[29] Y. Iijima and K. Hirano, Trans. Jap. Inst. Met. **13** (1972) 419

[30] W.J. Debonte and J.M. Poate, Thin Solid Films **25** (1975) 441

[31] F.J.A. den Broeder, D. Kuiper, A.P. van de Mosselaer, and W. Hoving, Pys. Rev. Lett. **60** (1988) 2769

[32] H. Zijlstra, "Experimental Methods in Magnetism" vol. 2, North-Holland, Amsterdam (1967)

[33] J. Burd, M. Huq, and E.W. Lee, J. Magn. Magn. Mater. **5** (1977) 135

[34] A.J. Bennet and B.R. Cooper, Phys. Rev. B **3** (1972) 1642

[35] J.G. Gay and R. Richter, Phys. Rev. Lett. **56** (1986) 2728

[36] Y. Yafet and E.M. Gyorgy, "Ferromagnetic Domains in an Atomic Monolayer" (to be published)

[37] J.D. Jackson, "Classical Electrodynamics" (2nd ed.) John Wiley, New York (1975)

[38] J.H.P. Colpa, Physica **56** (1971) 185

[39] P.H. Christensen and S. Mørup, J. Magn. Magn. Mater. **35** (1983) 130

[40] A.S. Arrott, B. Heinrich, S.T. Purcell, J.F. Cochran, and K.B. Urquhart, J. Appl. Phys. **61** (1987) 3721

[41] L.L. Hinchey and D.L. Mills, J.Appl.Phys. **57** (1985) 3687

Chapter 6 SUMMARY AND CONCLUSIONS

This thesis contains an experimental study of the magnetic properties of multilayers. Multilayers are thin films which are prepared by alternating deposition of different materials on a substrate. In the introduction the relevance of these new type of materials, which concerns both the fundamental magnetic properties and applications in magnetic recording, is sketched.

Chapter 2 gives a description of the preparation of multilayers by vacuum deposition methods. In the present study an electron beam evaporation and an ion beam sputtering apparatus have been used. In chapter 3 results of the characterization by various methods are presented. X-ray diffraction is employed to measure the modulation length that is realized in the preparation, but a detailed composition profile can not be determined. This is demonstrated by a computer simulation of the diffraction on incommensurable, artificial superlattices. In the transmission electron microscope a dark field image of a cross-section of a Pd/Co multilayer containing layers of 2 Å Co (i.e. one monolayer) shows that this film is indeed modulated, which strongly suggests that Pd/Co multilayers have relatively sharp interfaces. Auger spectroscopy with depth profiling has been applied to Cu/Fe, Au/Ni and Pd/Co multilayers, but proved to be only useful for multi-

layers in which the seperate layers are thicker than 20 Å. For Cu/Fe multilayers Mössbauer spectroscopy has been used to obtain a composition profile of the interface. In these multilayers, which were prepared by the ion beam sputtering method, the interfaces showed mixing over three atomic planes.

In chapter 4 the magnetic measurement techniques that have been used in this study, are discussed. The results of these measurements on Pd/Co multilayers are presented in chapter 5. The saturation magnetization (per volume unit Co) at room temperature in these films is higher than for pure Co. The polarization of Pd atoms is considered as the cause for this increase, but its dependence on the Pd and Co layer thicknesses is not fully understood. The most remarkable property however, is the magnetic anisotropy in these layers. The anisotropy depends linearly on the inverse of the Co layer thickness. Therefore it can be described by an interface (Pd/Co) and a volume (Co) anisotropy. When the Co layer thickness is lower than 8 Å, the interface anisotropy dominates and the preferential direction for the magnetization is perpendicular to the plane of the film, whereas when the Co layer thickness is larger than 8 Å it is parallel to the film. The perpendicular magnetization curve for the films with a perpendicular preferential direction depends on the Pd layer thickness. A magnetic domain model of the multilayer, which explains this property very satisfactory, is described in this thesis.

The values of the interface and volume anisotropy depend strongly on the preparation technique and conditions. In the samples prepared by ion beam sputtering no perpendicular preferential direction was

found and two series of samples prepared by electron beam evaporation yielded different values for the two contributions to the anisotropy. Heat treatments up to 400 ^{o}C and 600 keV Kr^{+} ion bombardment affected the anisotropy strongly, indicating that the interface diffuseness is an important parameter for the anisotropy. A model for the influence of the interface diffuseness on the anisotropy, assuming a pair interaction, is described. The model shows, that the interface anisotropy is indeed very sensitive to the exact composition profile at the interface. It would be very useful if an independent measurement of this diffuseness could be made.

The dipole-dipole interaction energy for crystalline films of 1 to 10 atomic layers has been calculated. When the film is thick enough, the usual demagnetization energy for a thin film is found, but for films of only several atomic layers the result deviates from the continuum value. It is shown, that the anisotropy caused by the dipole-dipole interaction can be split up in a volume and a surface contribution. These contributions are evaluated for various crystal structures. In the case of Pd/Co the surface contribution is too small to be important, but for other structures it may not be neglected.

In general, it has been shown that the magnetic properties of multilayer thin films, especially the magnetic anisotropy, can be understood and modified by the influence of the interfaces between the different materials, as has been demonstrated for Pd/Co in this thesis.

SAMENVATTING

Dit proefschrift beschrijft een experimenteel onderzoek naar de magnetische eigenschappen van multilagen. Dit zijn dunne films die vervaardigd worden door afwisselende depositie van verschillende materialen op een substraat. De belangstelling voor dit nieuw soort materialen betreft zowel fundamentele magnetische eigenschappen als toepassingen in magnetische signaalregistratie.

Hoofdstuk 2 beschrijft de preparatie van multilagen met vacuüm-depositiemethoden. In dit onderzoek is gebruik gemaakt van een elektronenstraal-verdamper en een ionenbundel-sputterapparaat. In hoofdstuk 3 komen de resultaten van de karakterisatie aan de orde. Röntgendiffraktie is gebruikt om de modulatielengte die bij de preparatie is gerealiseerd, te meten. Een gedetailleerd samenstellingsprofiel kan hiermee niet bepaald worden, zoals gedemonstreerd wordt aan de hand van een computer-simulatie van diffraktie aan incommensurabele, kunstmatige superroosters. Een donker veld opname in een transmissie elektronen microscoop van een doorsnede van een Pd/Co multilaag met lagen van 2 Å Co (dit is één monolaag) laat zien dat deze film inderdaad gemoduleerd is. Dit suggereert dat Pd/Co multilagen relatief scherpe grensvlakken hebben. Auger-spectroscopie met diepte profilering is toegepast op Cu/Fe, Au/Ni en Pd/Co multilagen, maar bleek alleen zinvol voor multilagen waarin de afzonderlijke lagen dikker dan 20 Å

waren. Mössbauer-spectroscopie is gebruikt om een samenstellingsprofiel van de grensvlakken in Cu/Fe multilagen te verkrijgen. De menging aan het grensvlak bleek zich over ten minste drie atoomlagen uit te strekken.

In hoofdstuk 4 worden de magnetische meetmethoden die in dit onderzoek gebruikt zijn, behandeld. De resultaten van deze metingen aan Pd/Co multilagen worden in hoofdstuk 5 beschreven. Het blijkt dat de verzadigingsmagnetisatie (per volume-eenheid Co) bij kamertemperatuur in deze films hoger is dan voor puur Co. Dit wordt toegeschreven aan de polarisatie van Pd atomen, maar de afhankelijkheid van de Pd en Co laagdikten wordt nog niet goed begrepen. De meest opmerkelijke eigenschap is echter de magnetische anisotropie in deze films, die omgekeerd evenredig is met de Co laagdikte. Dit betekent, dat deze beschreven kan worden door een grensvlak- (Pd/Co) en een volume- (Co) anisotropie. Bij een Co laagdikte kleiner dan 8 Å overheerst de grensvlak anisotropie en is de voorkeursrichting voor de magnetisatie loodrecht op het filmvlak gericht, terwijl bij een Co laagdikte groter dan 8 Å de voorkeursrichting parallel aan het filmvlak is. De loodrechte magnetisatiekromme voor de films met een loodrechte voorkeursrichting blijkt van de Pd laagdikte af te hangen. Een magnetisch domein model van de multilaag, dat deze eigenschap zeer bevredigend verklaart, wordt in dit proefschrift beschreven.

De waarden van de grensvlak- en volume-anisotropie hangen sterk af van de preparatietechniek en omstandigheden. In de preparaten vervaardigd met ionenbundelsputteren werd totaal geen loodrechte voorkeursrichting gevonden en twee reeksen preparaten vervaardigd met elektro-

nenstraalverdamping gaven verschillende waarden voor de twee bijdragen tot de anisotropie. Verhitting tot 400 ^{o}C en ionen-bombardement met 600 keV Kr^{+} gaven een sterke verandering van de anisotropie. Dit geeft aan dat de diffuusheid aan het grensvlak een belangrijke parameter is voor de anisotropie. Een model voor de invloed van de grensvlakdiffuusheid op de anisotropie, uitgaande van een paar-interactie, wordt beschreven. In dit model blijkt dat de grensvlak anisotropie inderdaad zeer gevoelig is voor het precieze samenstellingsverloop aan het grensvlak. Het zou daarom zeer nuttig zijn om een onafhankelijke meting van deze diffuusheid te kunnen doen.

De energie van de de dipool-dipool wisselwerking voor kristallijne films van 1 tot 10 atoomlagen is berekend. Wanneer de films dik genoeg zijn, wordt de gebruikelijke demagnetisatie-energie voor een dunne film gevonden, maar voor films van slechts enkele atoomlagen wijkt het resultaat af van de continuüm-waarde. Aangetoond wordt, dat de anisotropie veroorzaakt door de dipool-dipool wisselwerking opgesplitst kan worden in een volume- en een oppervlakte-bijdrage. Deze bijdragen zijn voor verschillende kristalstrukturen berekend. In het geval van Pd/Co is deze oppervlakte bijdrage slechts klein, maar voor andere strukturen mag zij niet verwaarloosd worden.

Samenvattend kan gesteld worden, dat aangetoond is, dat de magnetische eigenschappen van multilagen, met name de magnetische anisotropie, begrepen en gemanipuleerd kunnen worden door de invloed van de grensvlakken tussen de verschillende materialen, zoals in dit proefschrift voor Pd/Co multilagen is beschreven.

DANKWOORD

Tot het werk dat in dit proefschrift is beschreven, hebben velen, zowel op het Philips Natuurkundig Laboratorium als bij de Technische Universiteit Eindhoven, bijgedragen. Op deze plaats wil ik hen hartelijk danken voor de medewerking. Speciaal genoemd moeten worden: Henk Donkersloot, Alex Kahle, Wim Gevers en Ad van den Mosselaer voor de preparatie van de multilagen; Dick Kuiper voor zijn assistentie bij Röntgendiffraktie en diffusiemetingen; Jan Bernards, Peter van Engelen en Jelto Smits voor het gebruik van hun magnetometer; Gerard Poodt voor de temperatuurafhankelijke magnetisatiemetingen; Willem van der Vleuten voor zijn hulp bij de Auger-diepteprofilering; Ronald van Rijn voor zijn optreden als computervraagbaak; Ben Janssen, Maarten Luyks, Arjan Plompen, Marc van den Putte en Henk Swagten die als student aan het werk hebben bijgedragen; Honny de Cronckel voor de NMR metingen; Harry van Noort voor de Mössbauermetingen; Harry Ligthart voor de ionen-beschietingen; Ruth Cruijters, Theo Schoenmakers en Marc Beeker voor hun hulp bij de uiteindelijke vormgeving; Helga Pouwels en Rianne van Vinken voor de administratieve ondersteuning; dr. U. Enz, Klaas Kopinga, Coen Swüste en Kich de Wit voor stimulerende gesprekken; Frits den Broeder voor de elektronen-microscopie, zijn continue belangstelling en het nauwkeurig doorlezen van het manuscript; en tenslotte Wim de Jonge voor zijn niet aflatend enthousiasme en zijn kritische begeleiding van het onderzoek.

DE AUTEUR

Henk Draaisma werd op 26 september 1959 geboren te Leidschendam. Van 1971 tot 1977 doorliep hij het gymnasium β aan het St. Maartenscollege in Voorburg. Van 1977 tot 1983 studeerde hij aan de Technische Hogeschool te Delft, Afdeling der Technische Natuurkunde. Zijn afstudeeronderwerp betrof kernoriëntatie-thermometrie in de groep Lage Temperaturen o.l.v. prof. dr. H. Postma. Van 1984 tot 1988 was hij als wetenschappelijk assistent in de groep Coöperatieve Verschijnselen o.l.v. prof. dr. ir. W.J.M. de Jonge verbonden aan de Technische Universiteit Eindhoven en was hij tevens werkzaam op het Philips Natuurkundig Laboratorium te Eindhoven in de groep van dr. P.F. Bongers en dr. U. Enz. In deze periode kwam het onderzoek dat in dit proefschrift is beschreven, tot stand.

STELLINGEN

behorende bij het proefschrift

Magnetic Multilayers

door

H.J.G. Draaisma

VIII

Er dient in de berichtgeving via massamedia over zaken die met radioaktiviteit te maken hebben, een veel duidelijker onderscheid gemaakt te worden tussen gevaren van straling en besmetting.

IX

Het uitspreken van "Ångström" als "Ängström" is net zo ongewenst als het uitspreken van "Rembrand" als "Rembrend".

X

In deze stelling maakt zwart een ko.

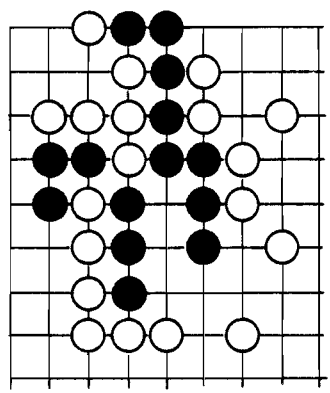

Eindhoven, 4 oktober 1988